Optically Detected Cyclotron Resonance in II-VI Compound Semiconductors

by

Kazuo Satoh

Dissertation in Physics

March 1999

Osaka University

Graduate School of Science

Toyonaka, Osaka

Abstract

Optically Detected Cyclotron Resonance (ODCR) is the combination technique of Cyclotron Resonance (CR) and Photoluminescence (PL), which gives full pay to its ability. In this work, the ODCR measurements together with PL and CR experiments were carried out to investigate the fundamental properties of typical II-VI compound semiconductors, CdTe and ZnSe. Both CdTe and ZnSe are useful semiconductors and have recently attracted a great deal of attention. CdTe is an attractive material for gamma-ray detection and optoelectronic devices. ZnSe, on the other hand, is one of the promising materials for fabricating optical devices.

Two types of ODCR signals can be obtained. One is the signal as a function of the applied magnetic field. The other is the signal as a function of the PL wavelength. From the analysis of results, the line shape of ODCR signal as a function of the magnetic field depends on the origin of the PL lines (free exciton, neutral bound exciton, neutral acceptor bound exciton, etc.). Hence the formation processes in excitonic system were determined through close examination of the difference in the ODCR signals as a function of the magnetic field.

The sign of the ODCR signals strongly depends on the mobility of the sample, i.e. whether the CR spectrum is sharp or broad. The mobility is determined by the concentration of neutral shallow impurity at low temperatures and under photoexcitation condition. The difference of the impurity concentration affects the energy distribution of carries. The situation can be indicated by means of the Monte Carlo simulation. The Monte Carlo simulation is a good tool to obtain the visual solution for the Boltzmann equation. The calculation makes clear that the relation between the sign of the ODCR signals and the energy distribution of carries.

The origins of ODCR signals are the variation in capture rate, impact ionization and resonant formation. The present experiments reveal that the competition between them determines the sign of the ODCR signals.

Contents

1 Introduction

If a charged carrier is set in a static magnetic field B, its motion is a spiral around the direction of the magnetic field. Its angular frequency is known as the cyclotron frequency given by

$$\omega_c = \frac{eB}{m}, \tag{1}$$

where e is the electronic charge and m is the mass of the carrier. The carrier can interact with the electromagnetic radiation and shows resonance absorption when the angular frequency of the radiation coincides with the cyclotron frequency of the carrier. The phenomenon is called cyclotron resonance (CR). This is the classical explanation of the phenomenon called cyclotron resonance. The CR may be also explained by theoretical consideration based on quantum mechanics. In this model the energy of carriers is described as a series of energy levels (known as Landau levels) owing to the quantization of the orbit of the carrier in the magnetic field. With the integer n denoting the Landau level number, the CR represents the absorption of one photon $\hbar\omega$, which corresponds to change of n by $\Delta n = 1$, limited by the selection rule for cyclotron transitions.

The technique was introduced into the solid state physics research in the early 1950s. Dorfmann and Shockley predicted that it could be a useful method to study various properties of solids and it was analyzed theoretically by Dingle and Shockley [1][2][3]. Dresselhaus, Kip and Kittel, and also the Lax group, succeeded separately in the first observation of CR in Ge [4][5]. Since then, it has been used to accurately determine the effective masses and the band structures of the conduction as well as the valence bands in many semiconductors. In addition, the CR line width gives information on the scattering relaxation time of carriers, allowing us to also investigate scattering processes in semiconductors. Accordingly, the CR has become a powerful tool for investigating the properties of semiconductors.

A separate phenomenon is that of luminescence. This is defined as a radiative recombination of carriers from excited electronic states to lower lying states. In order for

semiconductors to emit radiation, they first have to be excited by some means. One possible way is to excite the semiconductor by light with higher quantum energy than the band gap energy, which creates non-equilibrium electron-hole pairs. These then recombine with the emission of photons along a variety of the relaxation paths. This emission from a solid is called photoluminescence (PL). At low temperatures, free electrons and holes created by light in a pure semiconductor first recombine to form free excitons. In semiconductor containing impurities, free excitons are trapped by impurities as bound excitons, and free electrons or holes are captured by ionized impurities. The recombination radiation thus occurs from impurity bound excitons or donor to acceptor transitions. PL measurements also yield important information about the dynamical properties of photoexcited carriers. PL from states near the band edge provides information about the carrier distribution near the band edge. PL from excitons provides information about their binding energy. Electron-hole-drop PL helps to identify the phase transitions of carriers. These and other measurements make PL of great technical importance for the investigation of fundamental properties of semiconductors.

Optically detected cyclotron resonance, (ODCR), is the combination method of CR and PL measurements, and has the merits of each measurement to study various properties of semiconductors. The ODCR method has been developed since the end of the 1970's. It is an important tool to investigate the properties of semiconductors since Baranov et al. performed the first successful ODCR experiment for semiconductors [6], but until recently the poor signal-to-noise ratio limited the use of technique. In the last few years, our group has succeeded in observing very clear ODCR signals, and using the technique for investigating dynamical properties of a number of semiconductors such as Si, Ge and GaAs with many interesting results [7][8][9].

When electron CR occurs in semiconductors, the electrons resonantly absorb the electromagnetic radiation and are promoted into a 'hot' or non-equilibrium state, which is shifted from the normal thermal-equilibrium condition. The hot electrons affect other

particles in free and/or bound state, and the PL intensity and/or PL spectrum change. In the ODCR measurements, the signal is detected through observing the changes in PL intensity induced by CR. The ODCR signal is given by

$$\mathrm{ODCR(signal)} = \mathrm{PL(on)} - \mathrm{PL(off)}, \tag{2}$$

where PL(on) is the PL intensity with the electromagnetic radiation incident on the sample and PL(off) is the PL intensity without the electromagnetic radiation.

ODCR signals can be observed in two ways. One is to observe the changes in PL intensity monitored at the fixed wavelength of a certain PL peak, while scanning the applied magnetic field with the electromagnetic radiation applied. The other is to observe the change in PL spectra due to CR, where the magnetic field is adjusted to produce the CR peak. In the latter case, the ODCR signal is obtained as a function of wavelength for the PL spectrum.

Figure 1 shows the schematic ODCR spectra as a function of PL wavelength. The dotted line represents the PL spectra without electromagnetic radiation. The solid line represents the PL spectra with electromagnetic radiation. It follows from Eq. (2) that the ODCR signal is positive when the PL intensity is increased due to CR. The ODCR signal is, on the other hand, negative when the PL intensity is decreased due to CR.

The ODCR method has some important advantages relative to the ordinary CR. One can select electron or hole cyclotron resonance by changing the strength of the magnetic field, and can also select radiative objects, namely free excitons, bound excitons, bound multiple-exciton complexes and electron-hole droplets in PL, so that one can observe the interaction between radiative objects and carriers separately. In addition, the ODCR signal is detected using a highly sensitive optical detector, and leading to enhanced sensitivity. When the signal from a substrate is dominant and the signal from an epitaxial layer is obscured, it is impossible to investigate the properties of the epilayer by the ordinary CR. However, if the energy region of PL from the substrate is different from that of PL from the epilayer, the luminescence from the epilayer can be selected from that of the

substrate and one can study the properties of epilayer using the ODCR method. If the energy of the excitation source is sufficiently high, only PL from the epilayer is observed because the absorption coefficient of solids is sensitive to the energy of incident light. In this case, the epilayer can be studied by the ODCR method, as reported by Son et al. for SiC epilayers [10][11].

In ODCR experiments, it is possible to study the dynamical behavior in photoexcited carrier system. In the case of ODCR measurements, the sign of the signals can be positive and negative, according to the following factors:

1. **Reduction of the capture rate**

   The capture rate of free carriers decreases with increasing carrier kinetic energy. Thus, the probability of capture by ionized impurities or binding into exciton, is reduced when carriers are heated by CR [12][13].

2. **Impact ionization**

   If carriers have sufficient kinetic energy due to CR, they can ionize shallow impurities or dissociate excitons by collision. It is called impact ionization.

3. **Resonant formation**

   This process occurs when the interaction between carriers and LO-phonon is strong. Figure 2 shows the schematic energy diagram of an exciton state and a conduction band. A carrier resonantly enters the binding state with emission of n LO-phonons when the kinetic energy of the carrier $E(k)$ fulfills the following condition.

   $$n\hbar\omega_{LO} = E(k) + E(b), \tag{3}$$

   where $E(b)$ is the binding energy, $\hbar\omega_{LO}$ is the LO-phonon energy and n is the number of LO-phonons concerned. The phenomenon is called resonant formation and has been reported by Tomaru et al. for the free exciton resonant formation in ZnSe [14].

The competition between these factors determines whether the ODCR signal is positive or negative.

CdTe and ZnSe are useful II-VI semiconductors and have received attention for several decades. CdTe is an attractive material for gamma-ray detection, optoelectronic devices and near infrared optics [15][16]. It is also an ideal substrate for HgCdTe, which is important infrared detector material. ZnSe is one of the most promising materials for fabricating optical devices [17]. Sometimes ZnSe epitaxial layers are grown on GaAs substrates because of the relatively small lattice mismatch between ZnSe and GaAs. Some significant strain is introduced due to the lattice mismatch and differing thermal expansion coefficients. In order to avoid these problems it is necessary to grow ZnSe layers on ZnSe substrates, known as a homoepitaxial growth. The development of ZnSe homoepitaxy has been long hampered by the difficulty in obtaining high quality bulk ZnSe crystals for use as substrates. It is important to study the fundamental properties of high quality bulk CdTe and ZnSe both for basic research and device applications. In recent years, important progress in CdTe and ZnSe crystal growth has been achieved, and high quality bulk CdTe and ZnSe can be obtained.

There are few reports of ODCR measurements on CdTe and ZnSe. ODCR from CdTe has been observed by Romestain and Weisbuch using 70GHz microwave. They obtained the hole mass for the first time and analyzed the ODCR signals [18]. Le Si Dang et al. have determined the Luttinger parameters of CdTe from the ODCR spectrum as a function of magnetic field [19]. Tomaru et al. studied ZnSe using the ODCR method and reported the dynamical behavior of carriers [14]. However, detailed mechanisms of ODCR in CdTe and ZnSe have not been yet resolved.

The aim of this work is to investigate the fundamental properties of high quality bulk CdTe and ZnSe and present the new results on dynamical behavior of the carrier system.

2 Monte Carlo simulation

2.1 Introduction

The capture rate of electrons by ionized centers decreases with increasing kinetic energy of electrons. If carriers have sufficient kinetic energy, they can break by collision the bound exciton, free exciton, neutral donor and so on. These processes should be the origin of ODCR. Thus, it is important to estimate the distribution of carrier energy in analyzing the ODCR spectra. To estimate the distribution of carrier energy, the Boltzmann equation must be solved. However, it is very difficult to solve the Boltzmann equation by analytical methods. From the analytical method, only approximate solutions of the Boltzmann equation are obtained. In actual calculations, the analytical method needs to compute an enormous task.

A new numerical approach was introduced to solve the Boltzmann equation in 1966 [20]. The new method is the Monte Carlo technique. The Monte Carlo method is to simulate the motion of electrons in the condensed matter using a computer. The availability of fast computers enables us to obtain the exact solutions of the Boltzmann equation with the Monte Carlo method, which were afterwards developed to a high degree of refinement [21] [22] [23]. Accordingly the Monte Carlo simulation is now recognized as an important tool in various fields of physics.

2.2 Monte Carlo program

The distribution function and the mean energy of electrons in CdTe and ZnSe are obtained with the method proposed by Jacoboni et al. [24]. In this experiment the magnetic field and ac electric field (microwave) are applied to a sample, and thus the simulation of the motion of electrons in magnetic field and ac electric field is required. However, it is hard to simulate the motion of electrons in such a condition.

The electron trajectories are simulated in zero magnetic field and dc electric field in the present calculation. Karpińska et al. have succeeded in analyzing experimental results

of ODCR by the Monte Carlo simulation in zero magnetic field and dc electric field [25]. They have observed the ODCR spectrum related to DA emission in InGaAs as a function of the PL wavelength and calculated the mean energy and the distribution function of electrons by Monte Carlo simulation. They concluded that electrons have sufficient mean energy enough for impact ionization and the impact ionization is the dominant process for the ODCR signals.

Let us summarize here the Monte Carlo method proposed by Jacoboni et al [24]. One must start to define the physical situation and parameters, i.e. lattice temperature, electron effective mass, electric field, scattering processes and so on. Here values of physical parameters were chosen so as to be appropriate for CdTe and ZnSe employed in the present experiment. The determination of the initial conditions for the electronic system is needed on the heels of the definition of physical system. The next step is the determination of the flight duration of the electron that means the time interval between collision and next collision. The flight duration is determined using random sampling numbers created by a computer. When the flight duration is determined, the motion of a electron in dc electric field is calculated by the classical mechanics until first collision. Therefore it is possible to obtain the situation of the electron just before scattering. The next step is the choice of the scattering processes and the determination of the condition of the electron just after scattering using random sampling numbers. It is the one cycle of the Monte Carlo simulation. The condition of the electron just after scattering is the initial conditions of the electron at the next cycle. The cycle is repeated for sufficiently long time.

2.2.1 Fligth duration

The flight duration of electrons is determined by the random sampling numbers r which are uniformly distributed between 0 and 1. The collision is a random event, and according to the probability theory the random number r is related to collision time t_c by

$$r = \int_0^{t_c} P(t)dt / \int_0^{\infty} P(t)dt, \tag{4}$$

where $P(t)$ is the probability of collision at time t. When r is determined, t_c is obtained. The time t_c is the flight duration.

If $S(\boldsymbol{k}(t))$ is the scattering probability of the electron with wave vector $\boldsymbol{k}(t)$ at time t, the number of electrons which are scattered between t and $t+dt$ is $n(t)S(\boldsymbol{k}(t))dt$. $n(t)$ is the number of electrons which have not suffered a prior collision at time t. If $dn(t)$ represents the number of scattered electrons between t and $t+dt$,

$$-dn(t) = n(t)S(\boldsymbol{k}(t))dt. \tag{5}$$

Equation (5) can be solved by integrating:

$$n(t) = n(0)exp\left[-\int_0^t S(\boldsymbol{k}(t'))dt'\right]. \tag{6}$$

The probability of collision $P(t)$ at time t is given by

$$P(t) = n(t)S(\boldsymbol{k}(t))/n(0) = S(\boldsymbol{k}(t))exp\left[-\int_0^t S(\boldsymbol{k}(t'))dt'\right]. \tag{7}$$

If Eq. (7) is substituted in Eq. (4) and r is determined, the flight duration time t_c is obtained. However, it is hard to obtain t_c because of the integration at the exponent is quite complex. In order to avoid this problem, a self scattering term $W(\boldsymbol{k}(t))$ was introduced by Rees [22].

If Γ is the maximaum value of $P(t)$ in the region of $\boldsymbol{k}$ space of interest, the total scattering rate $S_T(\boldsymbol{k}(t))$ is now defined so that

$$S_T(\boldsymbol{k}(t)) = S(\boldsymbol{k}(t)) + W(\boldsymbol{k}(t)) \tag{8}$$

is a constant equal to Γ. Hence, the integration is easy and $P(t)$ is given by

$$P(t) = \Gamma exp(-\Gamma t). \tag{9}$$

If this is substituted in Eq. (4), the flight duration time t_c is given by

$$t_c = -\frac{1}{\Gamma} ln(1-r). \tag{10}$$

The simulation will lead to mistaken results because of including the self scattering. But, if the self scattering is chosen, the wave vector of the electron just after collision is taken to be equal to that of the electron just before the collision. Thus the trajectory of the electron is unperturbed as if no scattering at all had occurred. The simulation leads to correct results even including the self scattering.

The self scattering results in a waste of the computer time. The computation time is thereby increased but the integrals are rendered manageable. The simplification of the integrals is of great advantage to the simulation even wasting time.

2.2.2 Scattreing processes

If the flight duration time is determined, the motion of electron is calculated just before collision by classical mechanics. Then, the scattering process is chosen using random sampling numbers which are uniformly distributed between 0 and 1. The present simulation allowed for the scattering of electrons by acoustic and polar optical phonons (inelastic) as well as the scattering by neutral impurities (elastic). When intrinsic light is illuminated on a sample and electrons and holes are produced, these free carriers are promptly captured by ionized impurities and most of them are thereby neutralized. Accordingly one can neglect the contribution of the scattering by ionized impurities. The calculation was performed under the assumption that the conduction band is parabolic.

Acoustic phonon scattering

In the case of the high electric fields and/or the high temperatures are considered, the mean energy of electrons amounts to the optical phonon energy. Compared to the energy of acoustic phonon, the mean energy of electrons is considerably higher. Thus acoustic phonon scattering can be treated as an elastic process. But, acoustic phonon scattering must be treated as inelastic process at low electric fields and at low temperatures. In this case, the probability of the acoustic phonon absorption is different from that of the acoustic phonon emission. As the present experiments were performed under such a

Table 1: Definition of $x_{1,a}$, $x_{2,a}$, $x_{1,e}$ and $x_{2,e}$ classified by the electron energy ε, where ε_u is equal to be $\frac{1}{2}m^*u_l^2$ [24].

Absorption	Emission	Energy region
$x_{1,a} = \dfrac{4\varepsilon_u^{1/2}}{K_B T_0}\left(\varepsilon_u^{1/2} - \varepsilon^{1/2}\right)$	absent	$\varepsilon < \varepsilon_u$
$x_{2,a} = \dfrac{4\varepsilon_u^{1/2}}{K_B T_0}\left(\varepsilon_u^{1/2} + \varepsilon^{1/2}\right)$	absent	
$x_{1,a} = 0$	$x_{1,e} = 0$	$\varepsilon > \varepsilon_u$
$x_{2,a} = \dfrac{4\varepsilon_u^{1/2}}{K_B T_0}\left(\varepsilon_u^{1/2} + \varepsilon^{1/2}\right)$	$x_{2,e} = \dfrac{4\varepsilon_u^{1/2}}{K_B T_0}\left(\varepsilon_u^{1/2} - \varepsilon^{1/2}\right)$	

condition, the acoustic phonon scattering was treated as an inelastic process.

Jacoboni et al. have reported that the probability of the inelastic acoustic phonon scattering per unit time $P_{ac}(\varepsilon)$ is given by as a function of the electron energy

$$P_{ac}(\varepsilon) = \frac{m^{*1/2}(K_B T_0)^3 E_1^2}{2^{5/2}\pi\hbar^4 u_l^4 \rho}\varepsilon^{-1/2}\left\{ \begin{array}{l} F_1(x_{2,a}) - F_1(x_{1,a}) \\ G_1(x_{2,e}) - G_1(x_{1,e}) \end{array} \right\}, \tag{11}$$

where K_B, T_0, E_1, u_l and ρ are Boltzman constant, lattice temperature, electron acoustic phonon deformation potential, longitudinal sound velocity and crystal density. The upper and lower equations refer to phonon absorption and emission, respectively. F_1 and G_1 are given by

$$F_1(x) = \int_0^x N_q(x')x'^2 dx', \tag{12}$$

$$G_1(x) = \int_0^x [N_q(x') + 1]x'^2 dx', \tag{13}$$

where N_q is thermal equilibrium number of phonons with wave vector $\boldsymbol{q}$ and $x_{1,a}$, $x_{2,a}$, $x_{1,e}$ and $x_{2,e}$ are those given in Table 1. According to Jacoboni et al., the state of electrons after scattering is determined.

Polar optical scattering

In polar semiconductors such as CdTe and ZnSe, the interaction of carriers with the optical phonons is known as a polar optical scattering. The phonon associated with the

polar optical scattering is LO-phonon. As the energy of the LO-phonon is the order of several ten meV, the polar optical scattering must be treated as an inelastic scattering. Taking into account of the energy dispersion of LO-phonon, it is shown that few LO-phonons exist at low temperatures. This means that the LO-phonon absorption can be neglected at low temperatures.

According to the calculation performed by Fawcett, the polar optical phonon scattering process was treated as follows [23]. The scattering probability $P_{op}(\varepsilon)$ is given by

$$P_{op}(\varepsilon) = \frac{e^2 m^{*1/2} \omega_{op}}{4\sqrt{2}\pi\hbar} \left(\frac{1}{\epsilon_\infty} - \frac{1}{\epsilon_0} \right) \varepsilon^{-1/2} ln \left| \frac{\varepsilon^{1/2} + \varepsilon'^{1/2}}{\varepsilon^{1/2} - \varepsilon'^{1/2}} \right| \left\{ \begin{array}{l} N_{op} \\ N_{op} + 1 \end{array} \right\}, \tag{14}$$

where ω_{op}, ϵ_∞, ϵ_0 and N_{op} are optical phonon angular frequency, high frequency dielectric constant, static dielectric constant and thermal equilibrium number of optical phonons. The upper and lower equations refer to absorption and emission, respectively. ε' is given by

$$\varepsilon' = \varepsilon \pm \hbar\omega_{op}. \tag{15}$$

Here upper and lower signs refer to absorption and emission, respectively. According to Fawcett et al., the state of electrons after scattering is determined in this way.

Neutral impurity scattering

If a sample is illuminated by intrinsic light at low temperatures, the neutral impurity scattering is a dominant one. Electrons can be scattered by neutral donors and neutral acceptors. The neutral acceptors are deeper states, and so their wave functions are generally localized in real space. In addition the exchange scattering between electron and neutral donor occurs, but no exchange scattering between electron and neutral acceptor exists. As a consequence, the scattering probability of electrons by an neutral acceptor is smaller than that by an neutral donor, and one can consider only the neutral donor scattering for electrons. The electron scattering rate by neutral donors P_{imp} is well accounted for by the Erginsoy's formula [26],

$$P_{imp} = \frac{20\hbar a_B^* N_D}{m^*}, \tag{16}$$

where a_B^* is the effective Bohr radius and N_D is the donor concentration. According to the Eq. (16), P_{imp} was treated as independent of the energy of electrons.

3 Experimental procedures

3.1 Samples

The samples used in this study were high quality bulk CdTe and ZnSe, and their detailed specification are listed in Table 2 and Table 4 in chapter 4. They were obtained from several sources. Tohoku university (professor Isshiki group) has provided three bulk CdTe samples #A, #B and #P. Nippon Mining Co., Ltd. has provided a bulk CdTe sample #W. All bulk ZnSe samples were grown by Sumitomo Electric Industries, Ltd.

#B is the crystal which was annealed #A at 973K in 14mm Torr Cd atmosphere. It is believed that Cd vacancies and shallow donors form complexes which are worked as acceptors in CdTe [27]. The Cd vacancies in #B reduced due to the annealing and subsequently the complexes also reduced. As a result, the shallow donors in #B were activated and increased. Thus, the shallow donor concentration in #B is higher than that of #A. #A, #B and #P were grown by a vapor growth method. #W was grown by melt growth method.

All ZnSe crystals were grown by the recrystallization method. High quality ZnSe single crystals can be grown through the annealing of polycrystalline ZnSe in Se atmosphere, which is called as the recrystallization method. #8 was further annealed at 727K in Zn atmosphere for 100 hours. The PL line for neutral acceptor bound excitons, which was observed in #9, #N and #1, was not observed in #8. This suggests that the neutral acceptors in #8 were passivated by the annealing.

3.2 Experimental setup

Figure 3 shows a block diagram of experimental setup for PL, standard CR and ODCR measurements. The experimental setup was composed of a PL and a microwave CR measuring system. The sample was mounted on an immersion-type cryostat to avoid heating of the sample. The microwave system is a nonresonant reflection type waveguide system working at 35GHz. A klystron (OKI 35V11) was employed for microwave generation.

An external magnetic field was produced by a standard electromagnet whose maximum magnetic field is 0.6T. For the PL measuring system, two kinds of laser were employed as the excitation source. One was 488nm line of a cw Ar^+ laser (NEC GLG3200 : 100mW) for CdTe samples. The other was 325nm line of a cw He-Cd laser (KIMMOM IK3552R-G : 50mW) for ZnSe samples. The laser beam was guided to a sample face through an optical fiber and a silica rod. The luminescence was taken out through the same silica rod and the optical fiber. It was led to a monochromator (JASCO CT-50). The luminescence dispersed by the monochromator was detected by a photomultiplier. Three kinds of photomultipliers were used and one of them was selected for each measurement. The photomultiplier R943-02 (HAMAMATSU) was used for photon counting system (OXFORD SR400). The photomultiplier R2066 (HAMAMATSU) and the photomultiplier R980 (HAMAMATSU) were used for the lock-in amplifier detection system (NF 5610B). A personal computer was used for data processing and on-line display. All experiments were carried out at 4.2K.

In the PL measurements, the laser beam was mechanically chopped. The signal was analyzed by the gated photon counter or the lock-in amplifier system. The gated photon counter can open two gates simultaneously. One of them was open during exciting a sample by the laser and the other was open during not exciting it. The difference of the two signals obtained at the different gates was plotted to diminish dark noises for the photon counting system. Some proper filters were used to remove laser plasma lines and the laser light reflected from the sample.

In standard CR measurements, the laser was employed for exciting carriers. The laser beam was mechanically chopped. The CR signal was detected by a Schottky-type GaAs diode detector and the output was processed by the lock-in amplifier.

In ODCR measurements, the microwave was modulated by oscillating a reflector voltage for the klystron. The ODCR signal was caught by the lock-in amplifier or the gated photon counter. One gate of the gated photon counter was open during the irradiation

of the microwave to a sample. The other gate was open for the duration without the microwave irradiation to it. The difference of the two signals from two channels was plotted for the gated photon counting measuring system. In this case, some proper filters were again used to block laser plasma lines and laser light reflected from the sample.

4 Experimental Results

4.1 CdTe #A

4.1.1 Ordinary CR

Figure 4 shows the ordinary electron CR spectrum observed at 4.2K for 35GHz microwave. Carriers were excited by the 488nm line of the Ar^+ laser. It is noteworthy that the distinct resonant peak was observed and the line width of the CR spectrum was narrow. This means that #A is a high quality crystal. The effective mass m^* is derived from the following relation

$$m^* = \frac{eB_r}{\omega}, \tag{17}$$

where B_r is the resonance magnetic field and ω is the measuring microwave angular frequency. The effective mass of electron is estimated to be $0.0954m_0$, where m_0 is the free electron mass. It is in good agreement with previously reported values [28][29]. Strictly speaking, it is not band mass but polaron mass in such as II-VI semiconductors with a large electron-phonon interaction. The value of electron relaxation time τ is obtained from the width of the CR line. The resonance line width can be converted into τ by the following relation

$$\tau = \frac{B_r}{\omega \Delta B}, \tag{18}$$

where ΔB is the half-width and thus $\tau = 1.4 \times 10^{-11}$s is obtained. With this relaxation time, the electron CR mobility $\mu = 2.6 \times 10^5 \mathrm{cm}^2/\mathrm{Vs}$ is derived based on the relation

$$\mu = \frac{e\tau}{m^*}. \tag{19}$$

As for CdTe, above value is considerably large.

4.1.2 PL measurements

The PL spectrum measured in the range of 1.38 to 1.61eV at the magnetic field of 0.12T for the sample #A is presented in Fig. 5. Compared to the PL spectra at the magnetic field of 0T, the intensity of all the emission lines has decreased but the peak shift was

hardly observed with applying the magnetic field of 0.12T. The other CdTe samples also show the similar inclination.

The several PL lines in the near band edge were obtained. Several broad peaks were observed in the range of 1.40eV to 1.54eV. The broad peak at 1.47eV is generally labeled by Y line. Hoffman et al. have reported that the origin of Y line is donor to acceptor (DA) recombination involving an A center which is composed of a Cd vacancy and a Cl donor taking its position at a nearest Te site and acts as an acceptor [30]. Leopold has reported that the Y line is the recombination emission related to an impurity-Cd vacancy complex, although the real character of the impurity is unknown [31]. The broad peak at 1.49eV is due to DA recombination involving Ag acceptor [32]. The nature of peak at 1.52eV is unknown, but the peak is probably connected with the DA recombination. It is probable that all the broad peaks between 1.40eV and 1.54eV are due to DA recombination.

Figure 6 shows the PL spectrum at the magnetic field of 0.12T in the region of near band edge. The spectrum shows a sharp line at 1.590eV. This is a dominant line in the spectrum and it is attributed to the decay of an exciton bound to a neutral acceptor (A^0X) [27] [33]. The nature of this acceptor is controversial. The LO-phonon replica of the acceptor bound exciton (A^0X-LO) was observed. The difference between this line and the above mentioned main line corresponds to the established LO-phonon energy in CdTe, 21.3meV [33]. The spectrum shows some clear emission lines, due to a free exciton (X), a neutral donor bound exciton (D^0X) and an ionized donor bound exciton (D^+X) [27] [33]. D^+X line can accurately be the superposition of D^+X and D^0-h^+ which is radiative recombination between a free hole and a bound electron. The nature of the donor is unknown. Free exciton peak consists of two peaks. This would come from the exciton polariton branches. In addition the LO-phonon replicas of free exciton line (X-LO, X-2LO) were observed.

4.1.3 ODCR as a function of photon energy

Figure 7 shows the ODCR spectrum obtained by scanning PL wavelength at the magnetic field of 0.12T which corresponds to the field of the electron CR. Negative ODCR signals were observed in lower energy region, which are related to DA transitions. This means that the PL intensity of the DA recombination is decreased by the electron CR.

The ODCR spectrum as a function of photon energy near the band edge is shown in Fig. 8. The dominant ODCR peak related to A^0X was observed. At higher energy side of the main line, there were two ODCR signals associated with D^0X and D^+X. Although the PL intensity of free exciton itself was comparable to that of X-LO in the PL measurements, the intensity of X-LO peak was stronger than that of free exciton in the ODCR measurements. It is not clear that the reason why the relative intensity of the ODCR signal is different between free exciton and X-LO. From the near band edge ODCR spectrum, it is shown that D^+X was negative and D^0X, A^0X and X-LO were positive. This means that D^+X is decreased by the electron CR and the D^0X, A^0X and X-LO are increased by the electron CR.

The negative ODCR signal of D^+X was not evidently observed in Fig. 7 because of the difference in resolution of the monochromator.

4.1.4 ODCR as a function of magnetic field

Figure 9 shows the ODCR spectrum obtained through monitoring the X-LO line. The shape of the ODCR spectrum was similar to that of the ordinary CR. Unfortunately, the ODCR signal related to free exciton itself was not observed because its intensity was too weak. However, the line shape of the ODCR obtained from X-LO probably reflects that related to the original free exciton. This is confirmed by the following indirect evidences. As for both the ODCR signals related to original PL lines and those for LO-phonon replica, the line shape of these signals bears a striking resemblance each other in CdTe and ZnSe.

The microwave power dependence of ODCR spectrum monitored at A^0X PL line as a

function of magnetic field is shown in Fig. 10. The relative microwave power is indicated in the figure. The ODCR intensity decreases with decreasing microwave power. The line shape of the ODCR signal obtained from A^0X line at 0dB microwave power level is similar to that of X-LO.

The ODCR spectrum monitored at the D^0X line and obtained under the full microwave power level is shown in Fig. 11. The line shape is similar to the line shape of X-LO. Since this line is mixed with the D^+X line marked with the negative ODCR signal, the resultant ODCR signal obtained from D^0X line appears to be negative at the higher magnetic field.

Figure 12 shows the ODCR signal obtained from D^+X as a function of magnetic field. The ODCR signal was negative. As shown in Fig. 12, it is clear that a big fall of the D^+X PL line takes place at the electron CR. It is noteworthy that its line shape is anti-symmetric and rather different from that of the ODCR related to X-LO line.

4.2 CdTe #P

4.2.1 Ordinaty CR

Figure 13 shows the ordinary electron CR spectrum at 4.2K. This means that #P is also a high quality crystal and has low impurity concentration. The scattering relaxation time $\tau = 1.2 \times 10^{-11}$s and the CR mobility $\mu = 2.0 \times 10^5 \mathrm{cm}^2/\mathrm{Vs}$ were obtained from the line width of the CR spectrum.

4.2.2 PL measurements

Figure 14 shows the PL spectrum at the CR field of 0.13T. The PL peaks associated with excitons were observed at the region of near band edge. Several DA transitions and their LO-phonon replicas were observed at lower energy region. The positions of DA peaks obtained from #P are equivalent to those of DA peaks obtained from #A. Thus it is concluded that the origin of acceptors related to DA transitions in #P and in #A are the same. The intensity ratio of DA emission line to A^0X emission one in #P is larger than that in #A.

The PL spectrum measured in the region of near band edge at the CR field of 0.12T is presented in Fig. 15. The strong emission band at 1.590eV was identified as the superposition of several A^0X emission lines. The weak lines due to X and D^0X were also observed. Moreover the LO-phonon replicas of X and A^0X were observed.

4.2.3 ODCR as a function of photon energy

Figure 16 shows the ODCR spectrum as a function of the emitted photon energy at the CR magnetic field of 0.12T. Weak ODCR signals due to DA transitions were observed in the range of 1.43eV to 1.53eV. All ODCR signals due to DA transitions were negative, whereas A^0X line is positive. This means that DA recombination in #P was decreased by the electron CR.

In Fig. 17 the ODCR spectrum in the near band edge measured at the magnetic field of 0.12T is shown. The difference of signal-to-noise between Figs. 16 and 17 arises from a difference in detectors employed. A strong peak due to A^0X and its LO-phonon replica were observed. A weak LO-phonon replica associated with X was also observed. The signal due to X was hardly observed. In addition, a D^+X ODCR peak with the character of negative sign was observed, although the peak was not clear in the PL measurements. The D^+X peak was probably obscured by the strong A^0X line in the PL measurements, but the D^+X was clearly brought to light in the ODCR measurements because of the different sign between the ODCR signals for D^+X and A^0X lines. This greatly demonstrates the merit of ODCR measurements. The ODCR signals due to A^0X, A^0X-LO and X-LO lines were positive, but the D^+X signal was negative. These results obtained from #P are much the same as those from #A.

4.2.4 ODCR as a function of magnetic field

Figure 18 shows the microwave power dependence of the ODCR signal obtained from A^0X PL line as a function of magnetic field. The relative microwave intensity is indicated in the figure. The line shape of the ODCR signal for A^0X line resembles the spectrum of

the ordinary CR. The signal intensity of the ODCR decreases with decreasing microwave power.

Figure 19 shows the ODCR spectrum obtained from D^+X. Though it is rather noisy, it is noted that the ODCR signal is negative and the line shape is different from that for A^0X line. However, the ODCR spectrum resembles the ODCR spectrum obtained from D^+X in #A.

The ODCR signal related to the other PL lines could not be observed because they were too weak to detect. It is concluded that all the results obtained from #P are similar to those of #A.

4.3 CdTe #B

4.3.1 Ordinary CR

The ordinary CR spectrum taken at 4.2K is shown in Fig. 20. The definite CR peak was not observed in #B and the line width of the spectrum broadened, which was different from the result for #A and #P. This means that the relaxation time τ for electrons in #B is small. Since the scattering by neutral donors is dominant for electrons at lower temperatures, #B must have higher donor concentrations than #A and #P as expected from heat treatment.

4.3.2 PL measurements

Figure 21 shows the PL spectrum obtained at the CR field of 0.12T. Several broad peaks were observed in the range of 1.40eV to 1.48eV. The broad peak at 1.47eV was identified as the above mentioned Y line. The broad band at 1.45eV is DA transitions and due to Cu impurities on Cd sites which act as shallow acceptors [32] [34].The broad peaks at 1.43eV and 1.41eV are their LO-phonon replicas.

The detailed PL spectrum in the near band edge is shown in Fig. 22. The PL peak due to A^0X has shoulder at higher energy side, which is the contribution of different chemical species as acceptor. An LO-phonon replica of A^0X is also observed. In addition, a weak

line due to D^0X is observed at somewhat higher energy of the A^0X line. The clear signals due to free excitons and its LO-phonon replica were not observed. This suggests that the impurity concentration of #B is higher than that of #A and #P. It coincides with the results obtained from the CR experiment.

4.3.3 ODCR as a function of photon energy

Figure 23 shows the ODCR spectrum obtained at the CR field of 0.12T. The ODCR signals associated with DA transitions as well as Y line were observed in lower energy region. The ODCR signal at 1.47eV is Y line and the ODCR signal at 1.45eV is due to DA transitions involving Cu acceptors. The LO-phonon replicas of DA transitions were also observed. In the same way as other CdTe samples all of ODCR signals associated with DA transitions were negative.

The ODCR spectrum for the near band edge emission taken at the magnetic field of 0.12T is shown in Fig. 24. The ODCR signal at 1.591eV is due to the superposition of several A^0X lines. The LO-phonon replica of A^0X was observed. In addition, the ODCR signal obtained from D^0X was observed. It is remarkable that all of the ODCR signals for this sample were negative. One should note that the ODCR spectra obtained from #B are different with respect to the sign of the ODCR spectra for the near band edge emission, compared to those obtained from #A and #P.

Eventually, all of ODCR signals obtained from #B were negative, which means that the PL intensities of #B are sure to decrease by the electron CR.

4.3.4 ODCR as a function of magnetic field

Figure 25 shows the ODCR spectrum obtained from A^0X PL line. The resonance peak is broad and similar to the result of the ordinary CR. The change in PL intensity is decreased with increasing applied magnetic field.

Figure 26 shows the ODCR spectrum obtained from D^0X PL line. The line shape resembles the ordinary CR line shape. Again the ODCR signal intensity decreased with

increasing applied magnetic field.

4.4 CdTe #W

4.4.1 Ordinary CR

Figure 27 shows the ordinary CR spectrum at 4.2K. The definite CR peak was not observed, as in the case of #B. From the ordinary CR spectrum, it is concluded that #W has higher impurity concentration than #A and #P.

4.4.2 PL measurements

Figure 28 shows the PL spectrum obtained at the CR field of 0.12T. In the range of 1.40eV to 1.50eV, several broad peaks were observed. They were attributed to Y line, DA transitions involving Cu acceptors and their LO-phonon replicas. They were also observed in #B. In addition, several peaks were observed in the range of 1.55eV to 1.51eV. These lines have not been observed in other CdTe samples. Molva et al. have reported that the peak at 1.55eV is due to the DA transitions related to N acceptors and the peak at 1.54eV originates in the DA transitions involving Na or Li acceptors [35] [36]. The peaks at 1.53eV and 1.52eV are their LO-phonon replicas.

Figure 29 shows the PL spectrum for the near band edge emission at the magnetic field of 0.12T. The dominant peak is the recombination emission of A^0X. The LO-phonon replica of A^0X was observed. In addition, a weak line for D^0X was also observed. A free exciton line was hardly observed in this sample. This suggests that the impurity concentration of #W is considerably higher than that of #A and #P.

4.4.3 ODCR as a function of photon energy

Figure 30 shows the ODCR spectrum at the magnetic field of 0.12T. The ODCR peaks in the range of 1.40eV to 1.50eV were associated with DA transitions and their LO-phonon replicas. All of them show negative ODCR signals. The negative ODCR signals in the range of 1.55 to 1.51eV were DA transitions involving N and Na or Li acceptors. It is remarkable that the positive ODCR signals at 1.55eV and at 1.53eV were slightly observed.

The positive ODCR peak at 1.53eV is due to LO-phonon replicas of the positive ODCR peak at 1.55eV. They were not observed in PL measurements and probably obscured by other DA transitions involving N acceptors in PL measurements. The origin of them is unknown.

Figure 31 shows the ODCR spectrum in the near band edge at the magnetic field of 0.12T. The strong ODCR peak due to A^0X recombination and its LO-phonon replica were observed. In addition, the ODCR signal due to D^0X was also observed. All of the ODCR signals taken at the region of the near band edge were negative.

The ODCR signals obtained from #W were negative except for two peaks at 1.55eV and 1.53eV.

4.4.4 ODCR as a function of magnetic field

The ODCR spectra obtained from A^0X PL and D^0X PL lines as a function of the magnetic field are shown in Figs. 32 and 33, respectively. Both of ODCR signals resemble each other. Their line shapes are similar to that of the ordinary CR.

The results obtained from #W are wholly similar to those of #B.

4.5 Summary

The distinct CR peak was observed in #A and #P. Through the line width measurements, the CR mobility of these samples has been derived. The sign of ODCR signals obtained from #A is equivalent to that from #P. The line width of the CR spectra broadened in #B and #W. The sign of all the ODCR signals obtained from #B and #W are negative except for two weak peaks at 1.55eV and 1.53eV in #W. The CR mobility and the results of ODCR are listed in Tables 2 and 3.

Table 2: The specifications of CdTe. The circle means that the sample was annealed. The CR mobility was obtained from the line width of the ordinary CR spectrum at 4.2K.

sample	growth method	annealing	CR mobility at 4.2K(cm^2/Vs)
#A	vapor growth	×	2.6×10^5
#P	vapor growth	×	2.0×10^5
#B	vapor growth	◯	4.1×10^4
#W	melt growth	×	4.4×10^4

Table 3: The results of the ODCR in CdTe. The circle means the CR peak was observed in the sample. The plus means the sign of the ODCR signal was positive and the minus means the sign of the ODCR signal was negative. The ODCR signal for D^0X in #P and the ODCR signals for X-LO and D^+X in #B and #W were not observed. The ODCR signals for DA emission in #W were negative without two signals.

sample	CR	X-LO	D^+X	D^0X	A^0X	DA
#A	◯	+	−	+	+	−
#P	◯	+	−	absent	+	−
#B	×	absent	absent	−	−	−
#W	×	absent	absent	−	−	−(+)

4.6 ZnSe #9

4.6.1 Ordinary CR

Figure 34 shows the electron CR spectrum observed at 4.2K. The carriers were excited by the 325nm line of the He-Cd laser. A sharp resonance line related to the electron CR was observed at 0.18T, which means that #9 is a high quality crystal. The value of effective mass m^* derived from the resonance magnetic field is $0.143m_0$. It is in good agreement with the value of electron effective mass reported previously [37]. From Eqs. (18) and (19), the electron relaxation time τ and the CR mobility μ are estimated as 4.0×10^{-11}s and 4.9×10^5cm^2/Vs, respectively. It is noteworthy that the resonant spectrum did not have any structure.

4.6.2 PL measurements

The PL spectrum of #9 is shown in Fig. 35. Two strong PL lines and many weak ones are observed. The dominant PL peaks originate in recombination of excitons bound to neutral acceptors I_1 and ones bound to deep acceptors I_1^d. The deep acceptors are usually identified as substitutional Cu atoms Cu_{Zn} [38] [39]. Weak PL peaks due to free exciton line FE and shallow donor bound exciton line I_2 were observed. I_2 line consists of two peaks, which means that there exists more than two kinds of shallow donor in this sample. These origins are unknown. In addition, the LO-phonon replicas of FE, I_1 and I_1^d were also observed. It is said that the LO-phonon energy in ZnSe is 31.8meV [39], and it is consistent with this observation.

The inset of Fig. 35 shows the detailed PL spectrum in the range of lower energy. The R, Q series and the LO-phonon replicas associated with exciton were observed. Subscripts of R or Q indicate the number of LO-phonon emitted during the electronic transition. The origin of R and Q series is controversial and will be discussed later.

The peak shift of PL lines by applying of the magnetic field of 0.18T was hardly observed. The other ZnSe samples also show the similar inclination.

4.6.3 ODCR as a function of photon energy

Figure 36 shows the ODCR spectrum obtained at the magnetic field of 0.18T which corresponds to the electron CR. In this spectrum the dominant ODCR peak is due to I_1. In addition, the ODCR signals due to FE, I_2, I_1^d and their LO-phonon replicas were observed. The ODCR signals related to I_1 and I_1^d were positive, on the other hand, ones related to FE and I_2 were negative. Their LO-phonon replicas have the same sign as their original ones. Positive ODCR signals mean that the PL intensity is increased by the electron CR and negative ODCR signals, on the other hand, mean that the PL intensity is decreased by the electron CR.

The inset in the Fig. 36 shows the behavior of the ODCR signals in the region of lower energy. The prominent positive ODCR signals associated with Q series were observed. The negative signal observed at 2.71eV should be the superposition of FE-3LO and R_0 signals. The ODCR signal peak at 2.68eV is due to only R_1 transition because the FE-4LO is too weak to observe. Therefore it is concluded that the ODCR signals due to R series are negative.

4.6.4 ODCR signal as a function of magnetic field

The microwave power dependence of the ODCR spectra obtained from FE line is shown in Fig. 37. The relative microwave power is indicated in the figure. As shown in Fig. 37, it is obvious that the ODCR signals were different from the ordinary CR signal in shape. The ODCR spectrum obtained from FE peak at the microwave power level of 0dB has a shoulder. The shoulder is observed at 0.2T, which is higher magnetic field than that of the ordinary CR peak. The peak at 0.2T disappears at the low microwave power levels. Tomaru et al. have reported the similar results with respect to the peak at 0.2T [14]. They have concluded that the sign of the peculiar peak is positive and originates in the resonant formation of free exciton. The negative peak at 0.17T remains even at the -10dB microwave power level. This means that the ODCR spectrum obtained from FE line at the 0dB microwave power level consists of positive and negative signals. The

peak position of the negative ODCR signal at the 0dB microwave power level is 8% lower than that of the ordinary CR obtained at the 0dB microwave power level. It is possible that the observed ODCR peak outwardly shifts, because of the superposition of positive and negative ODCR signals. However, the peak shift is still observed even at the low microwave power levels where the positive ODCR peak completely disappears.

Figure 38 shows the ODCR signal due to I_2 line at the 0dB microwave power level. It is noted that the ODCR spectrum obtained from I_2 line is quite similar to the ODCR spectrum for FE line at the 0dB microwave power level. It has again a shoulder at the higher magnetic field of the CR. This line is also considered to be the superposition of two peaks.

Figure 39 shows the microwave power dependence of the ODCR spectra obtained from I_1 line. The ODCR signal at the 0dB microwave power level consists of two peaks as well. The positions of these two peaks are equivalent to those of FE. However, both peaks are positive. The peak at 0.2T disappears at the low microwave power levels. From this result, it is shown that the peak at 0.2T is due to the resonant formation of FE.

Figure 40 shows the ODCR spectra obtained from I_1^d line at various microwave power levels. The ODCR signal intensity decreases with decreasing microwave power as well. It is noted that the peak positions of the spectra obtained from I_1^d line are different from those of FE. The dependence of the ODCR signal for I_1^d on the microwave power is also different from that of FE.

4.7 ZnSe #N

4.7.1 Ordinary CR

Figure 41 shows the microwave power dependence of the electron CR spectrum taken at 4.2K. The CR intensity decreases with decreasing microwave power. However, the peak position as well as the line width is independent of the microwave power. With Eqs. (18) and (19), the relaxation time τ and CR mobility μ are estimated to be 3.9×10^{-11}s and

$4.8 \times 10^5 \mathrm{cm}^2/\mathrm{Vs}$, respectively. They are almost equivalent to the values of #9, which means that the crystal quality of #N is as high as that of #9.

4.7.2 PL measurements

The PL spectrum at the magnetic field of 0.18T in the range of 2.64eV to 2.82eV is shown in Fig. 42. The strongest peak is I_1. In addition, weak FE, I_2 and I_1^d line were observed. Their LO-phonon replicas were also observed. The relative intensity of I_1 to I_1^d in #N was different from that in #9. This means that the concentration ratio of shallow acceptors to deep ones is different in these two samples.

The inset in Fig. 42 shows the detailed PL spectrum in the range of lower energy. The above mentioned Q series were observed. The weak R series were observed as well.

4.7.3 ODCR as a function of photon energy

Figure 43 shows the ODCR spectrum at the magnetic field of 0.18T which corresponds to the electron CR. The ODCR signals due to FE, I_2, I_1, I_1^d and their LO-phonon replicas were observed. The ODCR signals associated with FE, I_2 and their LO-phonon replicas were negative. On the other hand, the ODCR signals associated with I_1, I_1^d and their LO-phonon replicas were positive.

The inset of Fig. 43 shows the detailed ODCR spectrum in the vicinity of 2.7eV. The ODCR signals related to Q series were observed and they were all positive. The distinct ODCR signals related to R series were hardly observed. It can be interpreted in two ways. One is that the ODCR signals for R series are negative and obscured by strong positive ODCR signals for Q series. The other is that in this sample the ODCR signals for R series are not affected by the electron CR. Since the ODCR signals for R series were clearly observed in #9, the former is probable interpretation.

4.7.4 ODCR as a function of magnetic field

Figure 44 shows the microwave power dependence of the ODCR spectra obtained from FE line. The spectra are similar to those of #9. The ODCR signal at the microwave power

level at 0dB has a shoulder which disappears at the low microwave power levels. The peak position of the shoulder lies in the higher magnetic field than that of the ordinary CR. Thus, it reflects the resonant formation of free exciton. The peak position of the negative ODCR signal is found at the lower magnetic field than that of the ordinary CR, of which peak shift is 9%.

The ODCR signal obtained from I_2 line is shown in Fig. 45. It is obvious that the ODCR signal has a shoulder at the higher magnetic field of the CR. The ODCR signal again consists of two peaks, of which peak positions are equivalent to those of the ODCR signal obtained from FE at the 0dB microwave power level.

Figure 46 shows the microwave power dependence of the ODCR signals obtained from I_1 line. The spectrum at the 0dB microwave power level also consists of two peaks. The peak at the higher magnetic field disappears at the lower microwave power levels like the results of #9. The peak positions of two peaks obtained from I_1 line are equivalent to those obtained from FE line.

4.8 ZnSe #1

4.8.1 Ordinary CR

Figure 47 shows the microwave power dependence of the ordinary CR taken at 4.2K. With Eqs. (18) and (19), the relaxation time τ and CR mobility μ are estimated to be 3.2×10^{-11}s and 3.9×10^5cm^2/Vs, respectively. The CR mobility for #1 is smaller than that of #9 and #N, which means that #1 has considerably higher donor concentrations because the neutral donor impurity scattering is dominant at low temperatures and under the condition of photoexcitation. It was found that the peak position as well as the line width of the CR was independent of the microwave power level.

4.8.2 PL measurements

Figure 48 shows the PL spectrum for #1 obtained at the magnetic field of 0.18T. The PL lines due to FE, I_2, I_1, I_1^d and their LO-phonon replicas were observed. The I_1^d peak

was stronger than the I_1 line. In this sample I_2 line was clearly observed, while this line was very weak in other samples as #9 and #N. This means that #1 contains much more shallow donors than #9 and #N. This result is consistent with the results of CR measurement.

The inset in Fig. 48 shows the detailed PL spectrum in the range of lower energy. The emission lines associated with Q series were observed. In addition, the weak emission lines associated with R series were observed.

4.8.3 ODCR as a function of photon energy

Figure 49 shows the ODCR spectrum at the magnetic field of 0.18T which corresponds to the electron CR. The ODCR signals due to I_1, I_1^d and their LO-phonon replicas were observed and they were positive ODCR signals. The ODCR signals due to FE and I_2 line with the negative sign were observed.

The inset in Fig. 49 shows the detailed ODCR spectrum in the range of 2.64eV and 2.75eV. The distinct ODCR signals associated with Q series were observed, while ODCR signals associated with Q series and a sharp phonon replica of I_1^d with the positive sign obscured those with R series.

4.8.4 ODCR as a function of magnetic field

Figure 50 shows the microwave power dependence of the ODCR spectra obtained from FE line. It was found that the ODCR signal decreased with decreasing microwave power. The ODCR signal has hardly shown any structure due to the resonant formation of FE even at the 0dB microwave power level.

Figure 51 shows the ODCR spectra obtained from I_2 line. The line shape is similar to that of the ODCR spectrum for FE line at the 0dB microwave power level. In this case the ODCR signal also shows no indication of the resonant formation of free exciton.

Figure 52 shows the microwave power dependence of the ODCR signal obtained from I_1 line. It is found that the intensity of the ODCR decreased with decreasing microwave

power. The prominent shoulder at 0.2T was not observed.

Figure 53 shows the microwave power dependence of the ODCR spectra obtained from I_1^d line. The intensity of the ODCR signals decreased with decreasing microwave power. The spectrum at the 0dB microwave power level consists of two peaks. The line shape of the ODCR signal at the 0dB microwave power level was different from that of FE line.

4.9 ZnSe #8

4.9.1 Ordinary CR

Figure 54 shows the CR spectrum at 4.2K. The relaxation time τ and CR mobility μ derived from the line width measurements are 2.4×10^{-11}s and 2.8×10^5cm^2/Vs, respectively. The CR mobility of #8 is the lowest one among ZnSe samples employed in this experiment.

4.9.2 PL measurements

The PL spectrum related to the near band edge emission at the magnetic field of 0.18T is shown in Fig. 55. The sharp PL peak due to I_1^d was observed. In addition, the PL peaks due to FE, I_2 and LO-phonon replicas of I_1^d were observed.

The inset in Fig. 55 shows the PL spectrum in the range of 2.1eV and 2.6eV. A broad peak at 2.4eV of which origin is unknown was observed.

It is characteristic behavior of #8 that I_1 line and the emission lines associated with R and Q series were not observed in the least. The broad peak at 2.4eV was observed only in #8 that is a unique sample with heat treatment. Accordingly, this broad line should originate in some kind of defects introduced by heat treatment.

4.9.3 ODCR as a function of photon energy

Figure 56 shows the ODCR spectrum obtained at the magnetic field of 0.18T. The change in PL intensity induced by the electron CR in #8 was smaller than that in other samples. The main ODCR peak was due to I_1^d line. The ODCR signals due to I_1^d and

their LO-phonon replicas were positive. The weak ODCR signals due to FE and I_2 were also observed. The ODCR signal due to I_2 was negative, while the ODCR one due to FE was positive. It is characteristic behavior of this sample that the ODCR signal obtained from FE is positive, because the ODCR signals for FE were always negative for other ZnSe samples employed.

4.9.4 ODCR as a function of magnetic field

Figure 57 shows the ODCR spectrum obtained from FE line. The signal was composed of two signals. One is the broad negative signal and the other is narrow positive one which might be due to the resonant free exciton formation. The negative ODCR signal is weaker than the positive ODCR one. Thus, the ODCR signal related to FE line shown in Fig. 56 exhibits the positive sign.

Figure 58 shows the ODCR spectrum obtained from I_2 line. Though the ODCR signal is rather noisy, its line shape is surely similar to that of the ODCR spectrum obtained from FE line. It is composed of two peaks, one is broad negative peak and the other is narrow positive one.

Figure 59 shows the ODCR spectrum obtained from I_1^d line. The ODCR signal has complicated structures. It is obvious that the ODCR line shape is completely different from those of FE and I_2 line.

Figure 60 shows the ODCR spectrum obtained from the broad PL peak at 2.4eV. The clear resonant peak was observed and the sign of the ODCR signal was positive.

4.10 Summary

The ordinary CR peaks were observed in all samples employed. The CR mobility was derived from the linewidth measurement of the CR spectrum. I_1 and the emission lines associated with R and Q series were observed except for #8. The broad peak at 2.4eV, on the other hand, was observed in only #8. The CR mobility and the characteristics of ODCR signals are listed in Tables 4 and 5.

Table 4: The specifications of ZnSe. The circle shows that the sample was heat treated. The CR mobility was derived from the linewidth measurements of the ordinary CR spectrum at 4.2K.

sample	growth method	annealing	CR mobility at 4.2K(cm^2/Vs)
#9	recrystallization	×	4.9×10^5
#N	recrystallization	×	4.8×10^5
#1	recrystallization	×	3.9×10^5
#8	recrystallization	◯	2.8×10^5

Table 5: The results of the ODCR in ZnSe at 0.18T. Circles mean that the clear CR peak was observed in the sample concerned. The plus and minus indicate the positive and negative sign of the ODCR signal, respectively. The notation 2.4eV means the broad emission peak observed at 2.4eV. The positive sign of the ODCR signal for FE in #8 is obtained at 0.18 T. One should note that it is negative at the different magnetic field.

sample	CR	FE	I_2	I_1	I_1^d	R	Q	2.4eV
#9	◯	−	−	+	+	−	+	absent
#N	◯	−	−	+	+	−	+	absent
#1	◯	−	−	+	+	absent	+	absent
#8	◯	+	−	absent	+	absent	absent	+

5 Discussion

5.1 CdTe

5.1.1 Formation process in exciton system

In #A and #P, the ODCR signal obtained from the X-LO line as a function of magnetic field was observed. The ODCR signals obtained from the LO-phonon replica lines as a function of magnetic field reflect those obtained from the fundamental lines. Namely it is found that the ODCR line shapes of the LO-phonon replica lines and the original PL line extremely resemble each other. Unfortunately the ODCR signal for free exciton line has not been observed because it was too weak, but the ODCR signal from the X-LO line was observed and this signal should reflect the ODCR signal from free exciton.

Formation process for neutral donor bound exciton, D^0X

From Figs. 9 and 11, one notes that the ODCR line shape obtained from D^0X is exceedingly similar to that from X-LO. This means that the change in PL intensity of free exciton line coincides with one of D^0X line. Based on these experimental observations let's discuss the formation process for the neutral donor bound exciton, D^0X. It is satisfactory to consider that there are three types of formation process for D^0X.

$$D^0 + e^- + h^+ \longrightarrow D^0 + X \longrightarrow (D^0X), \tag{20}$$

$$D^0 + e^- + h^+ \longrightarrow D^- + h^+ \longrightarrow (D^0X), \tag{21}$$

$$D^0 + e^- + h^+ \longrightarrow (D^+X) + e^- \longrightarrow (D^0X), \tag{22}$$

where, D^0, e^-, h^+, X, D^- and (D^+X) are neutral donor, electron, hole, free exciton, donor with an additional electron and ionized donor bound exciton, respectively. The formation process described by Eq. (20) means that first of all an electron and a hole form themselves into a free exciton and then the free exciton is captured by a neutral donor. Equation (21) means that an electron and a neutral donor form into D^- state and then a hole is captured by D^-. The final Eq. (22) means that a hole and a neutral donor

form into an ionized donor bound exciton and then an electron is captured by it.

If the formation process described by Eq. (22) is dominant, the ODCR signal obtained from D^0X is affected by that obtained from D^+X, because D^+X always exists at the intermediate state. Namely the change in the concentration of D^0X which corresponds to the change in PL intensity related to D^0X is surely affected by the change in the concentration of D^+X (the change in PL intensity of D^+X). From Figs. 12 and 19, it is shown that the ODCR signal obtained from D^0X as a function of magnetic field is different from that obtained from D^+X. This fact means that the change in PL intensity of D^0X is independent of that for D^+X. Thus, it is difficult to consider that the formation process of Eq. (22) is dominant.

Suppose that the formation process of Eq. (21) is dominant, the change in PL intensity of D^0X ought to be independent of the change in PL intensity of free exciton, because no free exciton exists at the intermediate state in this process. Accordingly it is hardly possible that the ODCR signal for D^0X is similar to the ODCR signal for free exciton.

If the formation process of Eq. (20) is dominant, the change in PL intensity of D^0X necessarily depends on the change in PL intensity of free exciton, because in this case free exciton always exists at the intimidate state. This suggests that the ODCR line shape of D^0X and free exciton obtained as a function of magnetic field should resemble each other and experimental results support the above argument. Thus, it is concluded that the formation process described by Eq. (20) is dominant for the formation process related to D^0X.

Formation process for neutral acceptor bound exciton, A^0X

In the next place the formation process of A^0X is considered . From Figs. 10 and 18, it is shown that the ODCR signal obtained from A^0X line as a function of magnetic field and that from X-LO resemble each other. As in the case of D^0X, there possibly exist three types of the formation process for A^0X.

$$A^0 + e^- + h^+ \quad \longrightarrow \quad A^0 + X \longrightarrow (A^0X), \tag{23}$$

$$A^0 + e^- + h^+ \longrightarrow (A^-X) + h^+ \longrightarrow (A^0X), \tag{24}$$

$$A^0 + e^- + h^+ \longrightarrow A^+ + e^- \longrightarrow (A^0X), \tag{25}$$

where A^0, A^-X and A^+ are neutral acceptor, ionized acceptor bound exciton and acceptor with an additional hole, respectively. The formation process described by Eq. (23) means that an electron and a hole first of all form themselves into a free exciton and then the free exciton is captured by a neutral acceptor. The formation process of Eq. (24) means that an electron and a neutral acceptor form into an ionized acceptor bound exciton and then a hole is captured by the ionized acceptor bound exciton. The formation process of Eq. (25) means that a hole and a neutral acceptor form into A^+ state and then an electron is captured by A^+.

The PL peak due to ionized acceptor bound exciton A^-X has not been observed in the present PL measurements, which implies that the formation process of Eq. (24) is not dominant. If the formation process of Eq. (25) is dominant, it is hardly understood that the line shape of the ODCR signal obtained from A^0X line as a function of magnetic field and that from X-LO line exceedingly resemble each other. If the formation process of Eq. (23) is dominant, it makes a point that the change in the concentration of free exciton (the change in PL intensity due to free exciton) should coincide with the change in the concentration of A^0X (the change in PL intensity due to A^0X). This requests that the line shapes of the ODCR signal obtained from A^0X line as a function of magnetic field and that from the X-LO line ought to resemble each other and experimental results are like that. Thus, it is concluded that Eq. (23) describes the dominant formation process for A^0X.

Formation process for ionized donor bound exciton, D^+X

On referring to Figs. 12 and 19, one notes that the line shape of ODCR signal obtained from D^+X is different from that from X-LO. The results from D^+X are in contrast to the results from D^0X and A^0X. It is considered that there are two types of D^+X formation

process.

$$D^+ + e^- + h^+ \longrightarrow D^+ + X \longrightarrow (D^+X), \tag{26}$$

$$D^0 + h^+ \longrightarrow (D^+X), \tag{27}$$

where D^+ is ionized donor. The formation process of Eq. (26) represents that a free exciton is captured by ionized donor after an electron and a hole form into a free exciton. The formation process of Eq. (27), on the other hand, represents that a hole is captured by D^0 and then they form into D^+X.

If the formation process followed by Eq. (26) is dominant, the change in the concentration of D^+X (the change in PL intensity of D^+X) must reflect the change in the concentration of free exciton (the change in PL intensity of free exciton). Thus, the change in PL intensity of D^+X needs to indicate the same behavior as that of X-LO. However, the line shapes of ODCR obtained from D^+X line and that from X-LO as a function of magnetic field are considerably different. Thus, it is concluded that the dominant process is described by the Eq. (27).

Summary

Dynamical properties for the formation mechanism in excitonic system are investigated through the ODCR measurements as a function of magnetic field. It is made clear that the dominant formation process is described by Eq. (20) for neural donor bound exciton (D^0X). The dominant formation process is given by Eq. (23) for neutral acceptor bound exciton (A^0X). As for the formation process of ionized donor bound exciton (D^+X), it is concluded that the dominant formation process is Eq. (27).

5.1.2 ODCR mechanism

Monte Carlo simulation

From Table 3, it is recognized that the sign of the ODCR signals for CdTe surely depends on the mobility of the sample, i.e., whether the ordinary CR is sharp or broad.

Here let us discuss the relation between the sign of the ODCR signal and the mobility of the sample based on the results of Monte Carlo simulation for CdTe.

Under the photoexcitation condition, the electron scattering is dominated by neutral donors at low temperatures. The neutral donor concentration can be estimated from Eq. (16). The relation between the scattering probability, P_{imp}, and the scattering time, τ, is

$$\tau = 1/P_{imp}. \tag{28}$$

Since the scattering time was obtained from the line width measurements of the CR line, the donor concentrations for #A and #P can be estimated to be $4.9\times10^{14}\mathrm{cm}^{-3}$ and $6.1\times10^{14}\mathrm{cm}^{-3}$, respectively. The donor concentrations for #B and #W, which did not show the distinct CR line, can be estimated at more than $3.2\times10^{15}\mathrm{cm}^{-3}$ and $2.9\times10^{15}\mathrm{cm}^{-3}$. The difference in donor concentration affects the mean kinetic energy of electrons under the application of dc electric field. According to Monte Carlo simulation the situation can be indicated. The details of the simulation are shown in the section of Monte Carlo simulation.

In Fig. 61 the mean kinetic energies of electrons with different donor concentrations, $5.0\times10^{14}\mathrm{cm}^{-3}$ and $3.0\times10^{15}\mathrm{cm}^{-3}$, are plotted against the applied dc electric field. It seems that the microwave power at the present experimental condition corresponds to the order of several ten V/cm of dc electric field [12][25]. From Fig. 61, one can note that the mean kinetic energy of the electron becomes lower with increasing concentration of neutral donors at the same electric field, i.e. the mean kinetic energy of electrons for #B and #W is lower than that for #A and #P at the same microwave power level.

The binding energy of the donor in CdTe is 13meV. The mean kinetic energy of electrons at 4.2K in a sample with the donor concentration of $5.0\times10^{14}\mathrm{cm}^{-3}$ is just 7meV even under 30V/cm dc electric field. Thus, it seems that the impact ionization for donors hardly occurs under such a situation. However, all electrons have not necessarily the mean kinetic energy, and a few electrons are sure to have larger energy than the mean kinetic energy. The energy distribution of the electronic system in a sample with the donor

concentration of 5.0×10^{14}cm^{-3} under 30V/cm dc electric field is shown in Fig. 62. As is obvious from the figure, there exist some electrons with the energy more than 13meV. This means that the impact ionization of the donor electrons possibly occurs in #A and #P under CR. However, it is found from Fig. 63 that the impact ionization of the donor electrons hardly occurs for the sample with higher donor concentration as #B and #W under CR. The difference in the donor concentration, thus, affects definitely the sign of the ODCR signals.

Rate equations for ODCR in CdTe

The excitonic system in CdTe is expressed by the rate equation. The system composed of free exciton, D^0X and A^0X is discussed. D^+X can be excluded from the system, because its formation process is not related to the free exciton as mentioned above. The energy diagram for free electron, free exciton, neutral donor bound exciton and neutral acceptor bound exciton is shown in Fig. 64. From Fig. 64, it is shown that the increase and decrease in free exciton, neutral donor bound exciton and neutral acceptor bound exciton concentrations are connected with each other.

The rate equation for the neutral donor bound exciton is given by

$$\frac{dn_d}{dt} = B_1(N_D - n_d)n_{ex} - A_1 n_d - C_1 n_e n_d - \frac{n_d}{\tau_d}, \tag{29}$$

where n_e, n_d, N_D, n_{ex} and τ_d are conduction electron concentration, neutral donor bound exciton concentration, total donor concentration, free exciton concentration and the life-time of neutral donor bound exciton, respectively.

The rate equation for the neutral acceptor bound exciton is given by

$$\frac{dn_a}{dt} = B_2(N_A - n_a)n_{ex} - A_2 n_a - C_2 n_e n_a - \frac{n_a}{\tau_a}, \tag{30}$$

where n_a, N_A and τ_a are neutral acceptor bound exciton concentration, total acceptor concentration and the lifetime of neutral acceptor bound exciton.

The rate equation for free exciton is given by

$$\frac{dn_{ex}}{dt} = B_3 n_e n_h - A_3 n_{ex} - C_3 n_e n_{ex} - \frac{n_{ex}}{\tau_{ex}}$$

$$-B_1(N_D - n_d)n_{ex} + A_1 n_d + C_1 n_e n_d$$
$$-B_2(N_A - n_a)n_{ex} + A_2 n_a + C_2 n_e n_a, \tag{31}$$

where n_h and τ_{ex} are hole concentration and the life time of free exciton. A_i, B_i and C_i are the thermal dissociation, the thermal capture and the impact ionization coefficients, respectively. Here i is 1, 2 and 3.

From the excitation intensity dependence of PL, it is shown that the PL intensity for bound exciton shows no saturation under the present experimental condition for ODCR. This means that total neutral donor/acceptor concentration is sufficiently higher than the neutral donor/acceptor bound exciton concentration. In this case, we may approximate with the following equations.

$$(N_D - n_d)n_{ex} \approx N_D n_{ex}, \tag{32}$$

$$(N_A - n_a)n_{ex} \approx N_A n_{ex}. \tag{33}$$

Thus, Eqs. (29), (30) and (31) are approximated by

$$\frac{dn_d}{dt} = B_1 N_D n_{ex} - A_1 n_d - C_1 n_e n_d - \frac{n_d}{\tau_d}, \tag{34}$$
$$\frac{dn_a}{dt} = B_2 N_A n_{ex} - A_2 n_a - C_2 n_e n_a - \frac{n_a}{\tau_a}, \tag{35}$$
$$\frac{dn_{ex}}{dt} = B_3 n_e n_h - A_3 n_{ex} - C_3 n_e n_{ex} - \frac{n_{ex}}{\tau_{ex}}$$
$$-B_1 N_D n_{ex} + A_1 n_d + C_1 n_e n_d$$
$$-B_2 N_A n_{ex} + A_2 n_a + C_2 n_e n_a. \tag{36}$$

Sign of ODCR signal (DA emission in #A and #P)

There are three types of factor to determine the sign of the ODCR signals as mentioned above. As the resonant formation of free exciton was not observed in CdTe, the reduction in the capture rate for ionized donor and free exciton and the impact ionization determine the sign of ODCR signals. In general B_i decreases monotonously with increasing of the kinetic energy of electrons [40]. Since the impact ionization should not occur until

the kinetic energy of electrons exceeds the binding energy of each radiative object, it seems that C_i increases rapidly when the kinetic energy of electrons surpasses a certain magnitude. However, since electrons have energy distribution, it seems that C_i is smooth function.

From the results of Monte Carlo simulation, it is noted that hot electrons give rise to the impact ionization of neutral donors in #A and #P under the CR condition. The impact ionization causes the increase in conduction electrons and the decrease in neutral donors. In addition, the capture rate of ionized donors decreases under CR condition because of the increase in the kinetic energy of electrons. Consequently the PL intensity for DA recombination decreases. It agrees with the observation for the ODCR experiments (see Figs. 7 and 16). In addition, it is noteworthy that neutral acceptors inversely increase because of reduction in DA recombination.

Sign of ODCR signal (Free exciton, D^0X and A^0X in #A and #P)

In a steady state condition, i.e. when $dn_d/dt = dn_a/dt = dn_{ex}/dt = 0$, from Eq. (36) we obtain for n_{ex}

$$n_{ex} = \frac{B_3 n_e n_h - n_d/\tau_d - n_a/\tau_a}{A_3 + C_3 n_e + 1/\tau_{ex}}, \tag{37}$$

where we may introduce α

$$\alpha = \frac{1}{A_3 + C_3 n_e + 1/\tau_{ex}}. \tag{38}$$

n_{ex} is expressed by

$$n_{ex} = \alpha(B_3 n_e n_h - n_d/\tau_d - n_a/\tau_a). \tag{39}$$

Hot electrons can give rise to the impact ionization for free excitons. If free excitons often obtain the kinetic energy from hot electrons, the temperature of free excitonic system will increase under CR condition, which causes the energy distribution of free excitons move to the higher energy. As a result, it is expected that the ODCR signal for free exciton line should become a derivative type of the original PL line [18]. Such a signal, however,

has not been observed in the present experiments. Accordingly, it can be concluded that the interaction of hot electrons with free excitons is not so strong and hot electrons rarely make to increase in the kinetic energy of free exciton. The change in A_3, $C_3 n_e$ and τ_{ex} is small under CR condition, therefore α is considered to be constant under CR condition. we can easily solve Eqs. (35) and (36) as follows:

$$n_d = \frac{B_1 N_D}{A_1 + C_1 n_e + 1/\tau_d} n_{ex}, \tag{40}$$

$$n_a = \frac{B_2 N_A}{A_2 + C_2 n_e + 1/\tau_a} n_{ex}, \tag{41}$$

where we may introduce β and γ

$$\beta = \frac{B_1 N_D}{A_1 + C_1 n_e + 1/\tau_d}, \tag{42}$$

$$\gamma = \frac{B_2 N_A}{A_2 + C_2 n_e + 1/\tau_a}. \tag{43}$$

n_d and n_a are expressed by

$$n_d = \beta n_{ex}, \tag{44}$$

$$n_a = \gamma n_{ex}. \tag{45}$$

Hence from Eqs. (39), (44) and (45), n_{ex} is given by

$$n_{ex} = \frac{B_3 n_e n_h}{1/\alpha + \beta/\tau_d + \gamma/\tau_a}, \tag{46}$$

where the numerator means the interaction between free excitons and conduction electrons. The term β/τ_d means the interaction free excitons and neutral donor bound excitons. The term γ/τ_a means the interaction between free excitons and neutral acceptor bound excitons.

Let us consider the change in n_d, n_a and n_{ex} under CR condition. Since the kinetic energy of free excitons scarcely changes under CR condition, it is assumed that B_1 and B_2 are constant. In addition, A_1, A_2, τ_d and τ_a are also constant at a fixed temperature.

N_D decreases under CR condition because of the reduction in capture rate of ionized

donors and impact ionization of neutral donors as above mentioned. $C_1 n_e$ increases under CR condition because of the increase in kinetic energy of electrons. Thus, from Eq. (42), it is shown that the change in N_D and $C_1 n_e$ under CR condition causes the decrease in β.

N_A increases under CR condition because of the reduction of DA recombination, which causes the increase in γ. $C_2 n_e$ increase under the CR condition, which causes the decrease in γ. Thus, from Eq. (43), it is shown that the competition between the change in N_A and $C_2 n_e$ determines the increase or decrease in γ. The increase and decrease in γ depends on the experimental condition. The sign of A^0X is more likely to be positive than that of D^0X because β always decreases, but γ can increase.

From the analysis of the ODCR signal for the DA recombination, it is shown that conduction electrons n_e increase under CR condition. In addition, B_3 decrease under CR condition because of the reduction in capture rate of free exciton.

Eventually the competition of the change in β, γ, n_e and B_3 determines the sign of the ODCR signals for excitonic system.

If the interaction between free exciton and conduction electron is smaller than the interaction between free exciton and bound exciton, which means that the change in B_3 and n_e is small and the change in β and γ is dominant, the total concentrations of n_d, n_a and n_{ex} scarcely change under CR condition. In this case, if a certain state (e.g. free exciton) increases, the other state (e.g. bound exciton) must decrease. However, all of the ODCR signals for excitonic system are positive. Hence the dominant factor for ODCR is the interaction between free exciton and conduction electron. The competition between the change in n_e and B_3 determines the sign of the ODCR signal. The ODCR signal for excitonic system is positive, which means that the increase in the concentration of excitonic system. Namely the dominant factor for ODCR signal must be the change in n_e which causes the increase in excitonic system concentration.

When the increase in n_e is dominant factor for the ODCR for excitonic system, from Eq. (46) it is shown that free exciton increases under CR condition. From Eq. (42)

and Eq. (43), it is shown that neutral donor bound exciton and neutral acceptor bound exciton increase when the increase in n_e is dominant.

n_e increases under CR condition because of the impact ionization of neutral donors, which causes the increase in free exciton. The increase in free exciton causes the increase in D^0X and A^0X. That is the scenario for the ODCR in #A and #P.

Sign of ODCR signals (D^+X in #A and #P)

Since the concentration of the neutral donors, D^0, decrease by the impact ionization due to electrons, D^+X decreases (see Eq. (27)). If the process of the formation for D^+X is dominated by Eq. (26), the concentration of D^+X should increase under CR condition because of increase in D^+ by the impact ionization. The experimental result for the ODCR related to D^+X is negative, which confirms that the dominant formation process for D^+X is given by Eq. (27).

Sign of ODCR signal (DA emission in #B and #W)

From the results of Mote Carlo simulation, it is shown that in #B and #W the impact ionization for neutral donors rarely occurs under CR condition. Thus, the reduction in the capture rate should be a dominant origin of the ODCR for the DA line. The neutral donors decrease under CR condition because of the reduction of the capture rate and subsequent decrease of the DA line (see Figs. 23 and 30).

A radiative and a nonradiative processes always compete with each other. The competition is affected by the change in the energy distribution of electrons. The reduction of the capture rate for electrons causes the increase in the number of electrons which are not trapped by the radiative centers. During their stay in the conduction band, they happen to meet nonradiative recombination centers. Hence the nonradiative recombination paths are enhanced in #B and #W. Actually DeLong et al. reported that the enhancement of nonradiative recombination process under microwave irradiation to the GaAs and InP samples [12]. Thus, all of the ODCR signal can be negative. The enhancement also takes

place in #A and #P. However, a number of electron ionized from neutral donors under CR condition are provided to excitonic system in #A and #P. It is different from the case of #B and #W. It is noteworthy that the impact ionization of neutral donors does not take place in #B and #W, therefore electrons are not provided to excitonic system.

Sign of ODCR (free exciton, D^0X and A^0X in #B and #W)

Once more Eqs. (44), (45) and (46) will be examined closely. In the case of #B and #W, under CR condition n_e is considered to be constant because impact ionization of neutral donors does not take place. It is different from the case of #A and #P. The competition of β, γ and B_3 determines the sign of the ODCR signals for excitonic system.

If the dominant factor is the change in B_3, the ODCR signals for excitonic system can be reasonably explained. B_3 decreases under CR condition because of the increase in kinetic energy of electrons. If the B_3 is dominant factor, which means that the change in B_3 is larger than that in β and γ, free exciton decreases under CR condition from Eq. (46). From Eq. (44) and (45), it is shown that the decrease in B_3 causes neutral donor bound exciton and neutral acceptor bound exciton decrease.

Namely free exciton decreases under CR condition because of the reduction in capture rate of free exciton. The decrease in free exciton causes the decrease in neutral donor bound exciton and neutral acceptor bound exciton. This is the scenario for the ODCR signals for excitonic system in #B and #W.

5.2 ZnSe

5.2.1 Formation process in exciton system

In a next step the formation process of the excitonic system in ZnSe is considered. Free exciton FE, neutral donor bound exciton I_2, neutral acceptor bound exciton I_1 and deep acceptor bound exciton I_1^d were observed in the PL measurements. Thus, One needs to consider FE, I_2, I_1 and I_1^d for the excitonic system.

Formation process for neutral donor bound exciton, I_2

The ODCR signals for I_2 line explored as a function of the magnetic field were observed in all the samples. There are three types of the formation process for I_2 line, same as the D^0X in CdTe. The formation process given by Eq. (22) can be neglected because D^+X lines in ZnSe have not been observed in PL measurements [41]. It is peculiar that the ODCR signal for I_2 line obtained as a function of the magnetic field is quite similar to that for FE line. When the ODCR signal for FE line obtained as a function of the magnetic field shows a prominent shoulder arising from the free exciton resonant formation, the ODCR signal for I_2 line also has a shoulder (#9, #N and #8). On the other hand, when the ODCR signal for FE line obtained as a function of the magnetic field does not show a prominent shoulder at higher magnetic field, the ODCR signal for I_2 line does not have any shoulder (#1). This fact indicates that the dominant formation process for I_2 line is described by Eq. (20), as described in the discussion about D^0X in CdTe.

Formation process for neutral acceptor bound exciton, I_1

The neutral acceptor bound exciton I_1 line is observed in #9, #N and #1. It is possibly considered that there are three types of the formation processes for I_1, same as A^0X in CdTe. The PL experiments reveal that A^-X almost never exists in ZnSe. Therefore the formation process followed by Eq. (24) can be excluded. The ODCR signal for FE consists of negative and positive signals, but the ODCR signal for I_1 consists of two positive signals. However, the ODCR spectrum for I_1 line as a function of magnetic field

is quite similar to that for FE except for the sign of the signal. As in the case of I_2 line, when the ODCR signal for FE line as a function of magnetic field has a shoulder due to the free exciton resonant formation, the ODCR signal for I_1 line has a shoulder (#9, #N). On the other hand, when the ODCR signal for FE line as a function of magnetic field does not have prominent shoulder, the ODCR signal for I_1 line does not have shoulder (#1). As the shoulder for I_1 line decreases with decreasing microwave power as in the case of the ODCR signal for FE, the structure is composed by the resonant formation of free exciton. This shows that the dominant formation process for I_1 is described by Eq. (23). The difference of the sign of the ODCR signal between FE and I_1 lines will be discussed later.

Formation process for neutral acceptor bound exciton, I_1^d

The ODCR signal for deep acceptor bound exciton I_1^d as a function of magnetic field is observed in #9, #1 and #8. The ODCR signals for I_1^d are positive and their line shapes are rather complicated. There are three types of the formation process for I_1^d, same as A^0X in CdTe. The formation process of Eq. (24) can be neglected because the A^-X line is hardly observed in PL experiments for ZnSe. The ODCR signal for I_1^d line is quite different from that for FE line. This experimental observation indicates that the formation process of I_1^d is different from one for I_1. It was made clear that the dominant formation process is described by Eq. (25). Tomaru et al. have obtained the same conclusion about I_1^d formation process [14].

Summary

The formation process for the excitonic system in ZnSe is explained by the ODCR signal as a function of magnetic field. It is made clear that the formation process for I_2 is Eq. (20). The formation process of I_1 is Eq. (23). The formation process for I_1^d is Eq. (25).

5.2.2 ODCR mechanism

The clear CR peak was observed in all ZnSe samples employed in this work. Assuming that the electron scattering due to neutral donors is dominant at low temperatures, the donor concentration can be estimated from the line width of CR peak, as analogous to the case of CdTe. The estimated donor concentration of ZnSe is $4.7 \sim 8.5\times10^{14}\mathrm{cm}^{-3}$. The Monte Carlo simulation was carried out with donor concentration of $8.5\times10^{14}\mathrm{cm}^{-3}$.

Figure 65 shows the energy distribution of electrons under the application of 30V/cm dc electric field. It is remarkable that the binding energy of usual shallow donors is 26meV. From Fig. 65, one notes that there are electrons which have kinetic energy above 26meV to some extent.

Sign of ODCR (R and Q series)

The first detailed studies of R and Q series were performed by Dean et al. [42]. They observed R_0, Q_0 and their LO-phonon replicas at liquid helium temperature. They reported that R and Q series come from the DA recombination emission, and that R_0 had the discrete structure arising from DA pair lines. Furthermore, the eA transition associated with Q_0, which a conduction electron recombines with a hole bound by an acceptor, was observed at higher temperatures. However, the eA transition related to R_0 was not observed. It is a strange phenomena.

Bhargava et al. have investigated the origin of R and Q series [43]. They concluded as follows: Both of the impurities associated with R_0 and Q_0 emission lines are the same acceptor, $\mathrm{Li_{Zn}}$. The shallow donor associated with R_0 is interstitial $\mathrm{Li_{int}}$ atom and one associated with Q_0 is substitutional group III donor $\mathrm{III_{Zn}}$. They think the binding energy of shallow donors, $\mathrm{Li_{int}}$, and $\mathrm{III_{Zn}}$, is close to each other (26mev). Why does the emission peak, R_0, differ from the line related to Q_0? The transition energy for DA emission E_{DA} is given by

$$E_{DA} = E_g - (E_D + E_A) + \frac{e^2}{4\pi\varepsilon_0\varepsilon r}, \tag{47}$$

where E_g is the band gap energy, E_D the donor binding energy, E_A the acceptor binding energy and r the distance between the donor and the acceptor. Since Li_{int} atom easily migrates even at 200C°, a certain correlation, as called preferential pairing, in the distribution of donors and acceptors comes into existence in a sample. Therefore, the Coulomb energy term between a donor and an acceptor is enhanced. Eventually the peak positions of DA transitions associated with R_0 shift to higher energy. Since the acceptors involved in the DA transitions concerned with R and Q series are the same ones, unique eA transitions are observed. This model proposed by Bhargava et al. is generally accepted now. However, the origin of DA emission lines is still controversial. Figure 66 shows the model proposed by Bhargava et al.

Emission lines for the R and Q series were observed in #9, #N and #1. I_1 line due to neutral acceptor bound exciton was also observed in them. These lines were not observed in #8, which did not show I_1 peak as well (see Fig. 55). As a strong FE line is observed in #8, it is concluded that there are few neutral shallow acceptors in this sample. If an above conjecture is pertinent, one is convinced of the experimental fact that the DA emission line is hardly observed in #8. This supports that the R and Q series are a kind of DA emission. The reason why neutral shallow acceptors are not contained in #8 should originate in the heat treatment effect of the sample, i.e., #8 was annealed in Zn atmosphere. It is noted that the annealing reduces the concentration of shallow acceptors, and from the experimental point of view the broad peak at 2.4eV appears. The details of the annealing effect have not been made clear yet.

From the results of ODCR, it is found that the ODCR signals for R series are negative and the ODCR signals for Q series are positive. It conflicts with the model proposed by Bhargava et al.. The probability of the impact ionization related to neutral donors associated with R and Q series should be exactly alike because their model said the donor binding energy associated with R and Q is nearly equal to 26meV. If their model is true, both of the ODCR signals for R and Q series should be negative from Monte Carlo sim-

ulation.

Isshiki et al. have proposed another model [44]. Through the PL measurements, they have studied the DA emission lines associated with R and Q series in detail. They concluded that the neutral acceptors associated with R and Q series are the common shallow acceptors, Li_{Z_n}, and the related donors are Ga_{Z_n} for Q emission and Li_{int} for R emission. In addition, they determined the donor binding energy of Li_{int} as 15meV. Ga_{Z_n} is the usual shallow donor, therefore the binding energy is 27meV. Figure 66 shows the model proposed by Isshiki et al.. From Fig. 66, it is shown that the unique eA transitions associated with R and Q series are observed.

Godlewski et al. observed the ODCR experiment and reported as follows [45]: For two overlapping DA transitions due to two donors with different binding energies, a reverse response of PL to carrier heating was observed in InGaAs. Hot carriers reach first the energy required for impact ionization of the shallower of the two donors, therefore the higher energy part of the DA bands is reduced and the lower energy part is enhanced because more carriers will recombine now via the deeper of the two donors.

The ODCR signal obtained from R and Q series shows the similar behavior reported by Godlewski et al. Namely DA emission associated with R series which is in higher energy region decreased and DA emission associated with Q series which is in lower energy region increased under CR condition. If the model proposed by Isshiki et al. is true, one can explain the results of the ODCR signals for R and Q series through the results reported by Godlewski et al. Hence hot electrons reach first the energy required for impact ionization of shallower donor Li_{int}, therefore the ODCR signal for R series is negative. The electrons released from Li_{int} donors are excited into the conduction band. Most of the conduction electrons excited from R series are inclined to recombine via the deeper donors Ga_{Z_n}, which causes the increase in the Q emission line. The ODCR experiments revealed that the model proposed by Isshiki et al. is reliable. Thus Isshiki et al.'s model is adopted here.

Although the decrease in R series is small, the increase in Q series is large. It seems strange. Neumark work gave indications of order magnitude differences in the transition probability between Li_{int} and substitutional donor [46]. Namely, the transition probability of R series is much lower than that of Q series. It may be the origin of the differences in the ODCR signal intensity between R and Q series.

Thus in the case of #9. #N and #1, most of the conduction electrons increased by impact ionization of Li_{int} incline to recombine via Q emission, therefore electrons increased by impact ionization of Li_{int} are not provided to excitonic system. It is different from the case of #A and #P CdTe samples. In the case of #A and #P, the conduction electrons increased by impact ionization of neutral donors come into excitonic system.

The impact ionization for neutral donors also takes place in #8. The positive ODCR signal for the broad peak at 2.4eV is observed in #8. It seems that most of electrons excited from shallow donors bring forth the broad peak at 2.4eV. Thus electrons increased by impact ionization of neutral donors are not provided to excitonic system, as in the case of #9. #N and #1.

Sign of ODCR (FE and I_1 in #8)

Since the formation process for I_1^d includes no free exciton at intermediate state, one may take into account the system composed of FE and I_2 in #8. In this case, the rate equations correspond to ones with $\gamma = 0$ for the system in CdTe. The solutions for the rate equations are given by

$$n_d = \beta n_{ex} \tag{48}$$

$$n_{ex} = \frac{B_3 n_e n_h}{1/\alpha + \beta/\tau_d}. \tag{49}$$

Let us consider the variation in n_{ex} and n_d under CR condition. The ODCR signal for FE did not show the line in the shape of the derivative type, which means that α is considered to be constant, as in the case of CdTe. Thus the competition of n_e, B_3 and β determines the sign of ODCR signals. From the results of DA emission lines, it is shown

that the electrons excited by the impact ionization for R series hardly contribute to the formation of free excitons. Thus n_e is considered to be constant and the competition between B_3 and β determines the sign of the ODCR signals for FE and I_2.

The numerator in Eq. (49) represents the interaction between free excitons and conduction electrons. The term β/τ_d in Eq. (49) represents the interaction between free exciton and neutral donor bound exciton. If the change in the numerator is small, which means the change in B_3 is smaller than that in β, the total concentrations of n_{ex} and n_d are almost constant. In this case, if a certain state (e.g. free exciton) decreases under CR condition, the other state (e.g. neutral donor bound exciton) must increase. However, it is found that both of the ODCR signals for FE and I_2 are negative. Thus it is concluded that the change in B_3 is dominant factor for the ODCR. It is obvious that the reduction in the capture rate of free exciton under CR condition causes the decrease in free exciton concentration. As a result, the decrease in free exciton concentration causes the decrease in neutral donor bound exciton concentration. This is the scenario for the ODCR for excitonic system in #8

Sign of ODCR (FE, I_1 and I_2 in #9, #N and #1)

Since the formation process for I_1^d has no connection with free exciton at intermediate state, one may take into account only the system composed of FE, I_1 and I_2. In this case, the rate equations for the system in ZnSe and in CdTe are described by the same form. From the results of DA emission lines, it is shown that the electrons excited by the impact ionization for R series hardly contribute to the formation of free excitons. Thus n_e is considered to be constant similar to the case of #8.

From Eqs. (44), (45) and (46), the competition among B_3, β and γ determines the sign of the ODCR signals, as in the case of CdTe. From the analysis of experimental results for #8, it is found that the change in β is smaller than that in B_3. Accordingly the change in β is ignored hereafter. Thus the competition between B_3 and γ determines the sign of the ODCR signals in #9, #N and #1.

The numerator in Eq. (46) represents the interaction between free excitons and conduction electrons. The term γ/τ_a in Eq. (46) represents the interaction between free exciton and neutral acceptor bound exciton. If the change in B_3 is dominant, which means that the change in γ is smaller than that in B_3, the concentrations of free exciton and bound exciton decrease as in the case of #8. Namely the decrease in free exciton due to the reduction of the capture rate causes the decrease in bound exciton. However, the ODCR signal for FE is negative, while the ODCR signal for I_1 is positive. Therefore the change in B_3 is not a dominant factor for the ODCR.

In this case it is concluded that the change in γ must be a dominant factor for the ODCR. γ can sometimes increase and sometimes decrease as mentioned above. In order to explain the positive ODCR signal for for I_1, however, γ must increase under CR condition. In such circumstance that γ increases, it is shown that the increase in N_A is larger than the decrease in $C_2 n_e$ as is evident from Eq. (43). If the dominant factor for the ODCR is the increase in neutral acceptor concentration, γ should increases, which causes the increase in neutral acceptor bound exciton. In this case, free exciton decreases due to the increase in γ and the decrease in B_3. Namely the increase in neutral acceptor under CR condition causes the increase in neutral acceptor bound exciton. The increase in neutral acceptor bound exciton and the reduction in the capture rate of free exciton cause the decrease in free exciton. Then, the decrease in free exciton causes the decrease in neutral donor bound exciton. This is the reason why the sign of the ODCR signal for FE is different from that for I_1. It is noteworthy that the reduction in free exciton is due to the change in γ and B_3 in this case. However, the reduction in free exciton is due to the change in B_3 in #8. Therefore, the line shape of the ODCR signal for FE as a function of magnetic field in #8 may be different from that in the other samples (see Fig. 57, Fig. 37, Fig. 44 and Fig. 50).

Why does the increase in neutral acceptor concentration under CR condition take place? The mechanism is not clear yet. The origin may be due to the decrease in DA transitions.

It seems that DA transitions increase under CR condition because the positive ODCR signal for Q series is strong. However, the transition probability of R series is smaller than that of Q series by order of magnitude as mentioned above. Hence, the decrease in the number of R series may be larger than the increase in the number of Q series under CR condition. This means that the decrease in total DA transition under CR condition. Since the change in neutral donor concentration causes the change in DA transition, the decrease in DA transition causes the increase in neutral acceptor. The decrease in total DA transition may be due to the enhancement of nonradiative recombination. Further study of the mechanism is needed.

Sign of ODCR ($\mathbf{I_1^d}$)

The origin of the ODCR signal for I_1^d is not clear. One model is as follows: A small part of electrons, which are excited from the neutral donors associated with R series by impact ionization, recombines via excitonic system. It seems that the electrons prefer to recombine via the deeper excitonic system, as in the case of DA emission line. Thus, I_1^d increases under CR condition.

6 Conclusion

ODCR, CR and PL measurements on high quality bulk CdTe and ZnSe samples were carried out. The results are as follows:

- The line shape of the ODCR signal obtained as a function of the magnetic field certainly depends on the origin of each PL line. Consequently, the formation processes in excitonic system in CdTe and ZnSe are determined through the analysis of the difference in the line shape of the ODCR signals as a function of the magnetic field. The formation process of neutral donor bound exciton in CdTe and ZnSe is shown by Eq. (20) which means that first of all an electron and a hole form themselves into a free exciton and then the free exciton is captured by a neutral donor. The formation processes of neutral acceptor bound exciton in CdTe and ZnSe are given by Eq. (23) which means that an electron and a hole first of all form themselves into a free exciton and then the free exciton is captured by a neutral acceptor. The formation process of ionized donor bound exciton in CdTe is described by Eq. (27) which means that a hole is captured by a neutral donor and then they form into an ionized donor bound exciton. The formation process of deep acceptor bound exciton in ZnSe is given by Eq. (25) which means that a hole and a neutral acceptor form into A^+ state and then an electron is captured by A^+.

- The sign of the ODCR signals of CdTe depends on whether the CR peak is sharp or broad. The line width of the CR peak is connected with the scattering relaxation time of electrons. Under photoexcitation condition at low temperatures, the relaxation time of the electron is dominated by neutral donors. The mean energy and energy distribution of electrons were calculated by means of Monte Carlo simulation under the condition of different donor concentrations. This calculation reveals that the energy distribution depends on the donor concentration, and the difference of energy distribution affects the competition between the reduction in the capture

rate and the impact ionization, which determines the sign of the ODCR signals.

- The increase and the decrease in PL intensity take place under CR condition. It is noted that the argument based on the rate equations is an effective way to analyze the rise and fall of PL intensity for excitonic system under CR condition. From the analysis of rate equations, the mechanism of the ODCR in CdTe could be made clear.

Acknowledgements

I would like to express my gratefulness for Professor T. Ohyama for his supporting my study and encouragement.

I am also grateful to Professor H. Nakata, Dr. K. Fujii, Dr. H. Kobori and the other members of Ohyama laboratory for their kind help in suggestion and discussion.

I am grateful to Professor M. Isshiki, Sumitomo Electric Industries, Ltd. and Nippon Mining Co., Ltd. for providing high quality samples, and indebted to Asahi Woodtech, Ltd., for the award of a scholarship.

I am especially thankful to my parents and sisters for supporting me financially and mentally for a long time.

References

[1] J. Dorfmann, Dokl. Acad. Sci. U.S.S.R. **81**, 765 (1951).

[2] R. B. Dingle, Proc. R. Soc. London. Ser. A **212**, 38 (1952).

[3] W. Shockley, Phys. Rev. **90**, 491 (1953).

[4] G. Dresselhaus, A. F. Kip and C. Kittel, Phys. Rev. **98**, 368 (1955).

[5] B. Lax, H. J. Zeiger, R. N. Dexter and E. S. Rosenblum, Phys. Rev. **93**, 1418 (1954).

[6] P. G. Baranov, Yu. P. Veshchunov, R. A. Zhitnikov, N. G. Romanov and Yu. G. Shreter, JETP Lett. **26**, 249 (1977).

[7] T. Tomaru, T. Ohyama and E. Otsuka, J. Phys. Soc. Jpn. **61**, 1798 (1992).

[8] T. Tomaru, T. Ohyama and E. Otsuka, Phys, Rev. B **44**, 10622 (1991).

[9] H. Nakata, T. Iwao and T. Ohyama, Jpn. J. Appl. Phys. **36**, L209 (1997).

[10] N. T. Son, O. Kordina, A. O. Konstantinov, W. M. Chen, E. Sörmann, B. Monemar and E. Janzén, Appl. Phys. Lett. **65**, 3209 (1994).

[11] N. T. Son, W. M. Chen, O. Kordina, A. O. Konstantinov, B. Monemar, E. Janzén, D. M. Hofman, D. Volm, M. Drechsler and B. K. Meyer, Appl. Phys. Lett. **66**, 1074 (1995).

[12] M .C. DeLong, W. D. Ohlsen, I. Viohl, X. Yin, P. C. Taylor, D. Sengupta, G. E. Stillmann, J. M. Olson and W. A. Harrison, Phys. Rev. B **48**, 5157 (1993).

[13] J. X. Shen, Y. Oka, W. Ossau, G. Landwehr, K. -J. Friedland, R. Hey, K. Ploog and G. Weimann, Solid State Commun. **106**, 495 (1998).

[14] T. Tomaru, T. Ohyama, E. Otsuka, M. Isshiki and K. Igaki, Phys. Rev. B **46**, 9390 (1992).

[15] R. Jäger-Waldau, N. Stücheli, M. Braun, M. Lux Steiner, E. Bucher, R. Tenne, H. Flaisher, W. Kerfin, R. Braun and W. Koschel, J. Appl. Phys. **64**, 2601 (1988).

[16] M. Soltani, M. Certier, R. Evrard and E. Kartheuser, J. Appl. Phys. **78**, 5626 (1995).

[17] H. Morkoç, S. Strite, G. B. Gao, M. E. Lin, B. Sverdlov and M. Burns, J. Appl. Phys. **76**, 1363 (1994).

[18] R. Romestain and C. Weisbuch, Phys. Rev. Lett. **45**, 2067 (1980).

[19] Le Si Dang, G. Neu, R. Romestain, Solid State Commun. **44**, 1187 (1982).

[20] T. Kurosawa, J. Phys. Soc. Jpn. Suppl. **21**, 424 (1966).

[21] P. J. Price, Proceedings of the 9th International Conference on the Physics of Semiconductors 753 (1968).

[22] H .D. Rees, J. Phys. Chem. Solids **30**, 643 (1969).

[23] W. Fawcett, D. A. Boardman and S. Swain, J. phys. Chem. Solids **31**, 1963 (1970).

[24] C. Jacoboni and L. Reggiani, Rev. Mod. phys. **55**, 645 (1983).

[25] K. Karpińska, S. Dedulewicz and M. Godlewski, Materials Sci. For. **143-147**, 681 (1994).

[26] C. Erginsoy, Phys. Rev. **79**, 1913 (1950).

[27] S. Seto, A. Tanaka and M. Kawashima, J. Aplpl. Phys. **64**, 3658 (1988).

[28] A. L. Mears and R. A. Stradling, Solid State Commun. **7**, 1267 (1969).

[29] K. J. Button, B. Lax, W. Dreybrodt and C. W. Litton, Solid State Commun. **8**, 2117 (1970).

[30] D. M. Hofmann, P. Omling, H. G. Grimmeiss, B. K. Meyer, K. W. Benz and D. Sinerius, Phys. Rev. B **45**, 6247 (1992).

[31] D. J. Leopold, J. M. Ballingall and M. L. Wroge, Appl. Phys. Lett. **49**, 1473 (1986).

[32] J. P. Chamonal, E. Molva and L. Pautrat, Solid State Commun. **43**, 801 (1982).

[33] J. Lee and N. C. Giles, J. Appl. Phys. **78**, 1191 (1995).

[34] E. Molva and Le Si Dang, Phys. Rev. B **27**, 6222 (1983).

[35] E. Molva, K. Saminadayar, J. L. Pautrat and E. Ligeon, Solid State Commun. **48**, 955 (1983).

[36] E. Molva, J. L. Pautrat K. Saminadayar, G. Milchberg and N. Magnea, Phys. Rev. B. **30**, 3344 (1984).

[37] T. Ohyama, E. Otsuka, T. Yoshida, M. Isshiki and K. Igaki, Jpn. J. Appl. Phys. **23**, L382 (1984).

[38] G. Cantwell, W. C. Harsch, H. L. Cotal, B. G. Markey, S. W. S. McKeever and J. E. Thomas, J. Appl. Phys. **71**, 2931 (1992).

[39] E. Tournié, C. Morhain, G. Neu, M. Laügt, C. Ongaretto, J. -P. Faurie, R. Triboulet and J. O. Ndap, J. Appl. Phys. **80**, 2983 (1996).

[40] T. Tomaru, Ph. D. thesis, Osaka university, (1991).

[41] M. Isshiki, T. Kyotani, K. Masumoto, W. Uchida and S. Suto, Phys. Rev. B **36**, 2568 (1987).

[42] P. J. Dean and J. L. Merz, Phys. Rev. **178**, 1310 (1969).

[43] R. N. Bhargava, R. J. Seymour, B. J. Fitzpatrick and S. P. Herko, Phys. Rev. B **20**, 2407 (1979).

[44] M. Isshiki, K. S. Park, Y. Furukawa and W. Uchida, J. Cryst. Growth **117**, 410 (1992).

[45] M. Godlewski, W. M. Chen and B. Monemar, J. Lumin. **60**&**61**, 52 (1994).

[46] G. F. Neumark, Phys. Rev. B **37**, 4778 (1988).

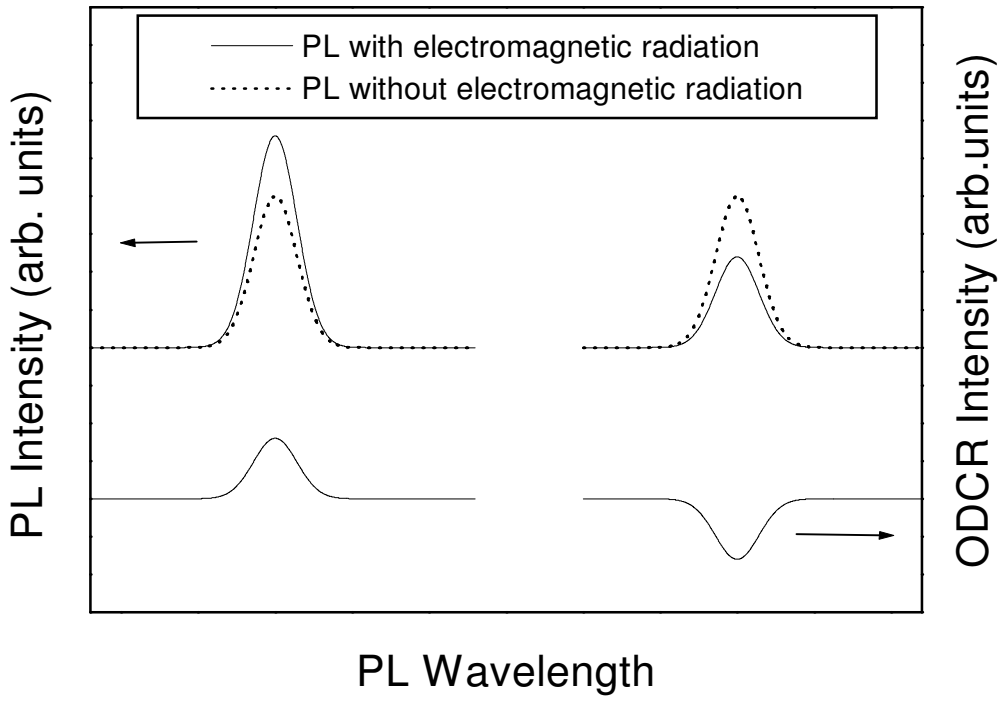

Figure 1: Schematic ODCR spectra shown as a function of the PL wavelength. The dotted line represents the PL spectra without electromagnetic radiation. The solid line represents the PL spectra with electromagnetic radiation.

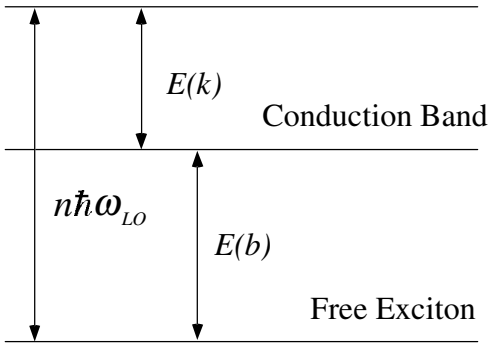

Figure 2: Schematic energy diagram of the exciton state and the conduction band. The resonant formation of free exciton takes place when the kinetic energy of the carrier $E(k)$ fulfills Eq. (3).

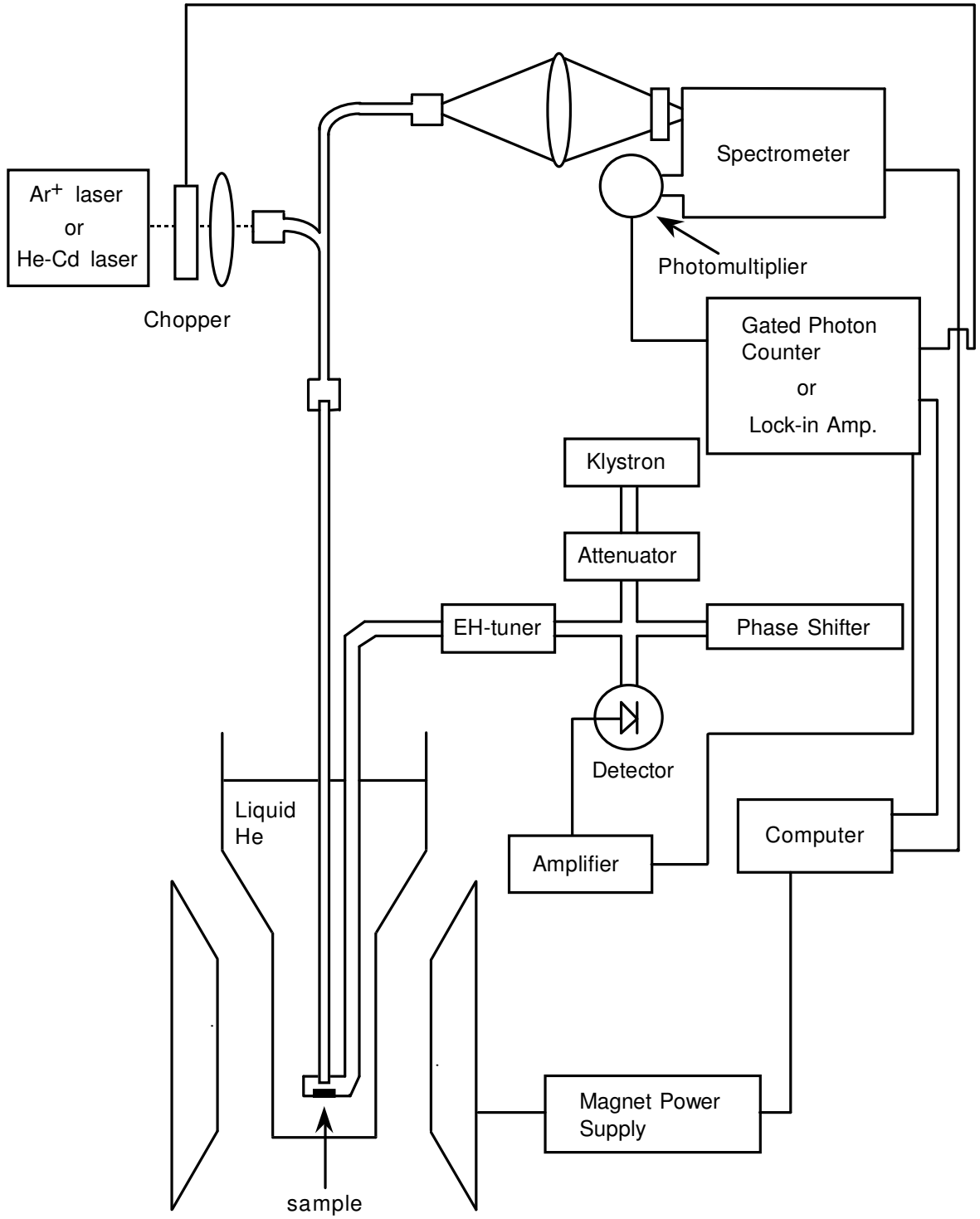

Figure 3: Block diagram of the experimental setup for PL, CR and ODCR measurements.

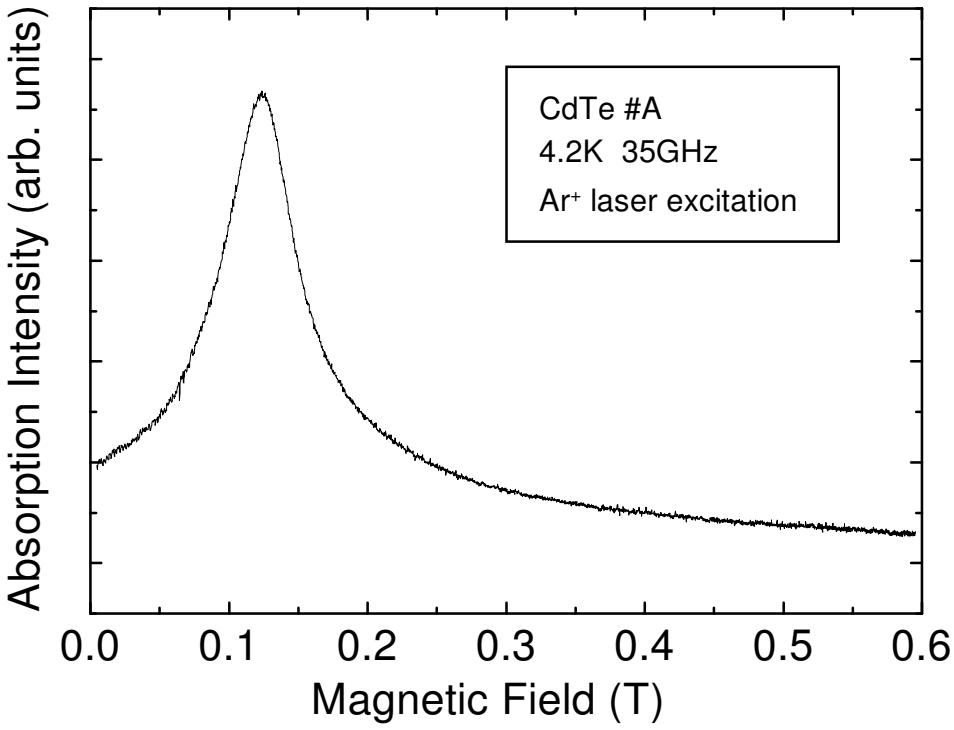

Figure 4: Ordinary electron CR spectrum taken at 4.2K. The sharp line of CR means that the employed sample is high quality.

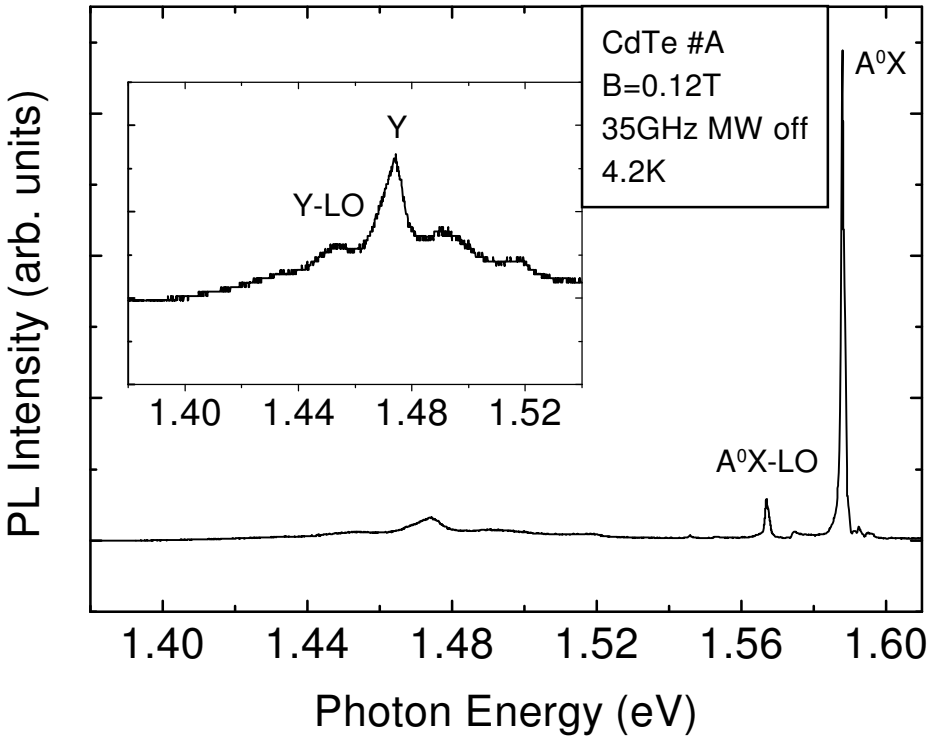

Figure 5: PL spectrum obtained at the magnetic field of 0.12T. The PL peaks associated with exciton and DA transitions were observed. The inset shows the same spectrum with an enlarged abscissa.

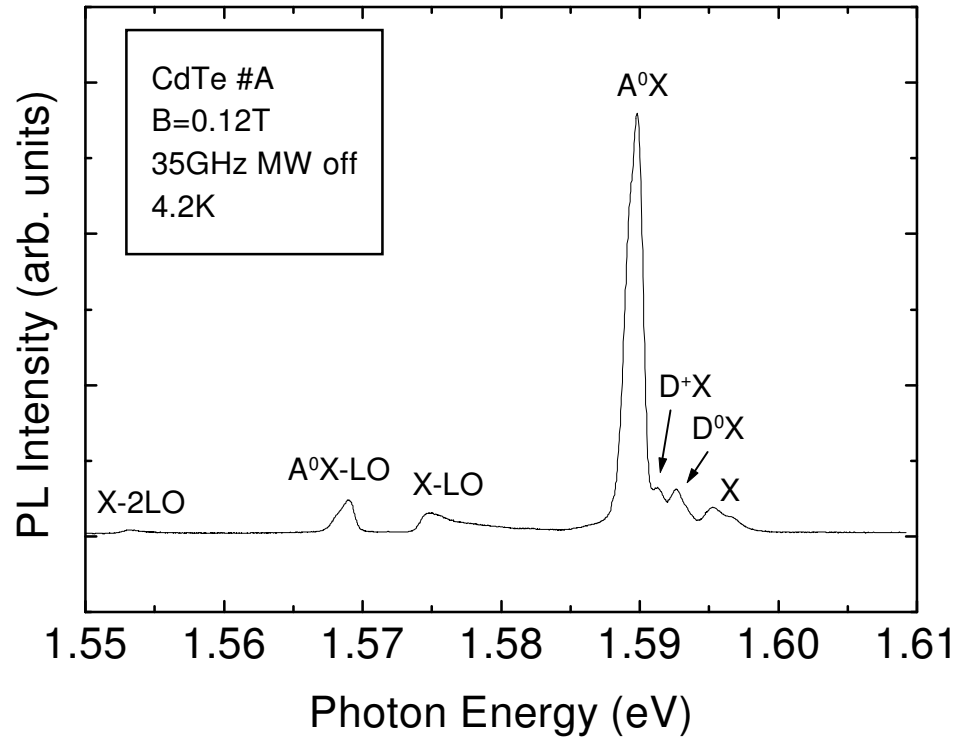

Figure 6: Detailed PL spectrum near band edge region at the magnetic field of 0.12T. Free exciton (X), neutral donor bound exciton (D^0X), ionized donor bound exciton (D^+X) and neutral acceptor bound exciton (A^0X) were observed.

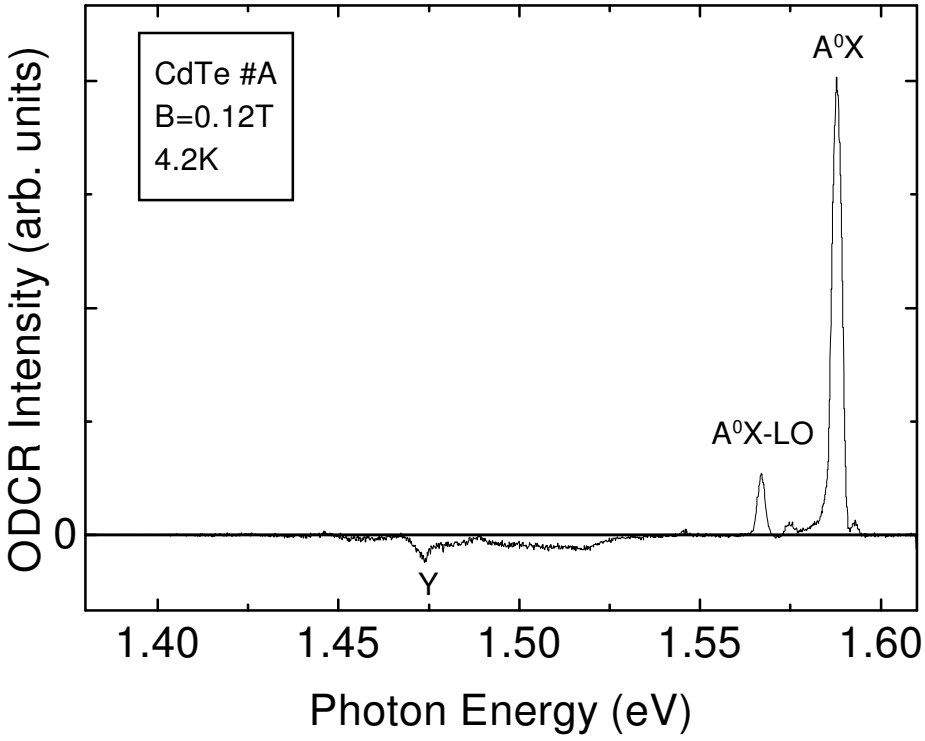

Figure 7: ODCR spectrum shown as a function of the photon energy at the magnetic field of 0.12T which corresponds to the electron CR. ODCR signals for exciton and DA transitions were observed.

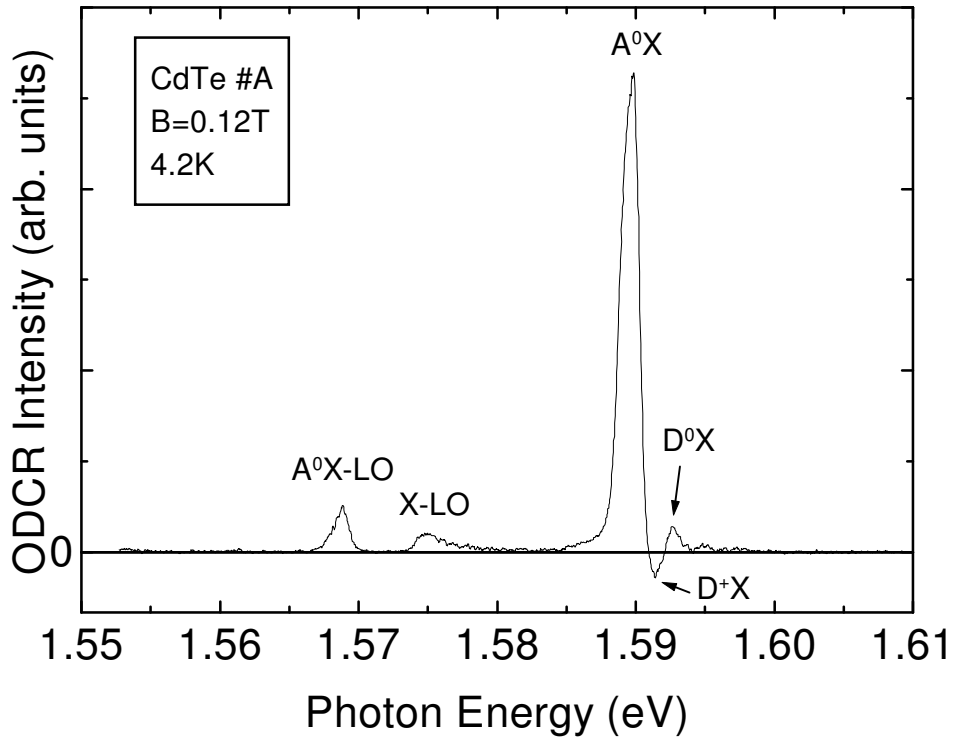

Figure 8: Detailed ODCR spectrum shown as a function of the photon energy near band edge. The strength of the applied magnetic field was 0.12T. The ODCR signals for free exciton phonon replica (X-LO), neutral donor bound exciton (D^0X), ionized donor bound exciton (D^+X) and neutral acceptor bound exciton (A^0X) were observed.

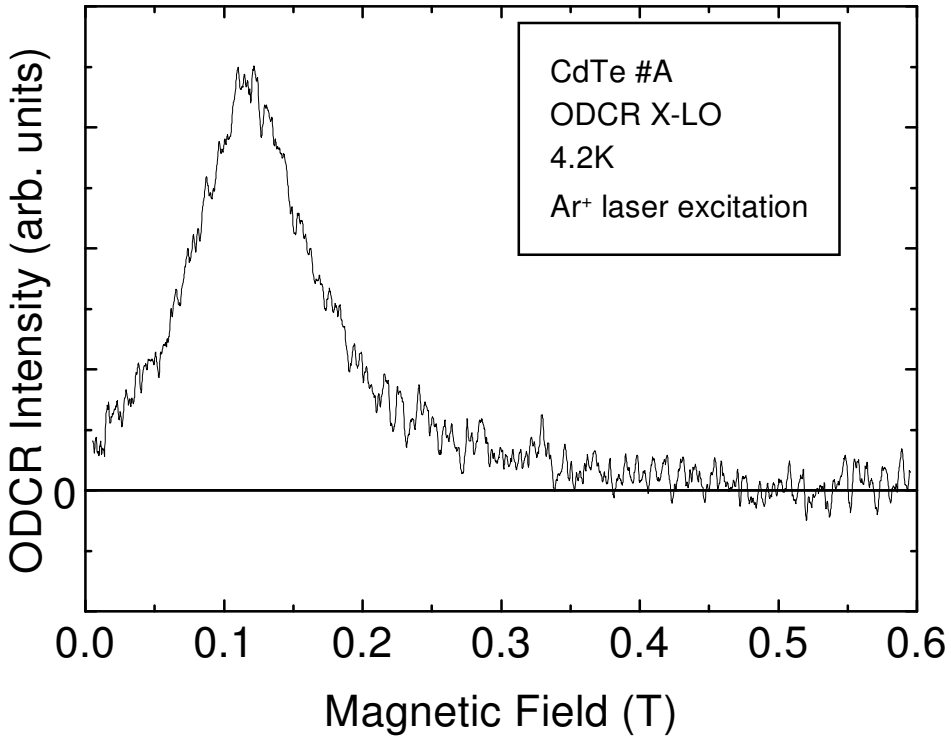

Figure 9: ODCR spectrum for free exciton LO-phonon replica (X-LO) shown as a function of the magnetic field. The microwave power level was maximum.

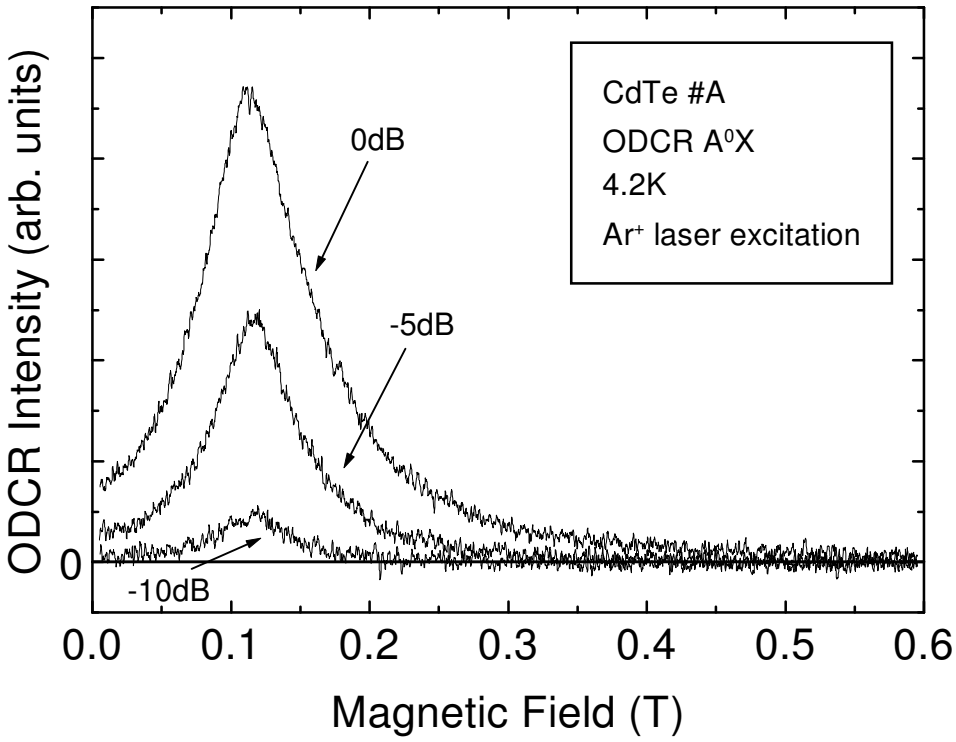

Figure 10: Microwave power dependence of the ODCR signal for neutral acceptor bound exciton (A^0X). The microwave power level is indicated in the figure. The ODCR signal decreased with decreasing microwave power.

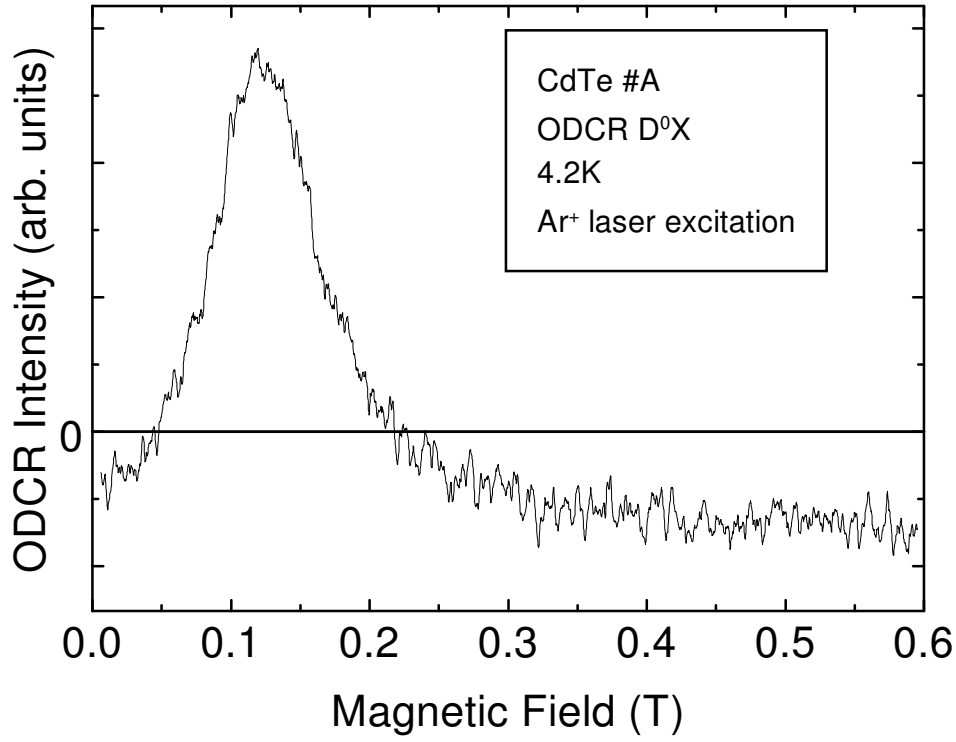

Figure 11: ODCR signal for neutral donor bound exciton (D^0X) shown as a function of the magnetic field. The microwave power level was maximum. The ODCR signal for D^0X and X-LO resembles each other.

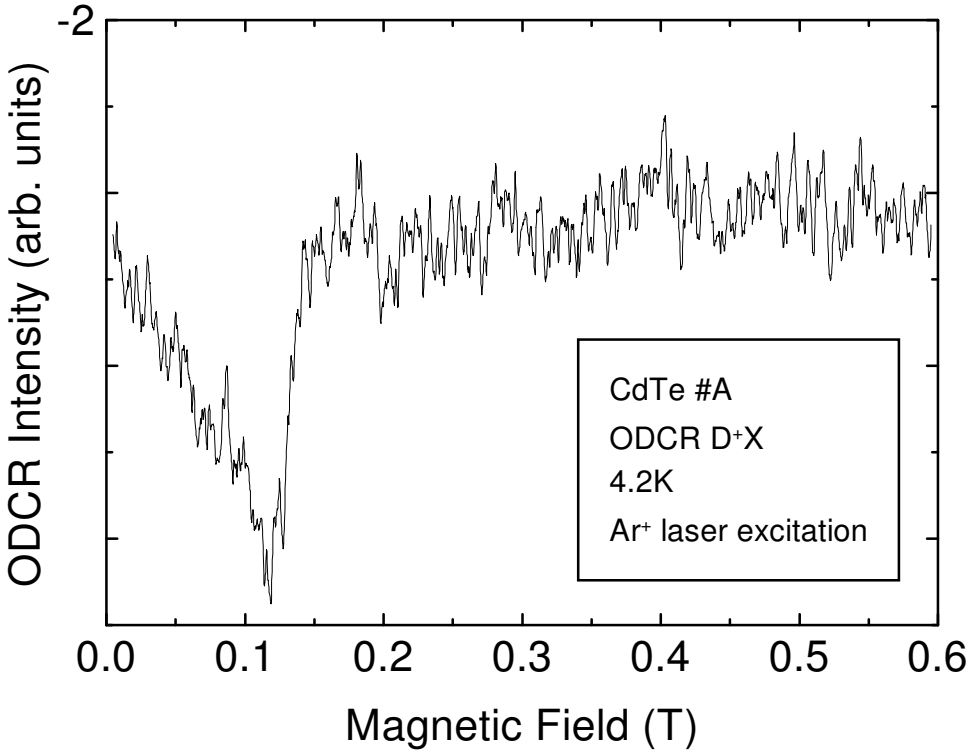

Figure 12: ODCR signal for ionized donor bound exciton (D^0X). The microwave power level was maximum. It is noteworthy that the ODCR signal is different from that for X-LO.

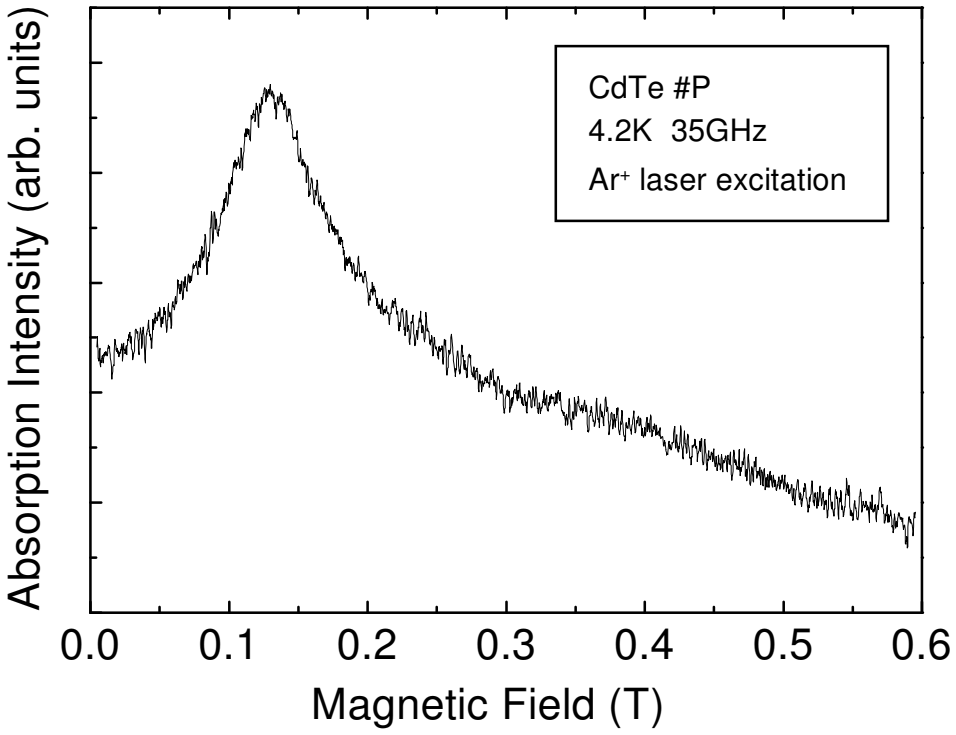

Figure 13: Ordinary CR spectrum taken at 4.2K. The sharp CR peak analogous to the case of #A was observed.

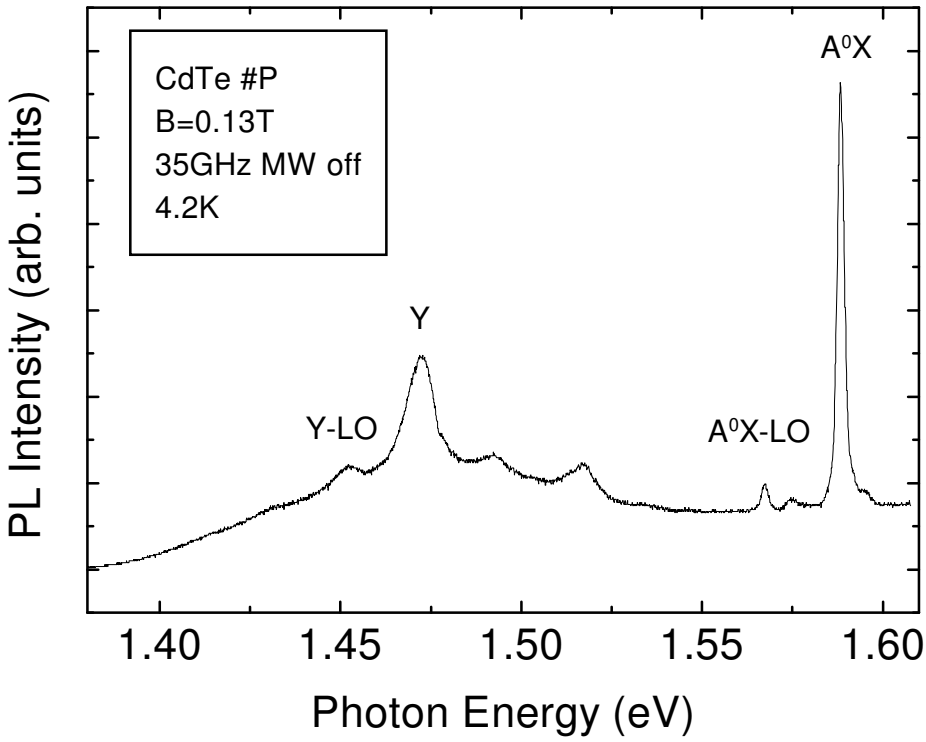

Figure 14: PL spectrum at the magnetic field of 0.13T. PL signals associated with exciton and several DA transitions were observed.

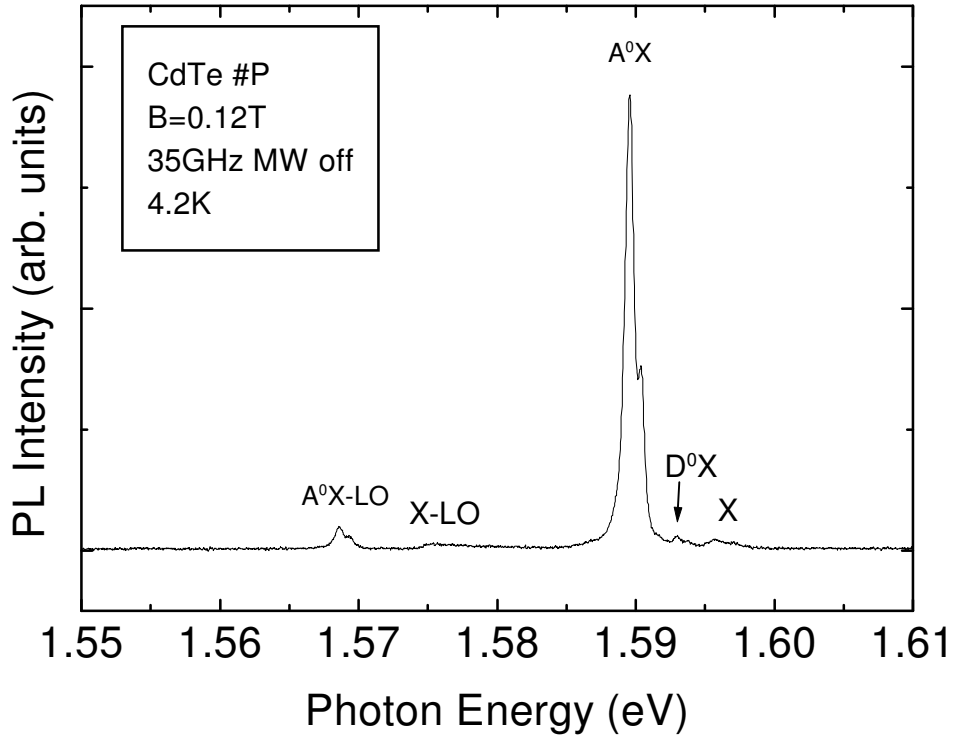

Figure 15: Detailed PL spectrum near band edge region at the magnetic field of 0.12T. PL signals for free exciton (X), neutral donor bound exciton (D^0X) and neutral acceptor bound exciton (A^0X) were observed.

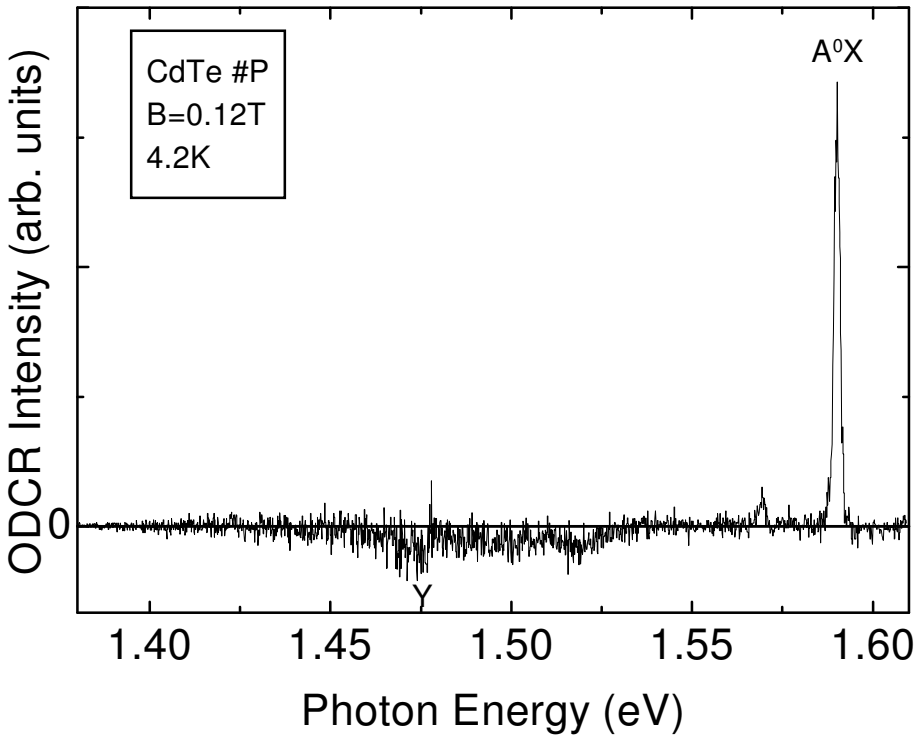

Figure 16: ODCR spectrum shown as a function of the photon energy. The applied magnetic field of 0.12T corresponds to that of electron CR. The ODCR signals for exciton and DA transitions were observed.

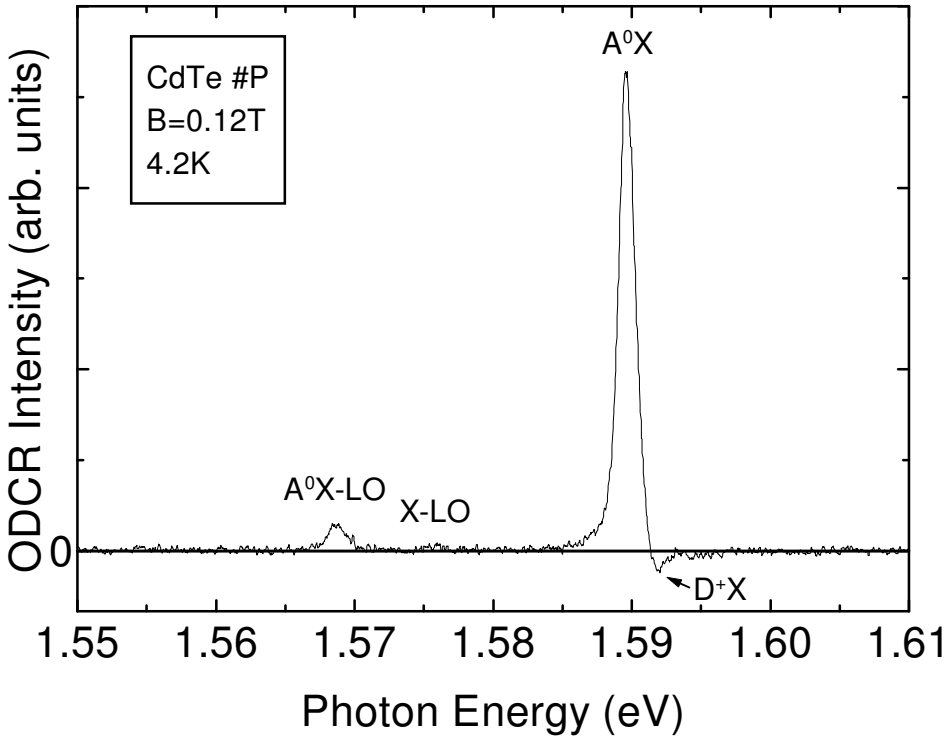

Figure 17: Detailed ODCR spectrum near band edge shown as a function of the photon energy. The applied magnetic field of 0.12T corresponds to that of electron CR. The ODCR signals for free exciton LO-phonon replica (X-LO), ionized donor bound exciton (D^+X) and neutral acceptor bound exciton (A^0X) were observed.

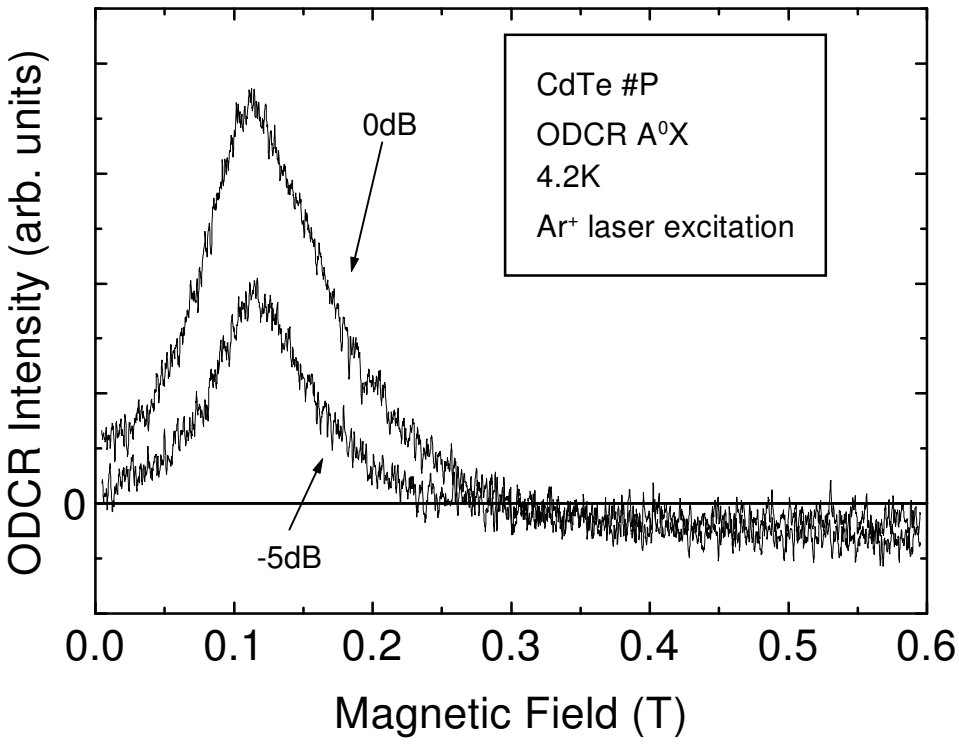

Figure 18: Microwave power dependence of the ODCR signal for neutral acceptor bound exciton (A^0X). The relative microwave power level is indicated in the figure. The ODCR signal decreased with decreasing microwave power.

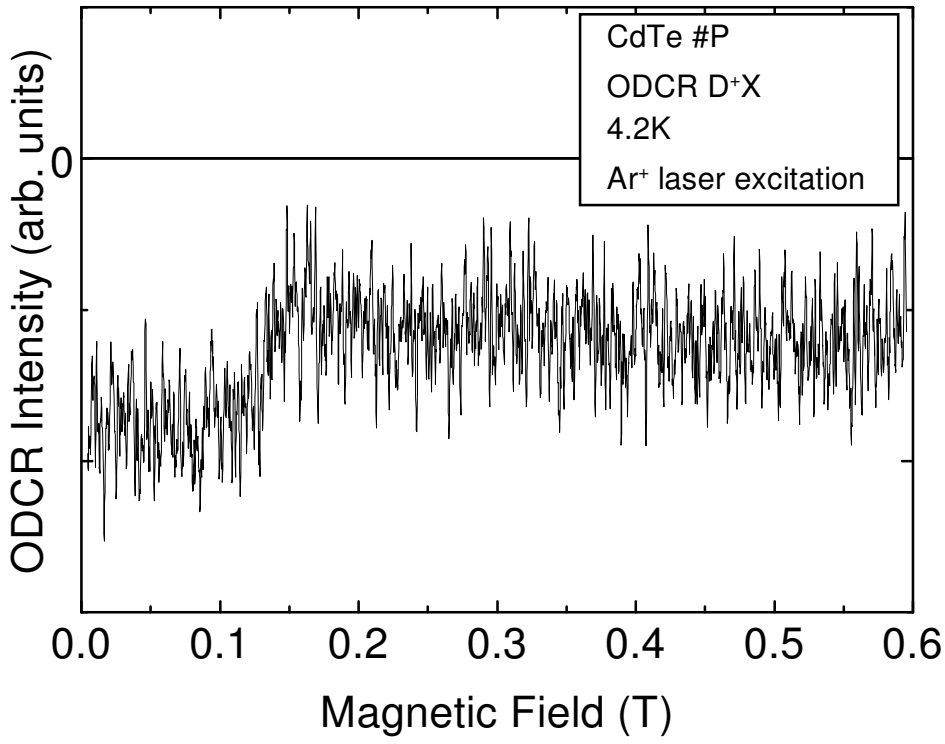

Figure 19: ODCR spectrum for ionized donor bound exciton (D^+X) shown as a function of the magnetic field. The microwave power level was maximum.

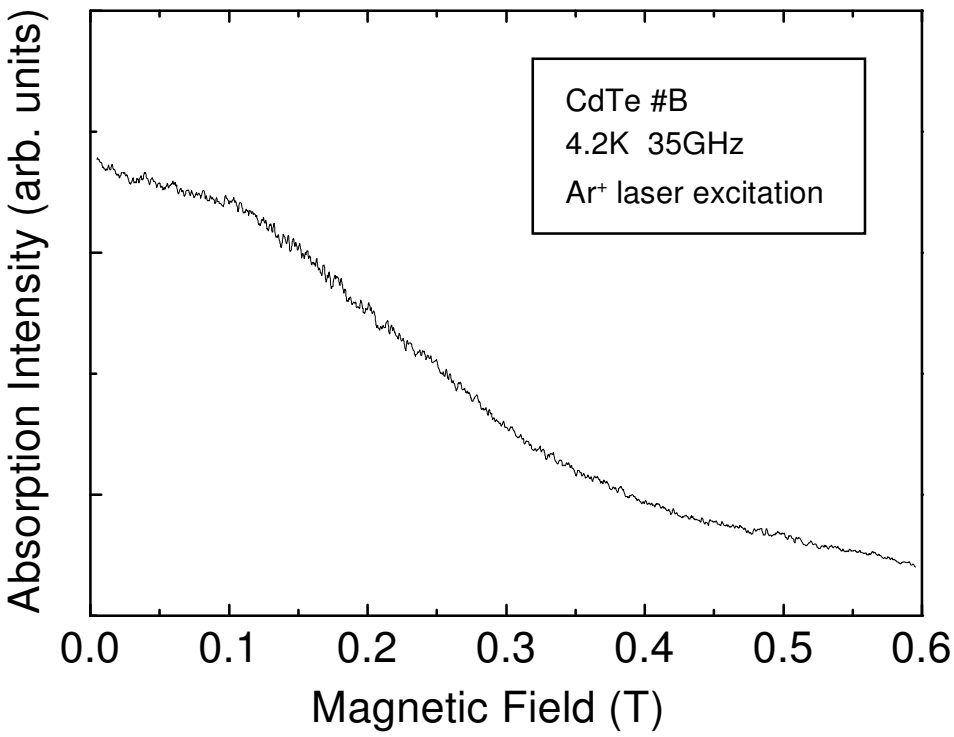

Figure 20: Ordinary CR spectrum taken at 4.2K. The broad CR peak means that the relaxation time is considerably small.

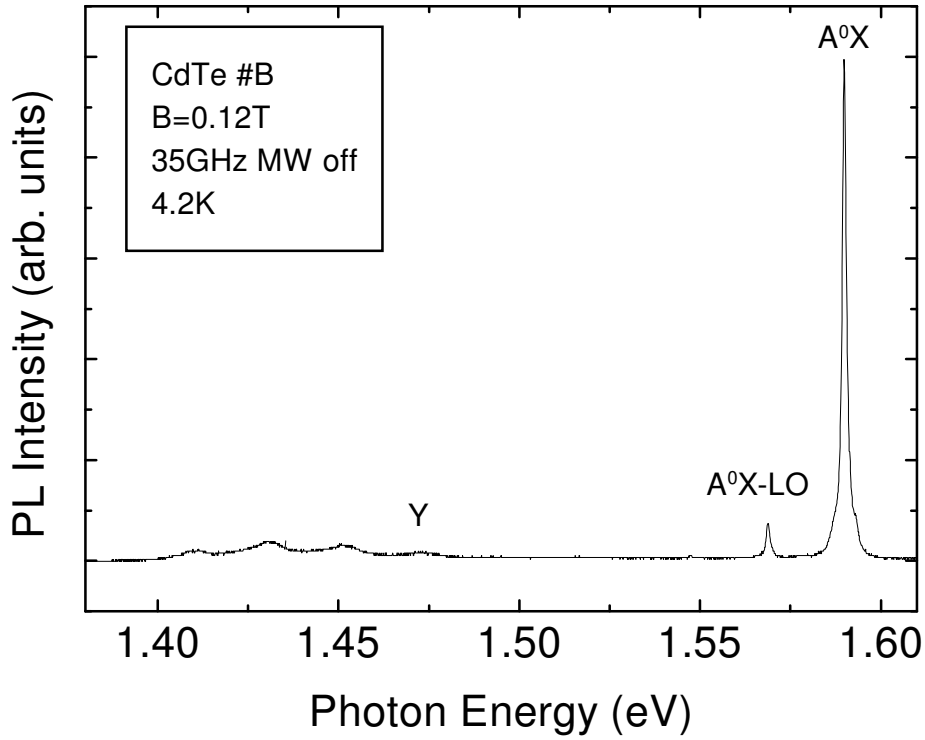

Figure 21: PL spectrum at the magnetic field of 0.12T. The PL signals associated with exciton and several DA transitions were observed.

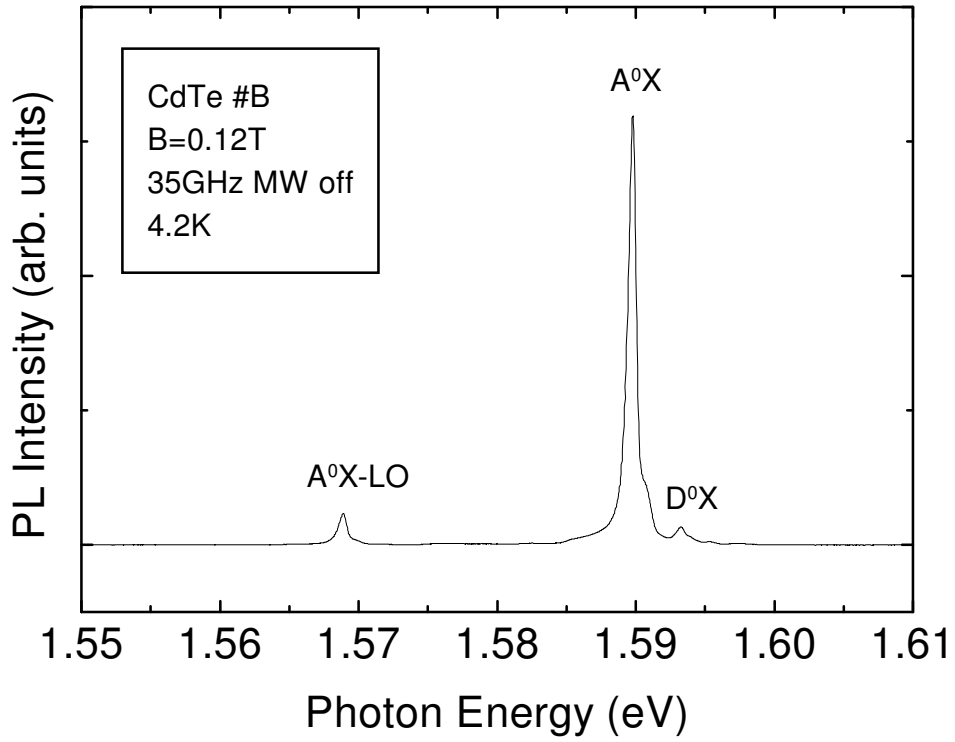

Figure 22: Detailed PL spectrum near band edge at the magnetic field of 0.12T. The PL signals for neutral donor bound exciton (D^0X) and neutral acceptor bound exciton (A^0X) were observed.

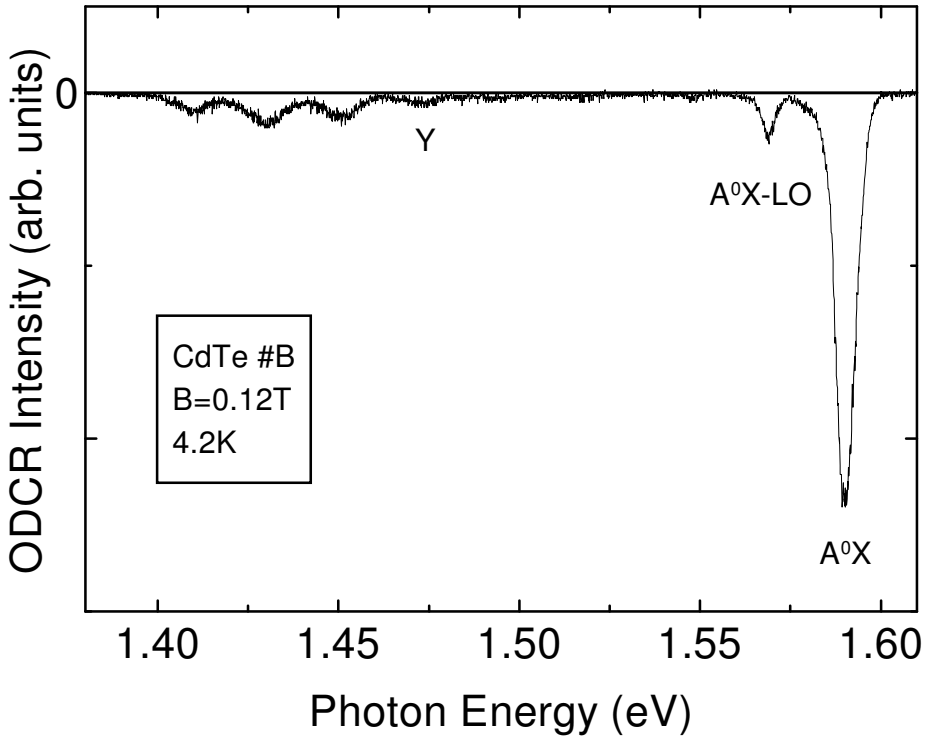

Figure 23: ODCR spectrum shown as a function of the photon energy. The applied magnetic field is 0.12T. The ODCR signals associated with exciton and DA transitions were observed.

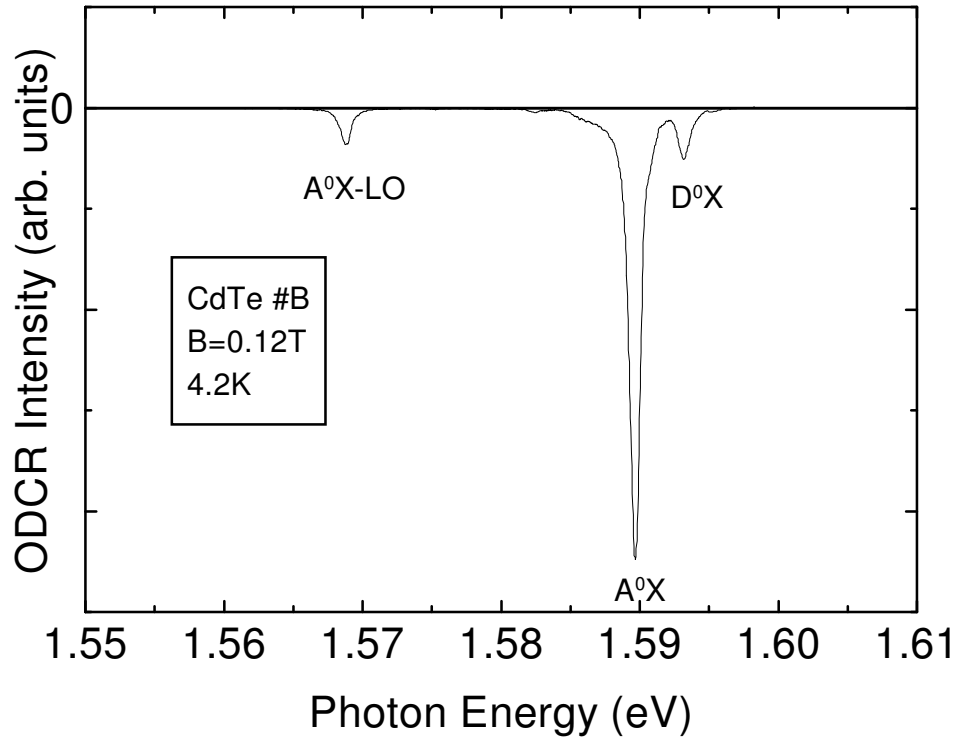

Figure 24: Detailed ODCR spectrum near band edge at the magnetic field at 0.12T. The ODCR signal for neutral donor bound exciton (D^0X) and neutral acceptor bound exciton (A^0X) were observed.

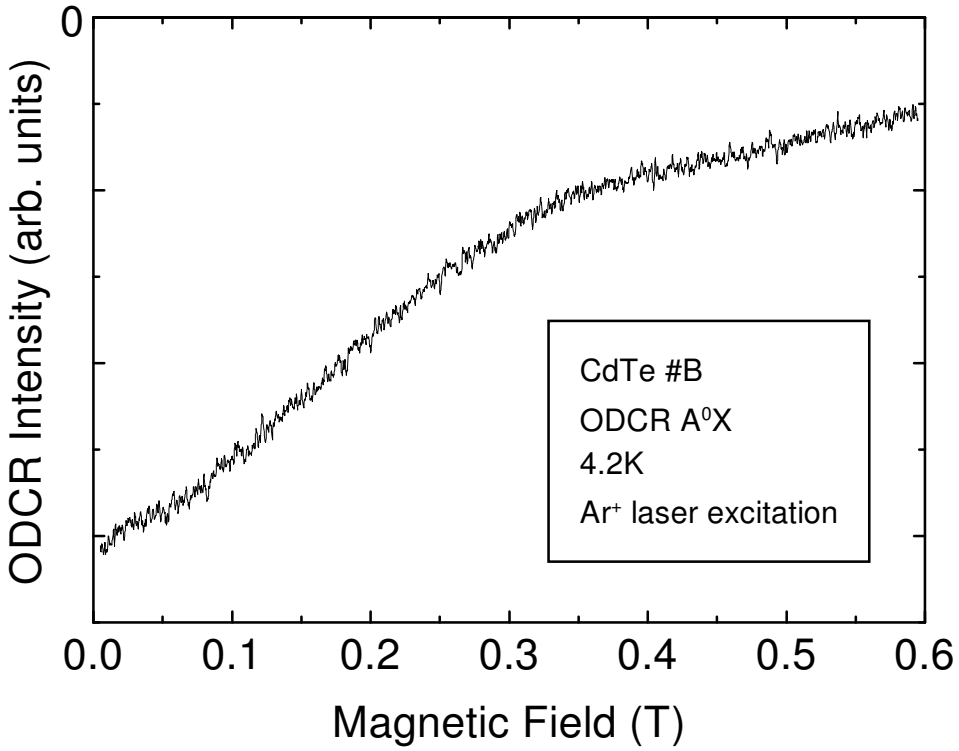

Figure 25: ODCR spectrum for neutral acceptor bound exciton (A^0X) as a function of the magnetic field. The ODCR signal shows a broad peak that is equivalent to the ordinary CR.

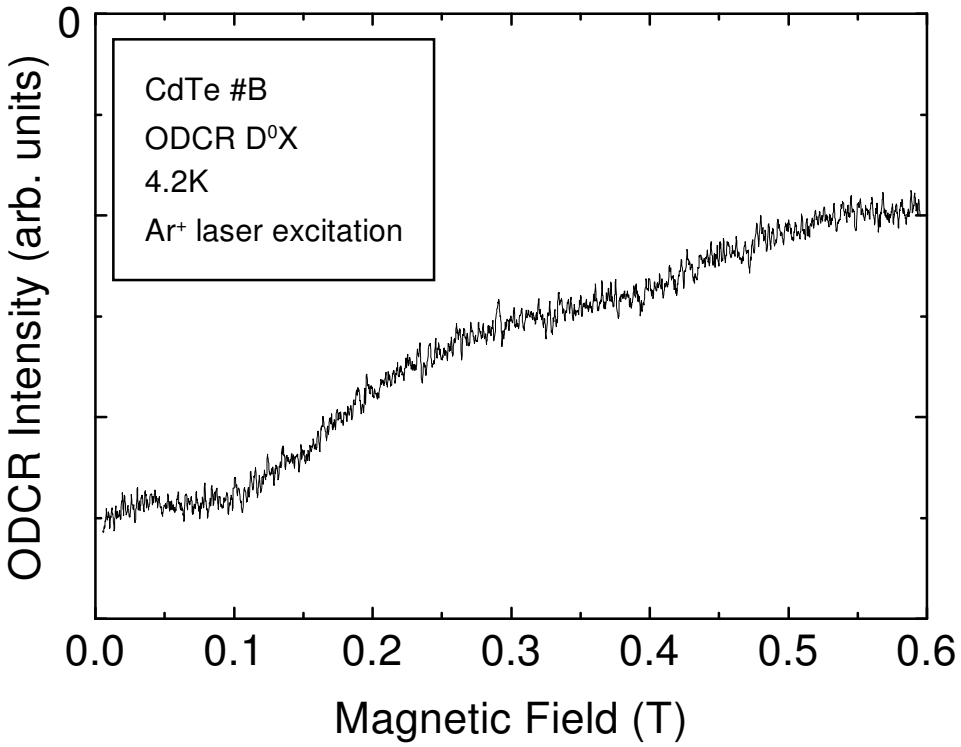

Figure 26: ODCR spectrum for neutral donor bound exciton (D^0X) as a function of the magnetic field. The ODCR signal shows a broad peak that is equivalent to the ordinary CR.

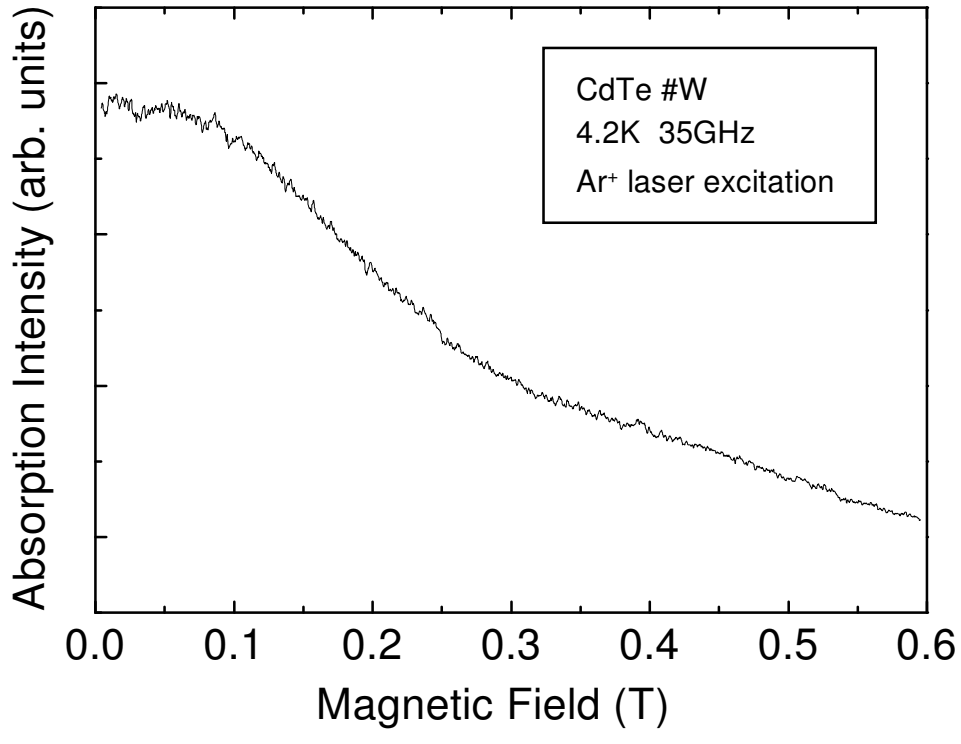

Figure 27: CR spectrum taken at 4.2K. The broad CR peak was observed.

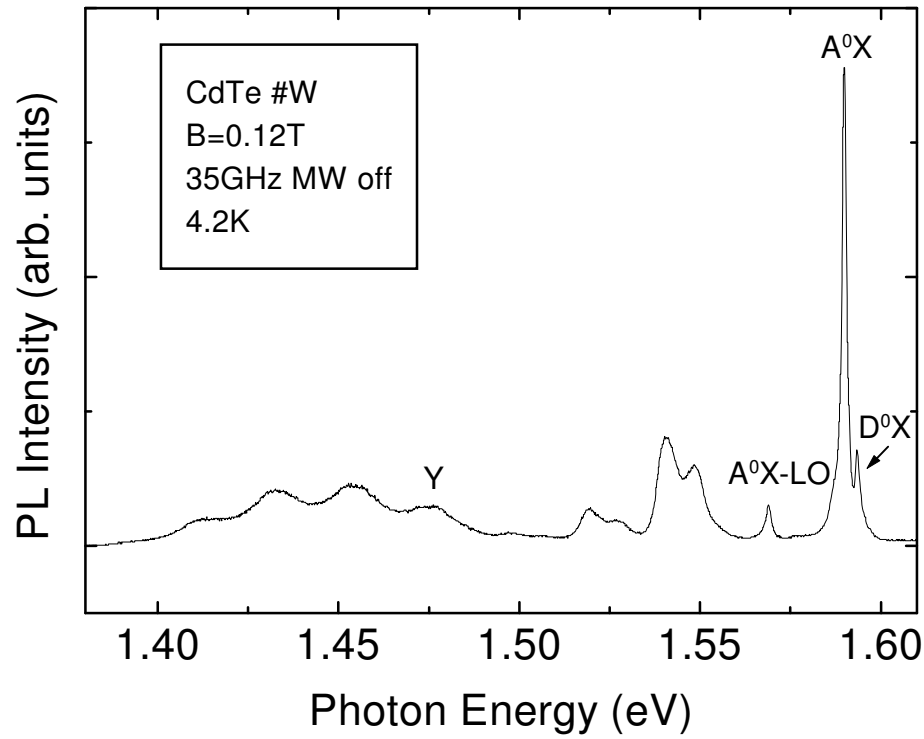

Figure 28: PL spectrum at the magnetic field of 0.12T. Many PL peaks were observed. They were attributed to DA transitions and exciton.

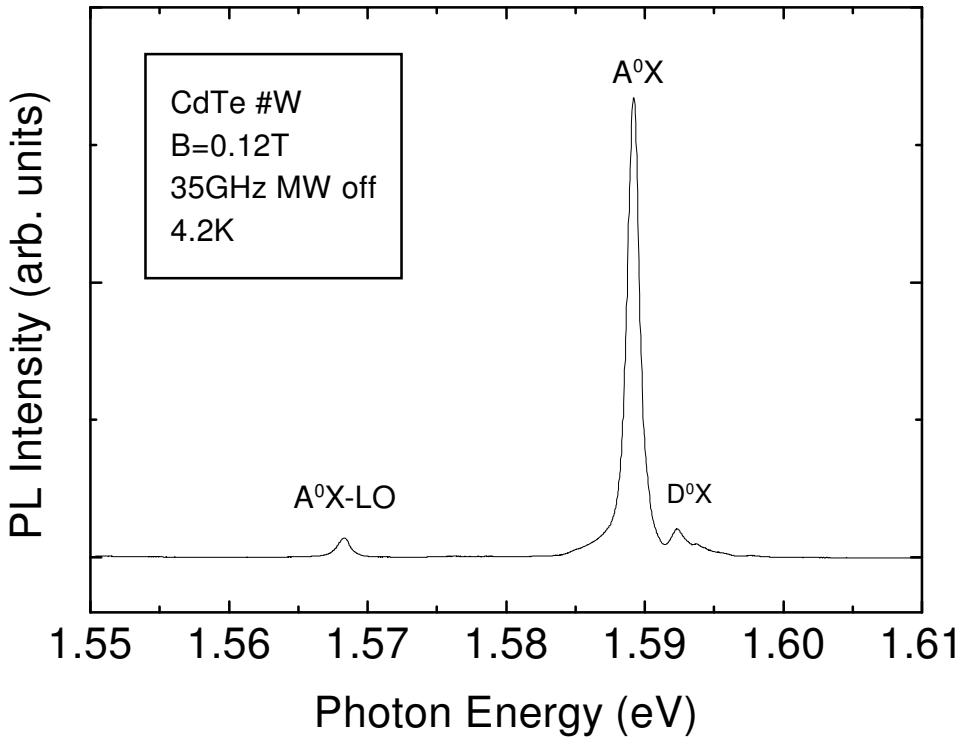

Figure 29: Detailed PL spectrum near band edge at the magnetic filed of 0.12T. The PL signals for neutral donor bound exciton (D^0X) and neutral acceptor bound exciton (A^0X) were observed.

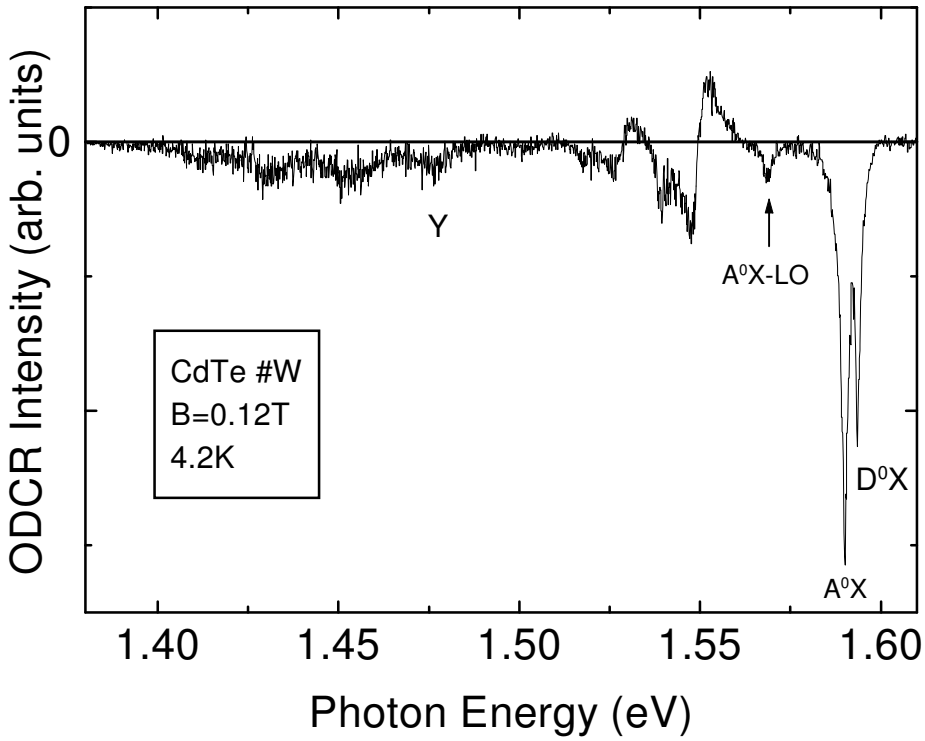

Figure 30: ODCR spectrum as a function of the photon energy. The applied magnetic field is 0.12T. The ODCR signals are associated with exciton and DA transitions. All of the ODCR signals were negative except for two peaks.

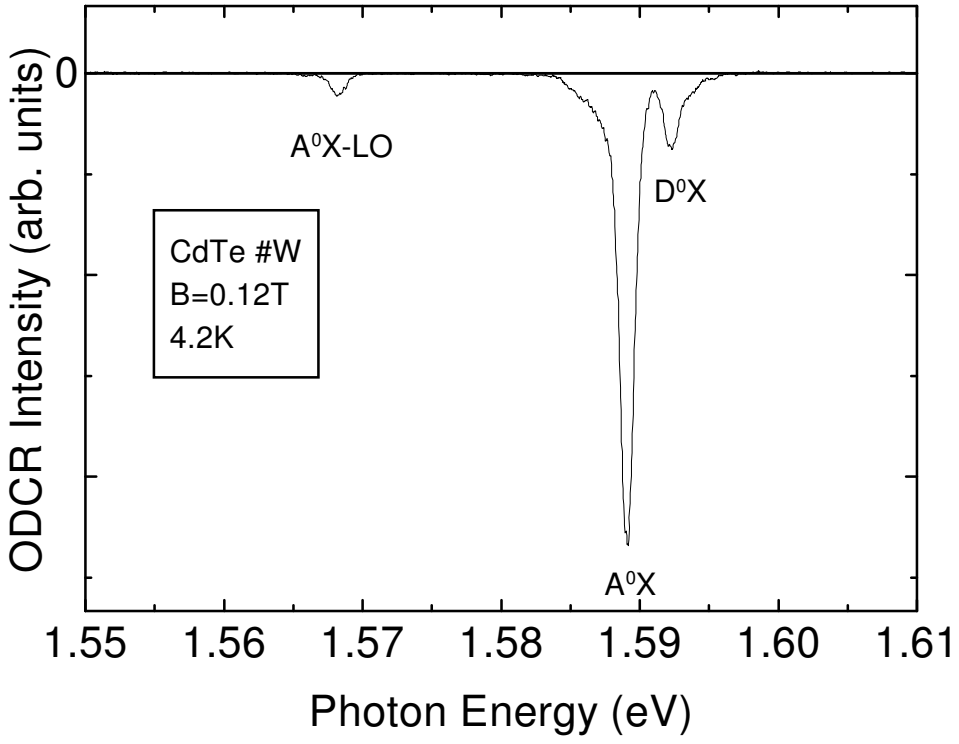

Figure 31: Detailed ODCR spectrum near band edge as a function of the photon energy. The ODCR signals for neutral donor bound exciton (D^0X) and neutral acceptor bound exciton (A^0X) were observed.

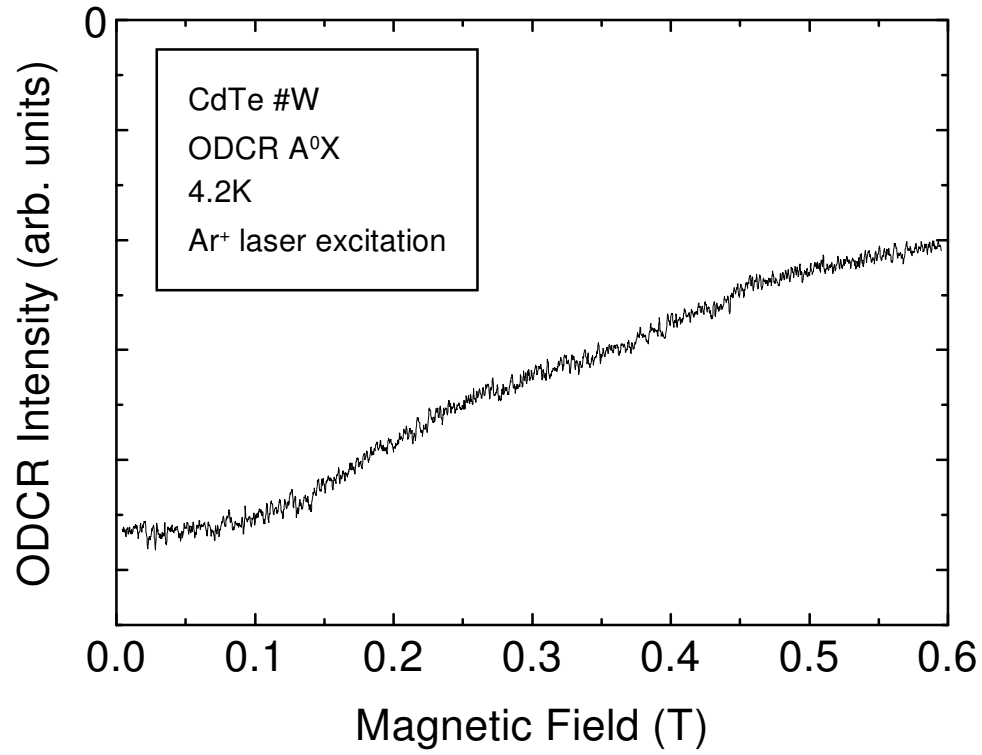

Figure 32: ODCR spectrum for neutral acceptor bound exciton (A^0X) as a function of the magnetic field. The ODCR signal shows a broad peak that is equivalent to the ordinary CR.

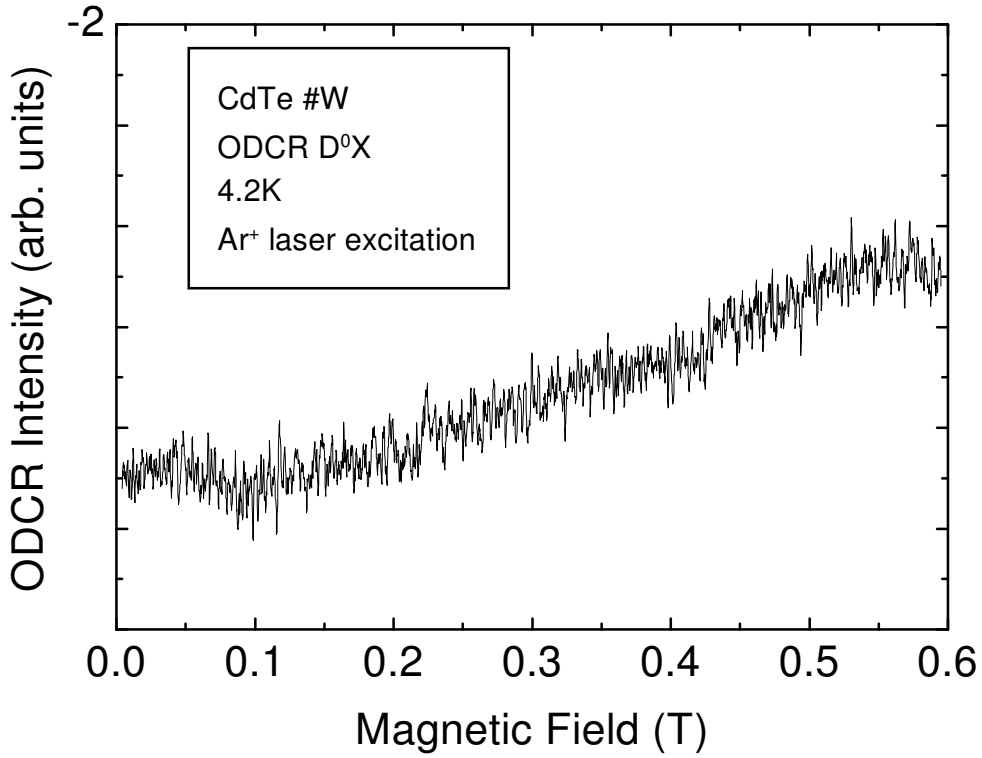

Figure 33: ODCR spectrum for neutral donor bound exciton (D^0X) as a function of the magnetic field. The ODCR signal shows a broad peak that is equivalent to the ordinary CR.

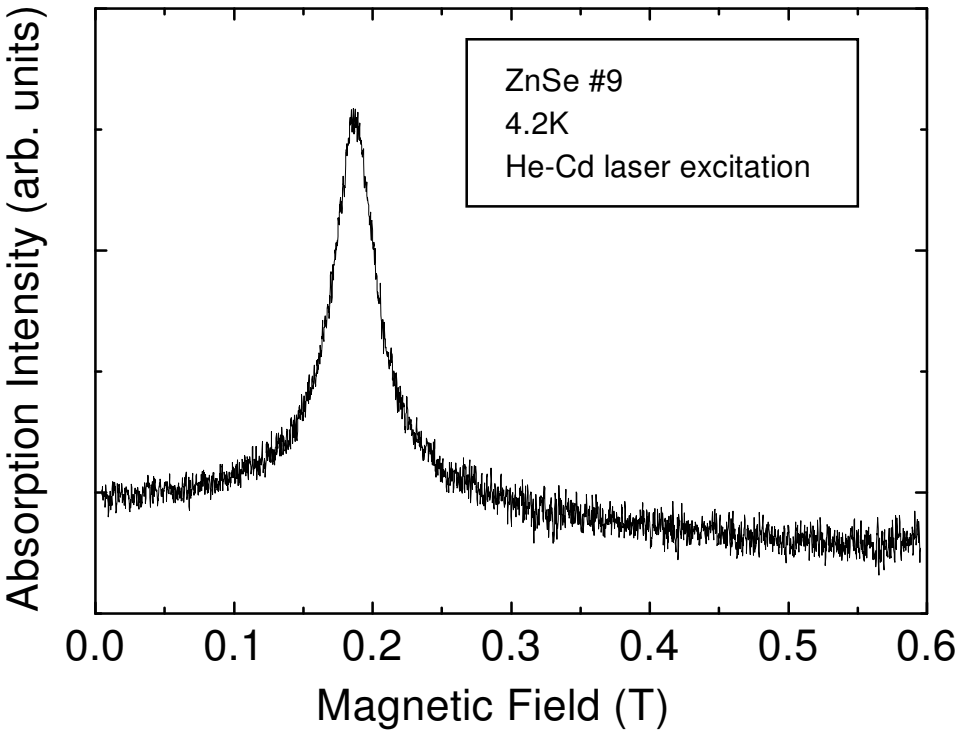

Figure 34: Ordinary CR spectrum taken at 4.2K. The sharp CR peak was observed, which represents high quality of the employed sample.

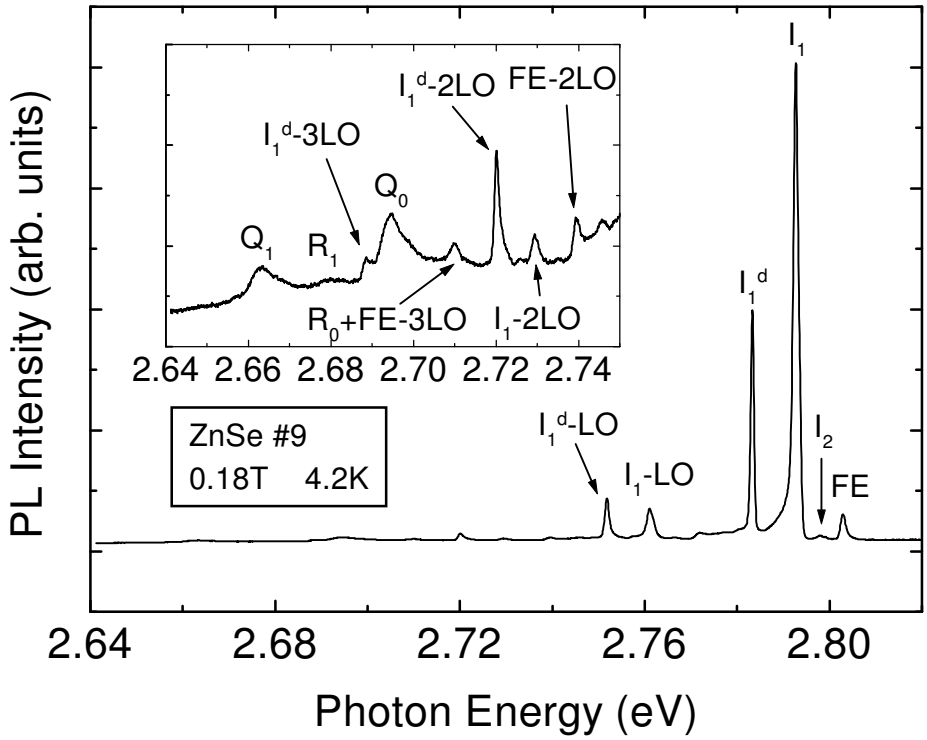

Figure 35: PL spectrum at the magnetic field of 0.18T. The PL peaks associated with exciton, R and Q series were observed. The inset shows the same spectrum with an enlarged abscissa.

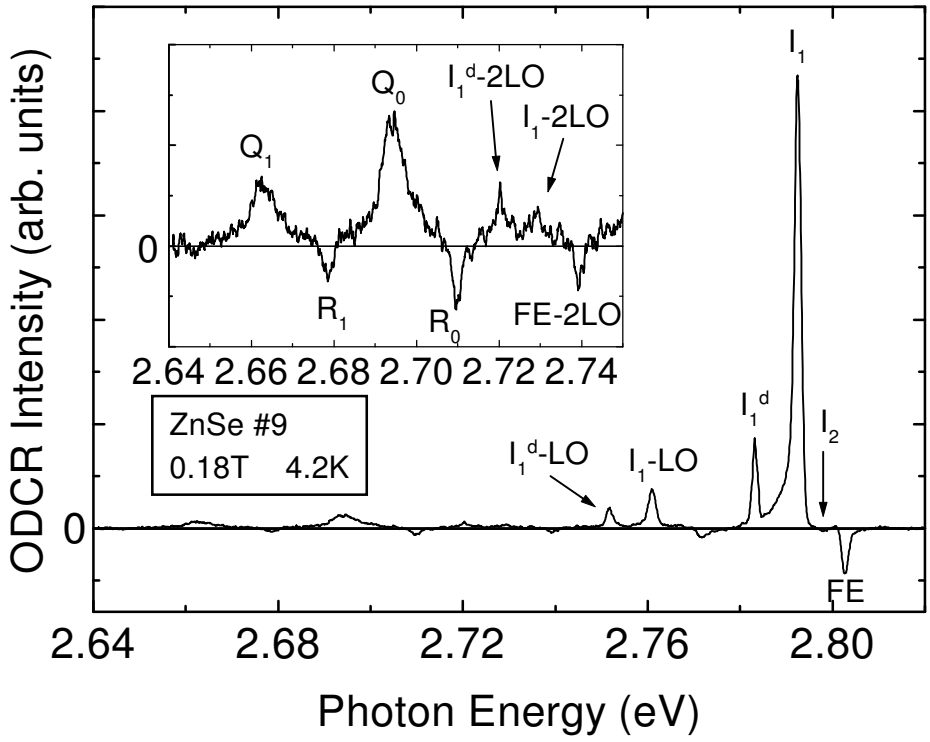

Figure 36: ODCR spectrum as a function of the photon energy. The applied magnetic field is 0.18T which corresponds to the electron CR. The ODCR signals for exciton and R and Q series were observed. The inset shows the same spectrum with an enlarged abscissa.

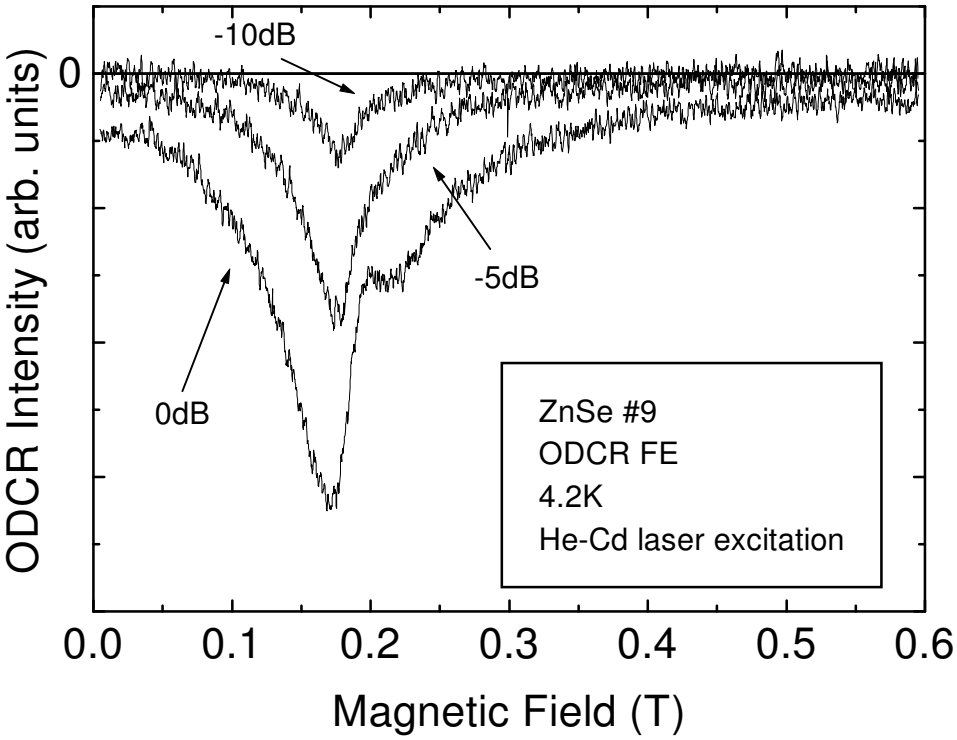

Figure 37: Microwave power dependence of the ODCR signal for free exciton. The relative microwave power level is indicated in the figure. The shoulder at 0.2T was observed at the maximum microwave power level.

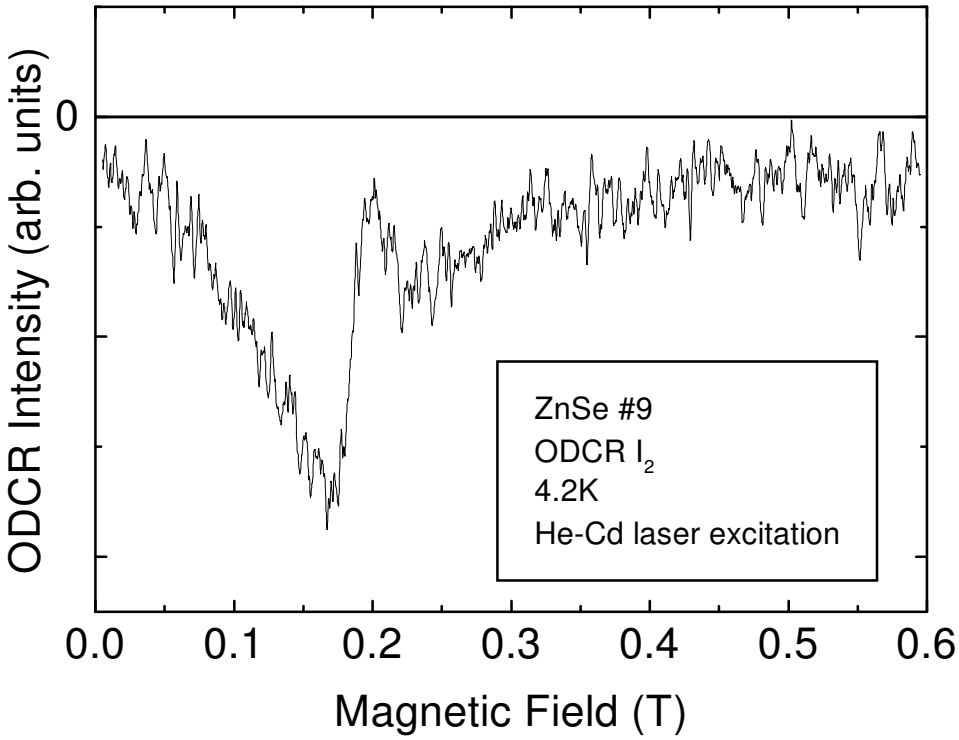

Figure 38: ODCR spectrum for neutral donor bound exciton I_2 shown as a function of the magnetic field. The microwave power level is maximum. The shoulder at 0.2T that is equivalent to the case of the ODCR signal for free exciton was observed.

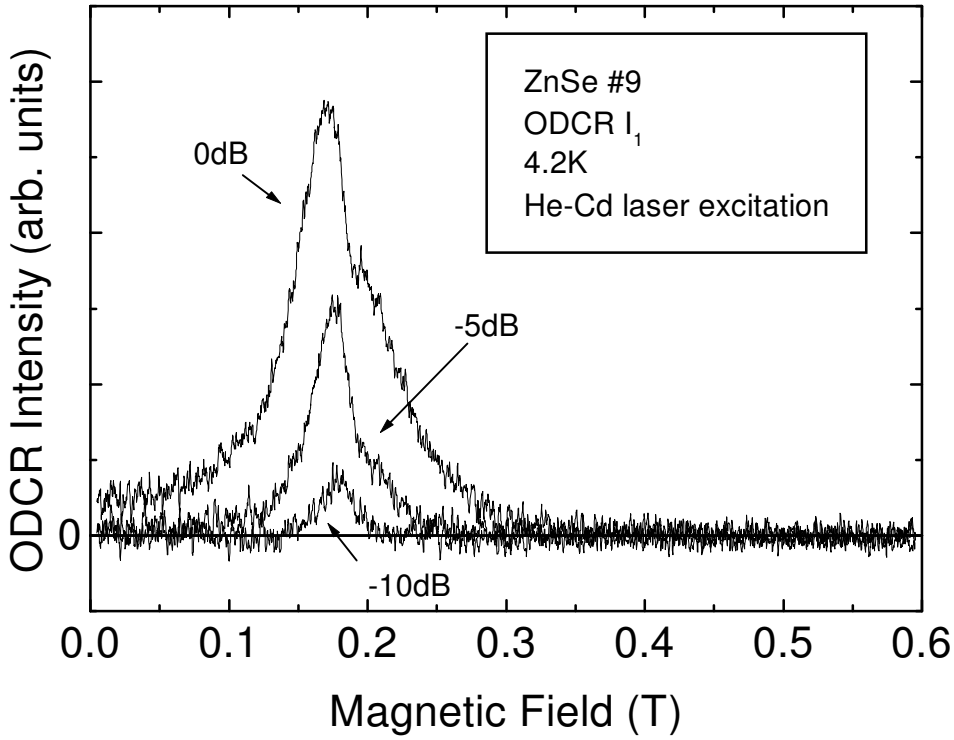

Figure 39: Microwave power dependence of the ODCR signal for neutral acceptor bound exciton I_1. The relative microwave power level is indicated in the figure. The shoulder 0.2T was observed at maximum microwave power level, as in the case of the ODCR signal for free exciton.

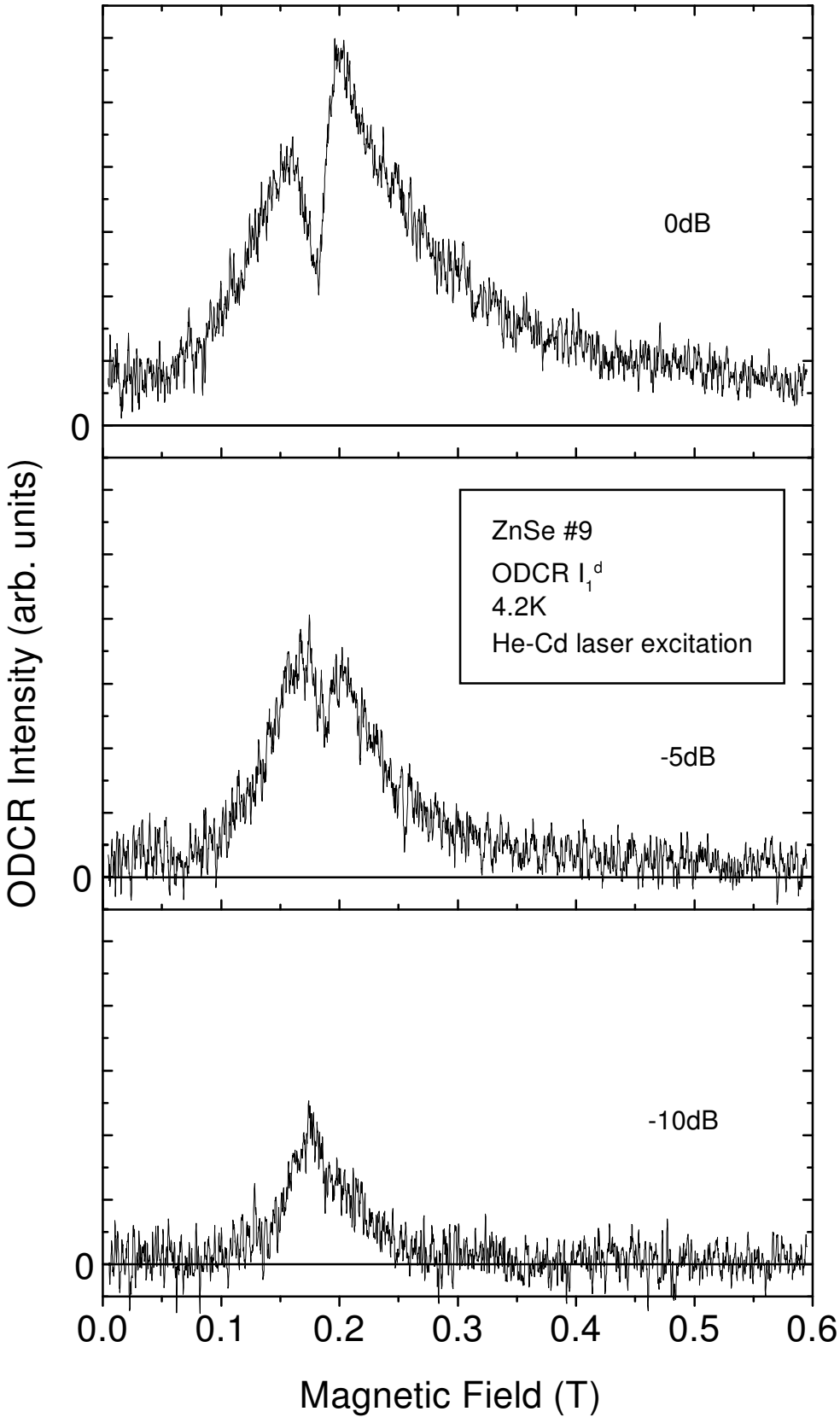

Figure 40: Microwave power dependence of the ODCR signal for deep acceptor bound exciton I_1^d. The relative microwave power level is indicated in the figure. The shape of the ODCR signal is different from that for free exciton.

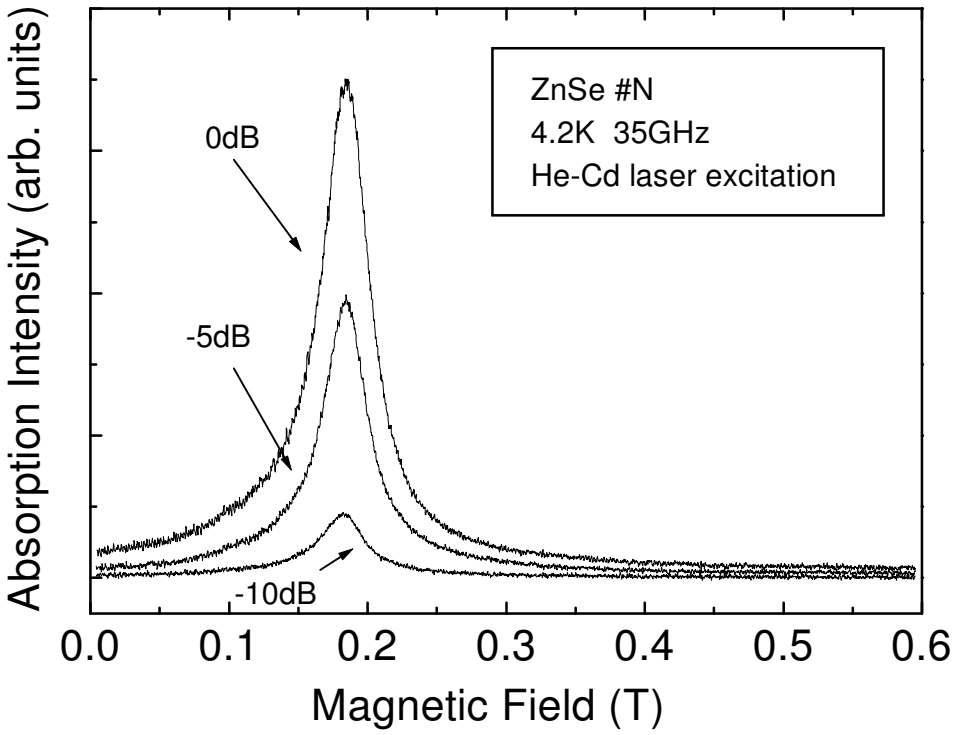

Figure 41: Microwave power dependence of the ordinary CR spectrum. The relative microwave power level is indicated in the figure. The sharp line suggests that the employed sample is a high quality one.

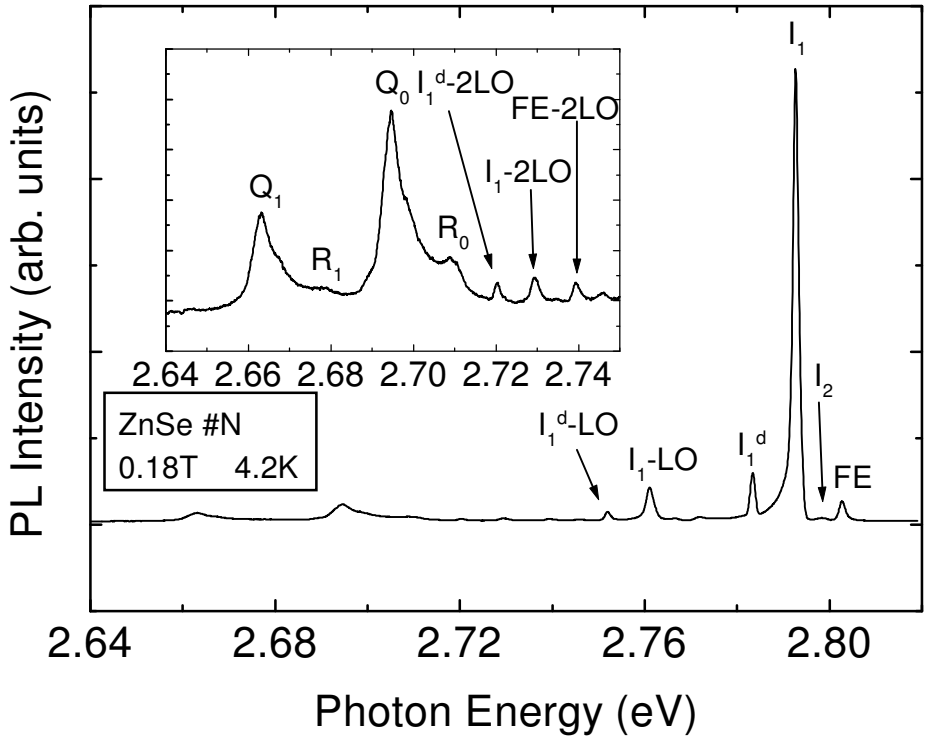

Figure 42: PL spectrum at the magnetic field of 0.18T. The PL peaks associated with exciton, R and Q series were observed.

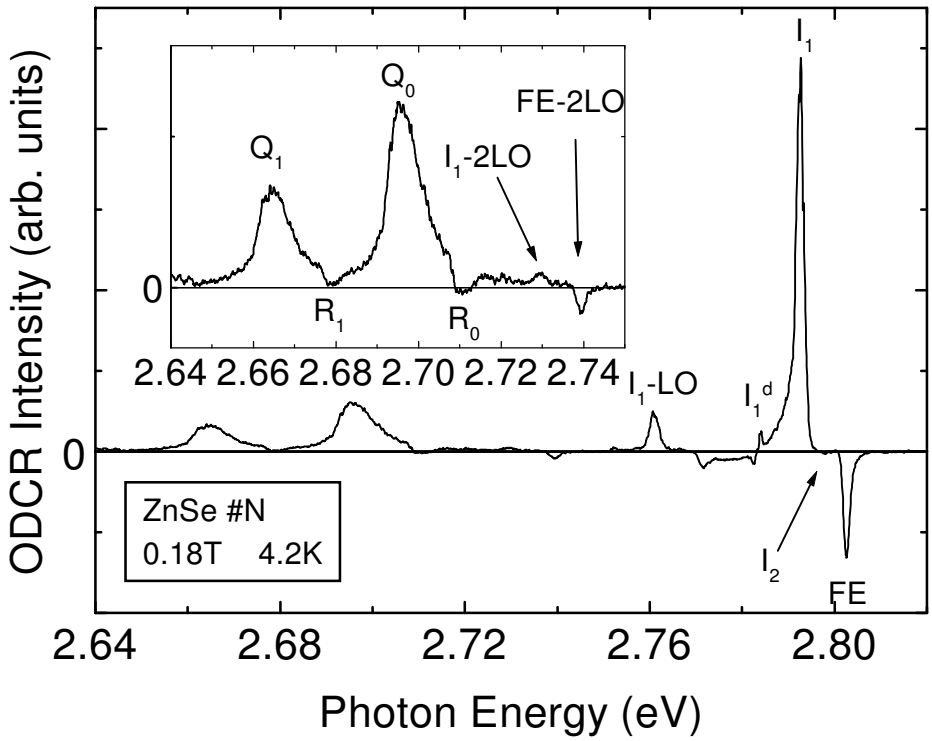

Figure 43: ODCR spectrum as a function of the photon energy. The applied magnetic field is 0.18T that corresponds to the electron CR. The ODCR signals for exciton and Q series were observed. The inset shows the same spectrum with an enlarged abscissa.

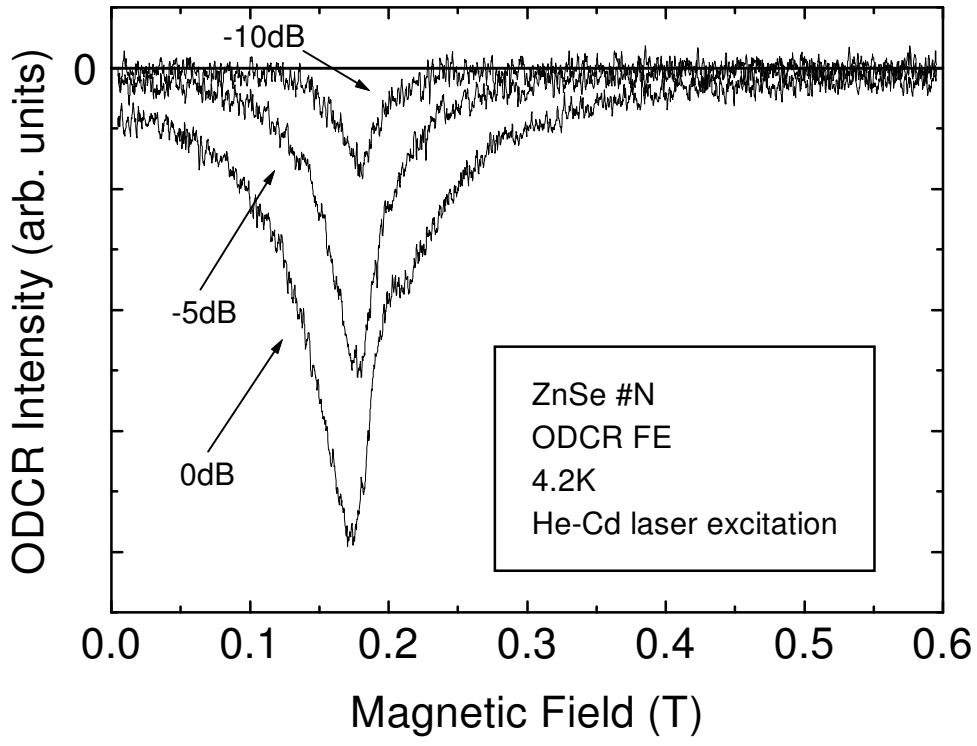

Figure 44: Microwave power dependence of the ODCR signal for free exciton as a function of the magnetic field. The relative intensity of microwave power is indicated in the figure. The shoulder at 0.2T is observed at maximum microwave power level.

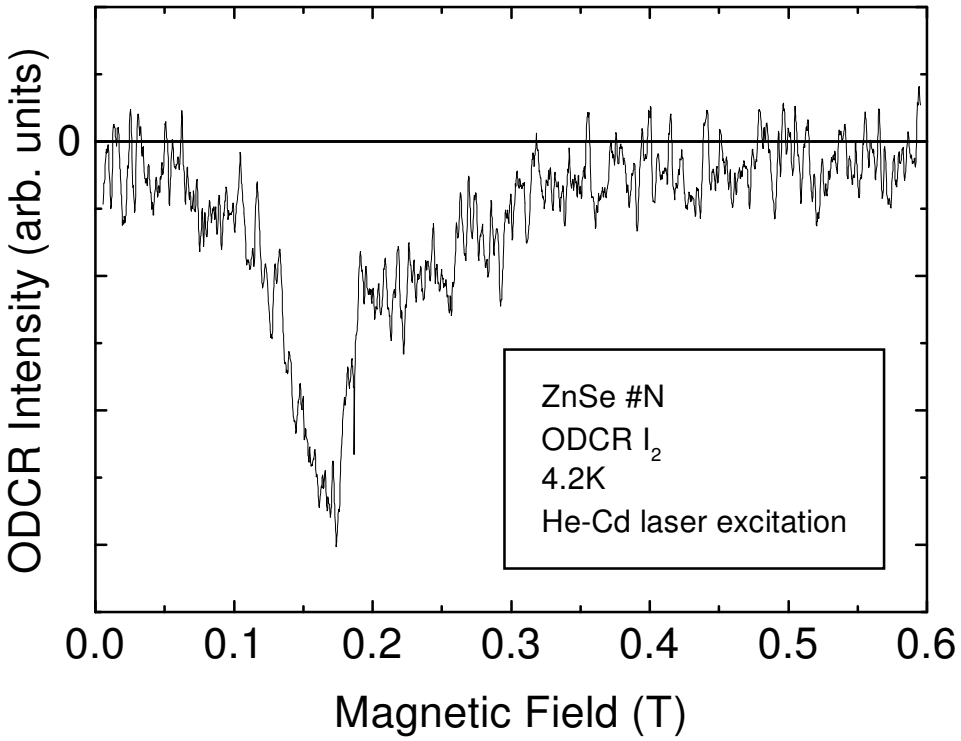

Figure 45: ODCR spectrum for neutral donor bound exciton I_2. The microwave power level is maximum. The shoulder at 0.2T was observed.

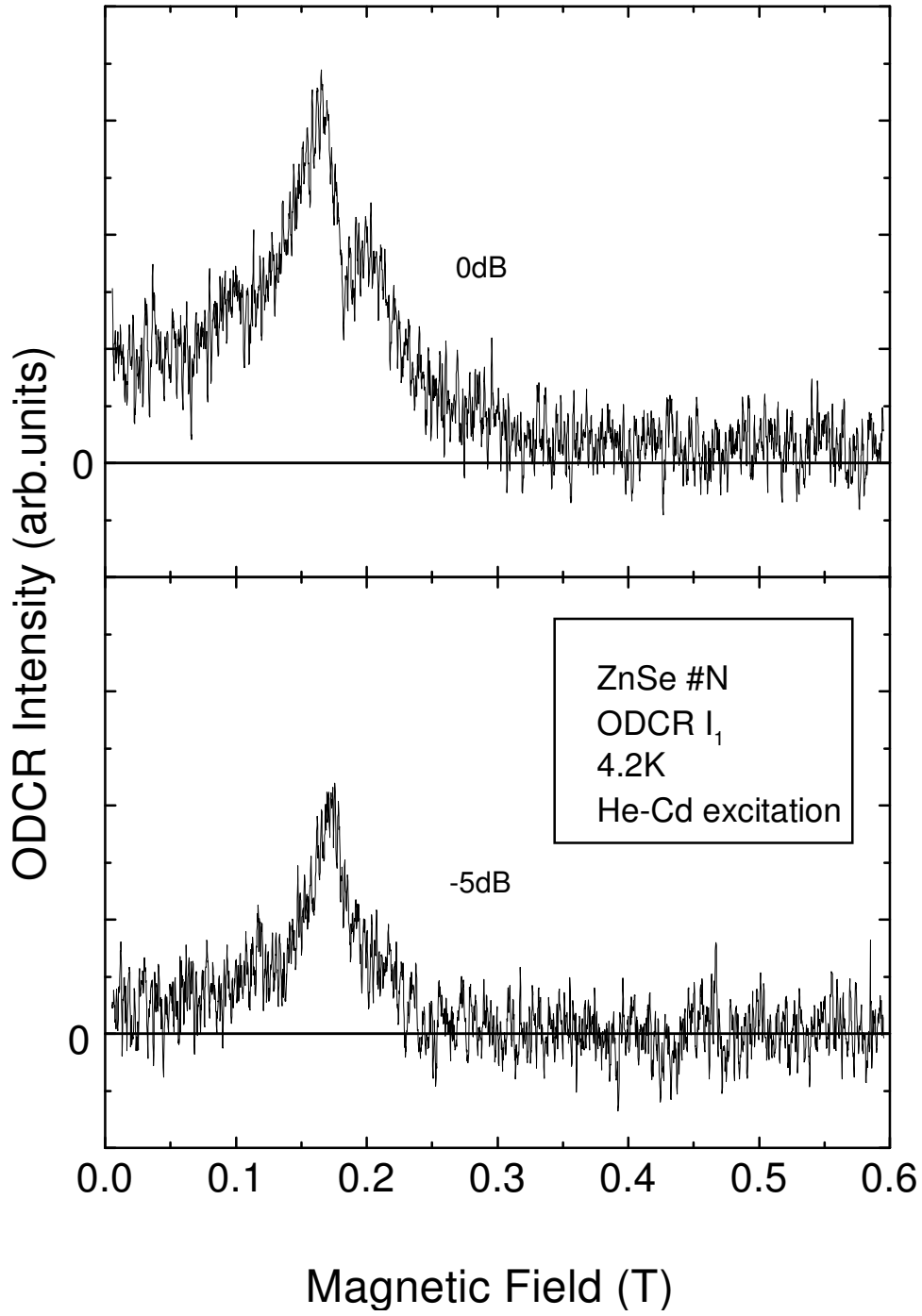

Figure 46: Microwave power dependence of the ODCR signal for neutral acceptor bound exciton I_1. The relative microwave power level is indicated in the figure. The shoulder at 0.2T was observed at maximum microwave power level, as in the case of the ODCR signal for free exciton.

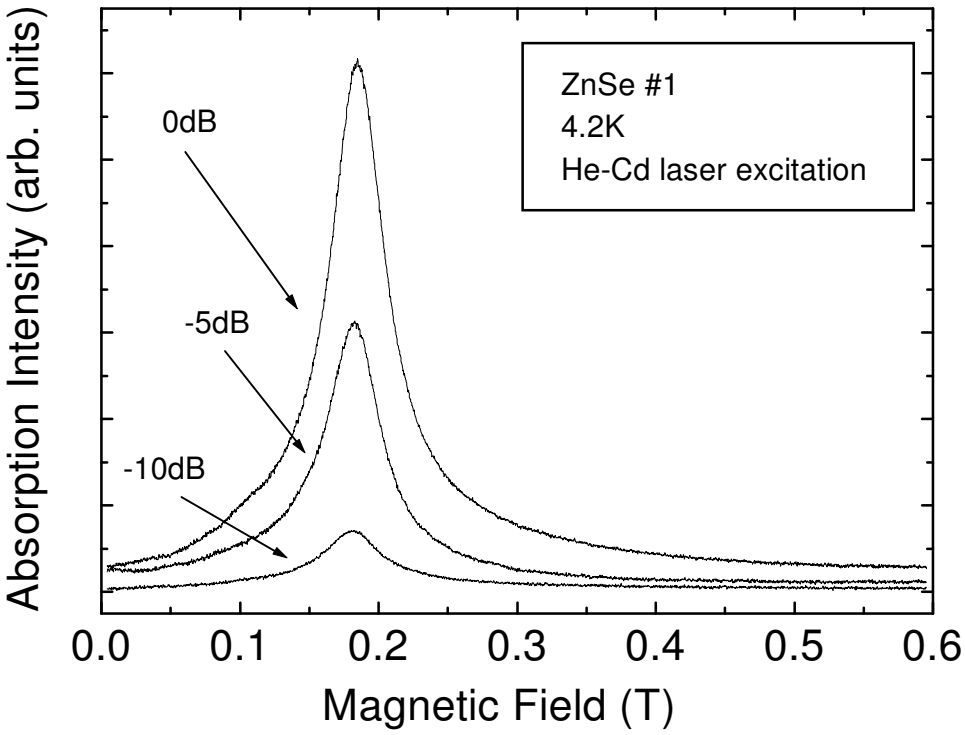

Figure 47: Microwave power dependence of the ordinary CR spectrum. The relative microwave power level is indicated in the figure. The sharp line suggests that the used sample is a high quality one.

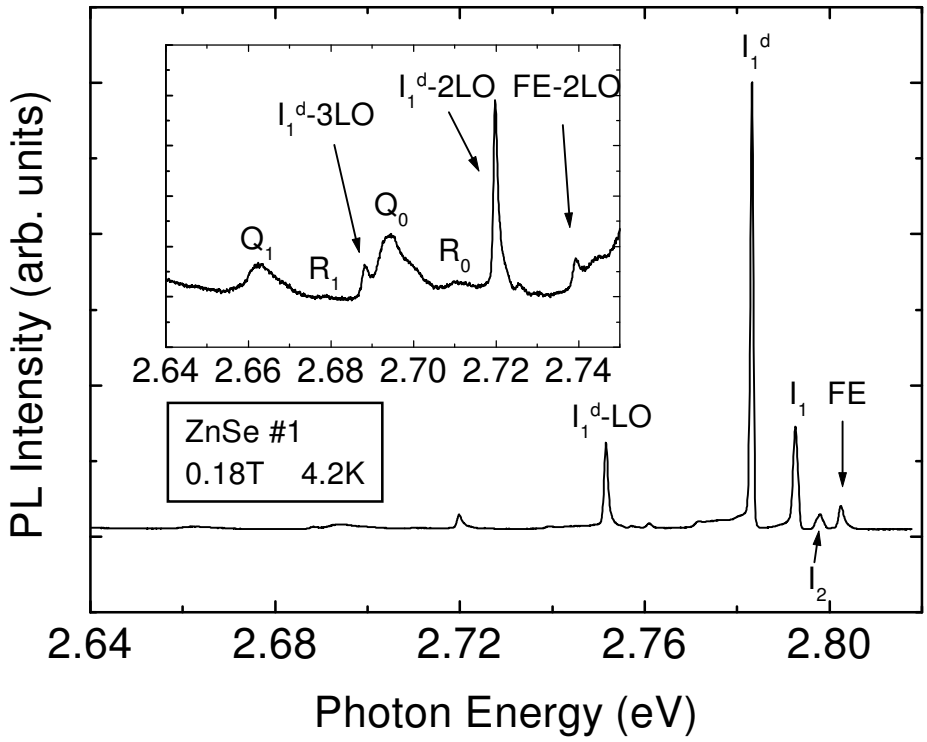

Figure 48: PL spectrum at the magnetic field of 0.18T. The PL peaks associated with exciton, R and Q series were observed.

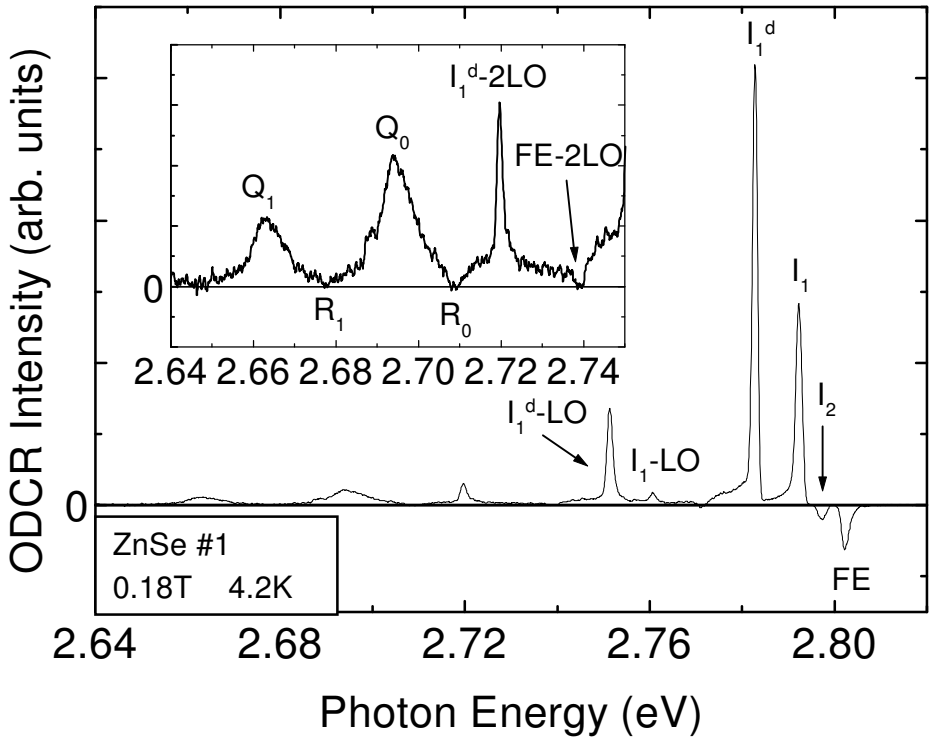

Figure 49: ODCR spectrum as a function of the photon energy. The applied magnetic field is 0.18T that corresponds to the electron CR. The ODCR signals for exciton and Q series were observed.

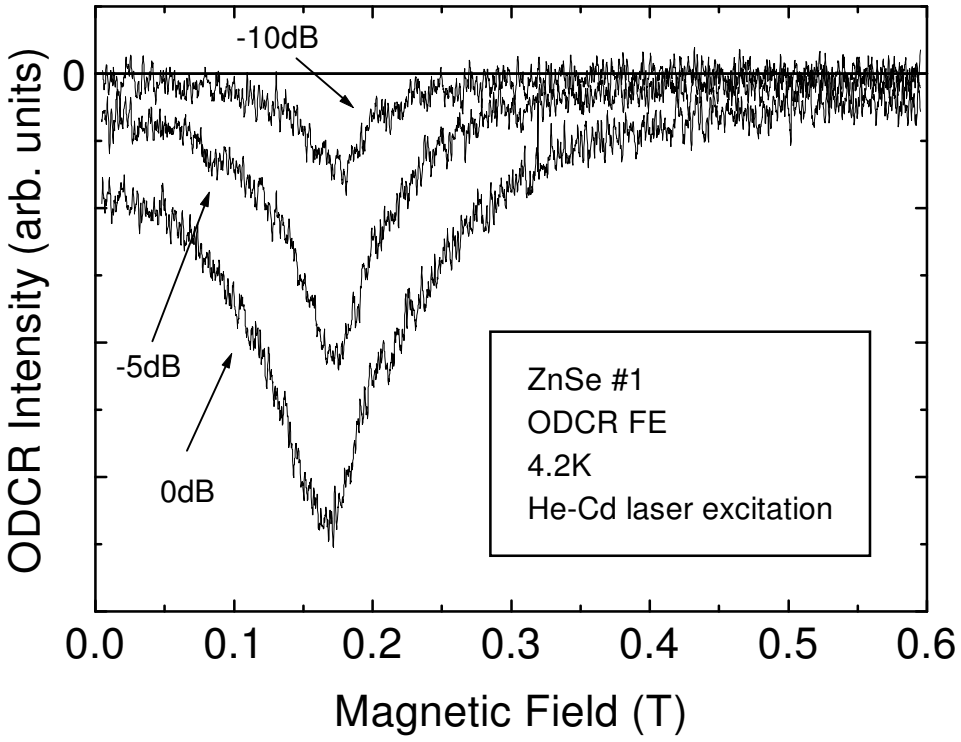

Figure 50: Microwave power dependence of the ODCR spectrum for free exciton. The relative microwave power level is indicated in the figure. The shoulder at 0.2T was not observed.

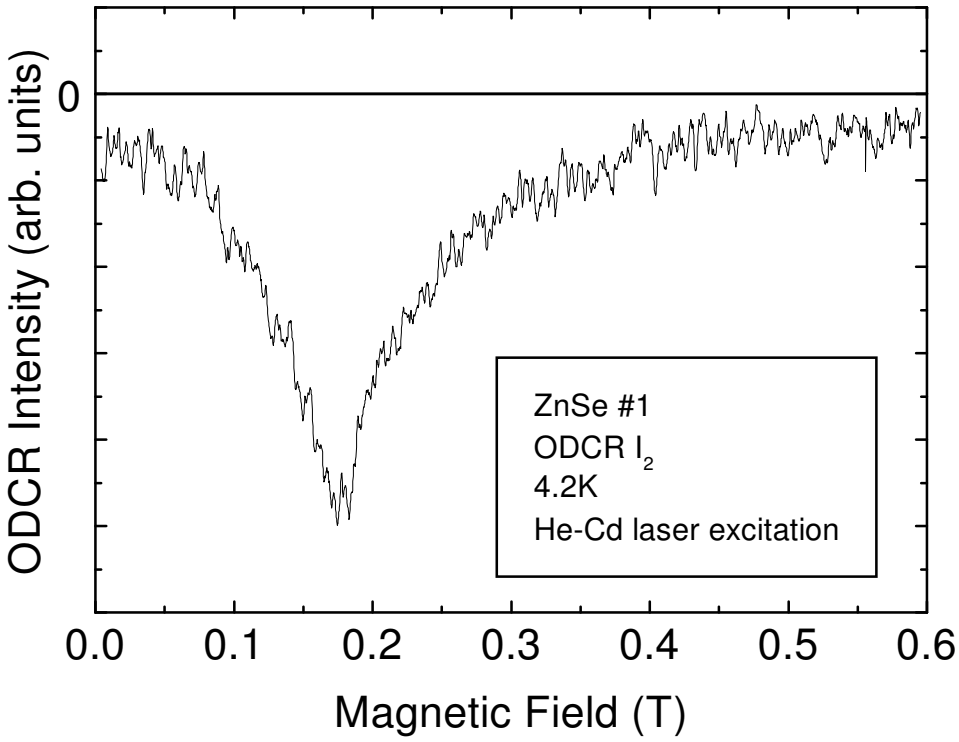

Figure 51: ODCR signal for neutral donor bound exciton I_2 as a function of the magnetic field. The microwave power is maximum. The shoulder at 0.2T was not observed, as in the case of the ODCR signal for free exciton.

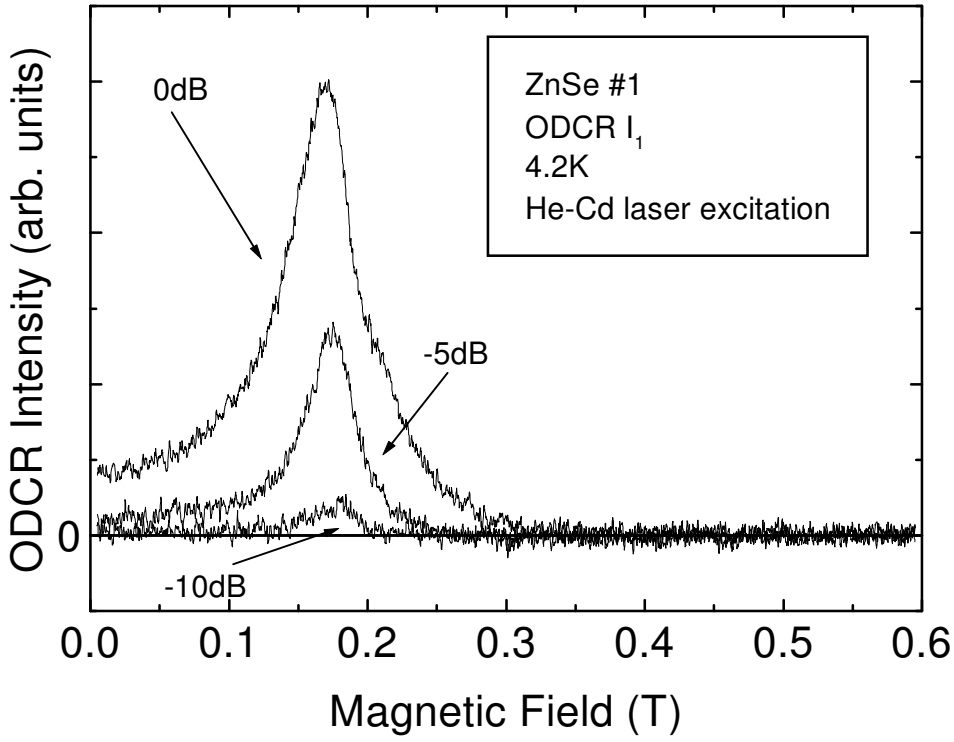

Figure 52: Microwave power dependence of the ODCR signal for neutral acceptor bound exciton I_1. The relative microwave power level is indicated in the figure. The prominent shoulder at 0.2T was not observed.

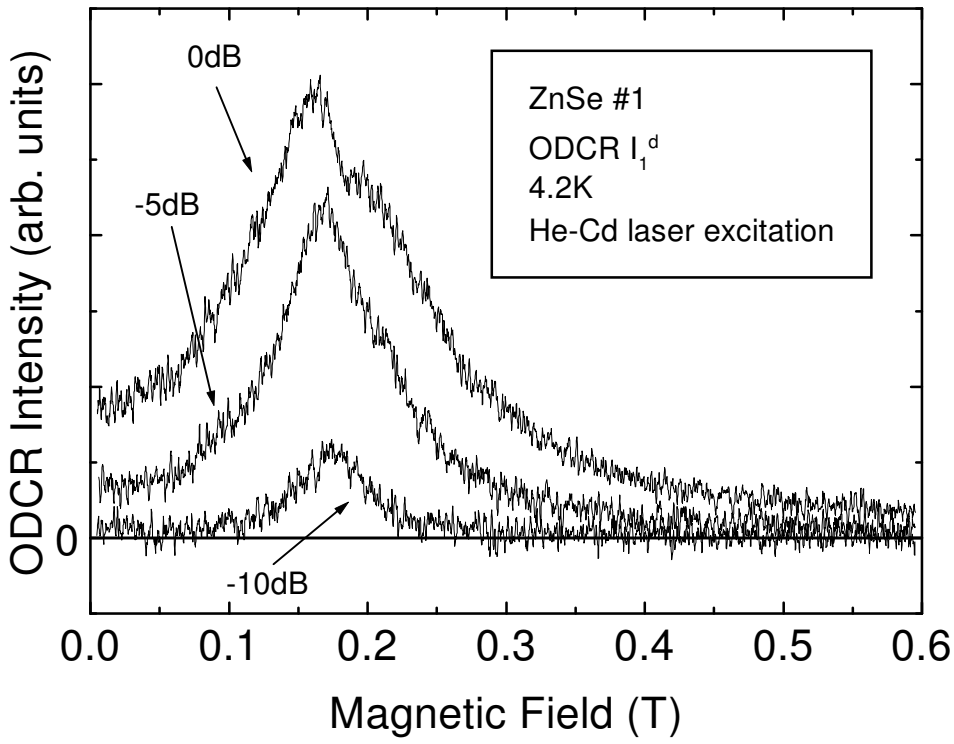

Figure 53: Microwave power dependence of the ODCR signal for deep acceptor bound exciton I_1^d. The relative microwave power level is indicated in the figure. The ODCR signal was composed of two signals at maximum microwave power level.

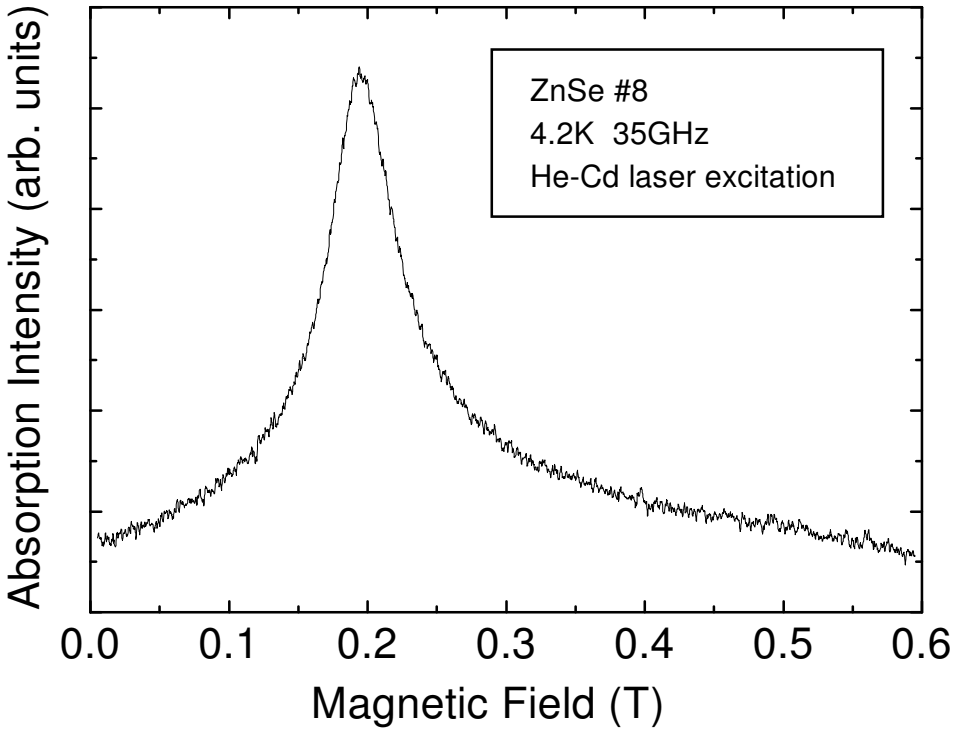

Figure 54: Ordinary CR spectrum at 4.2K. The sharp line represents that #8 is a high quality crystal.

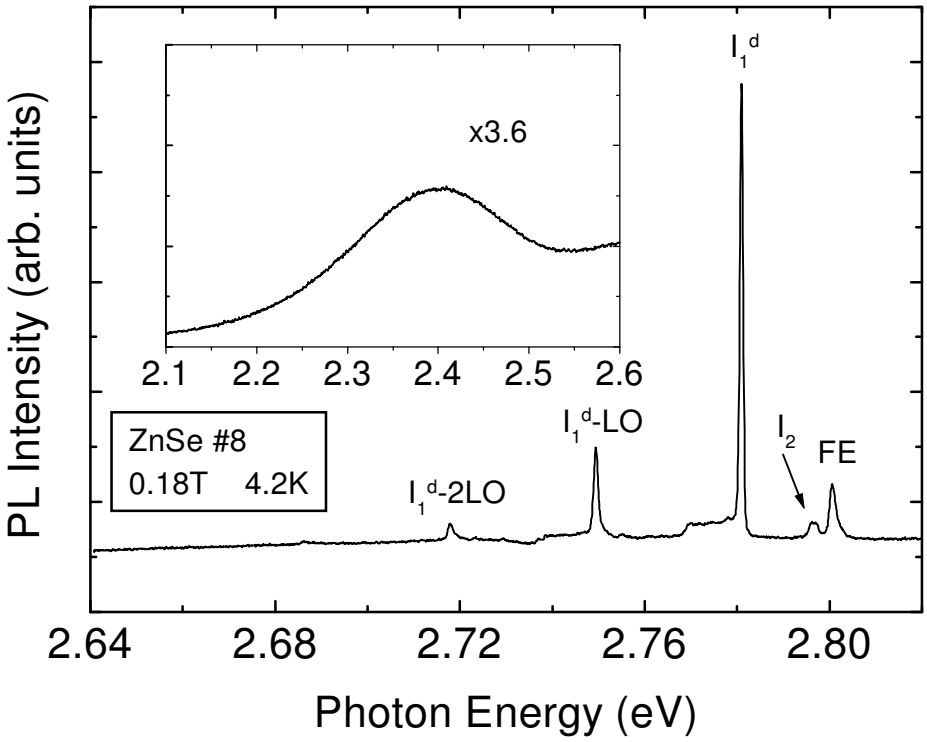

Figure 55: PL spectrum at the magnetic field of 0.18T. The PL peaks associated with exciton were observed. The PL peaks for neutral bound exciton I_1, R and Q series were not observed.

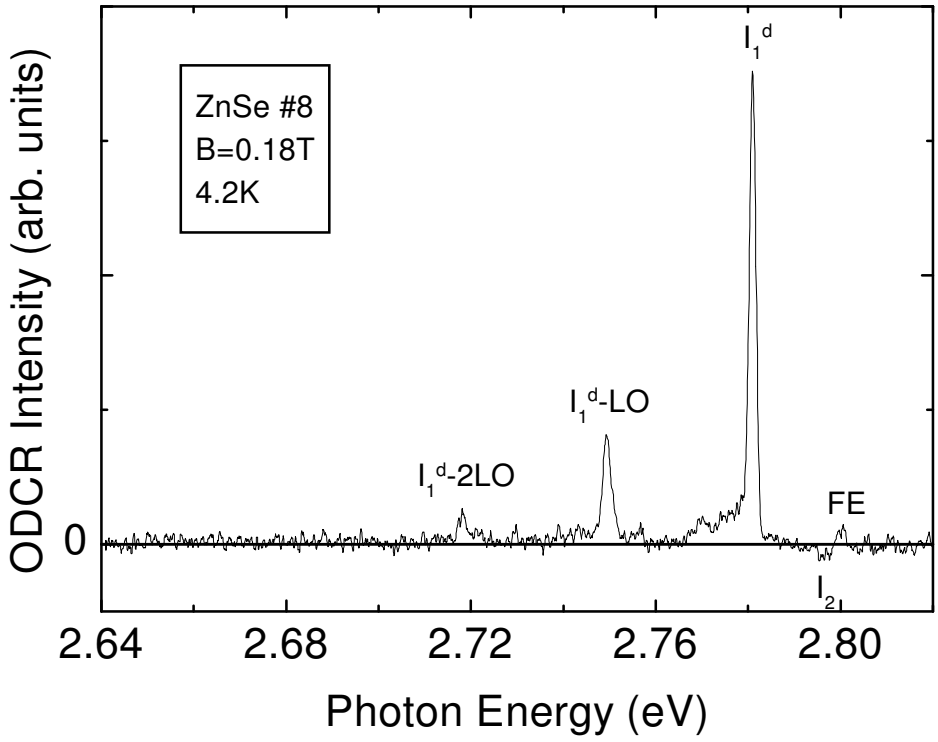

Figure 56: ODCR spectrum as a function of the photon energy. The applied magnetic field is 0.18T that corresponds to the electron CR. The ODCR signals associated with exciton were observed.

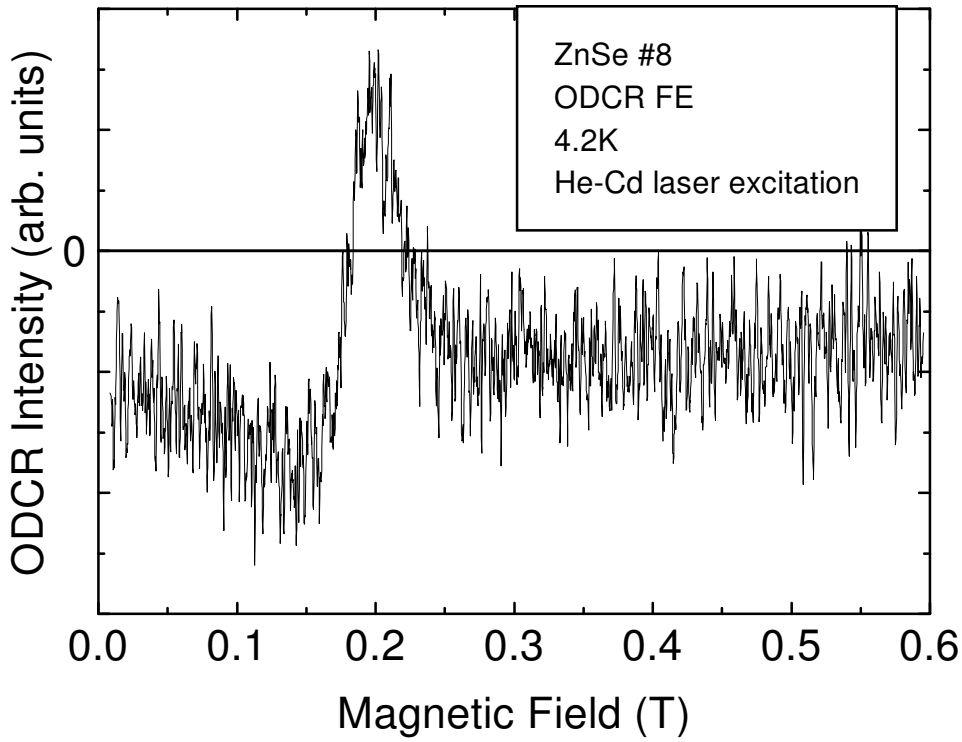

Figure 57: ODCR spectrum for free exciton as a function of the magnetic field. The microwave power level is maximum. The prominent signal at 0.2T due to the resonant formation of free exciton was observed.

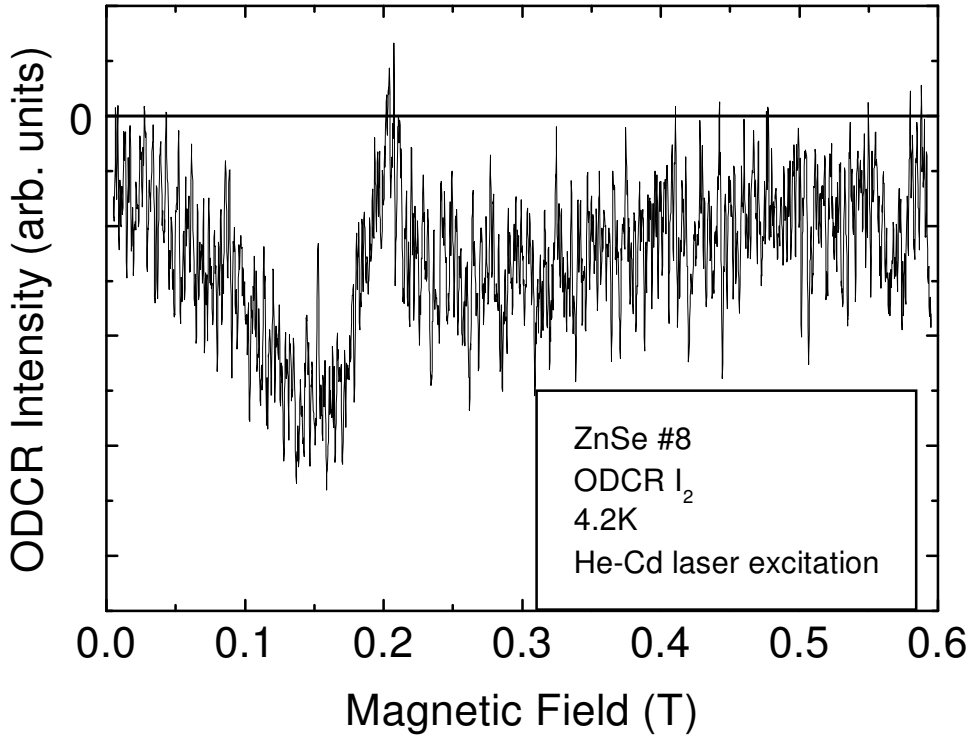

Figure 58: ODCR spectrum for neutral donor bound exciton I_2 as a function of the magnetic field. The microwave power level is maximum. The prominent signal at 0.2T due to the resonant formation of free exciton was observed, as in the case of the ODCR signal for free exciton.

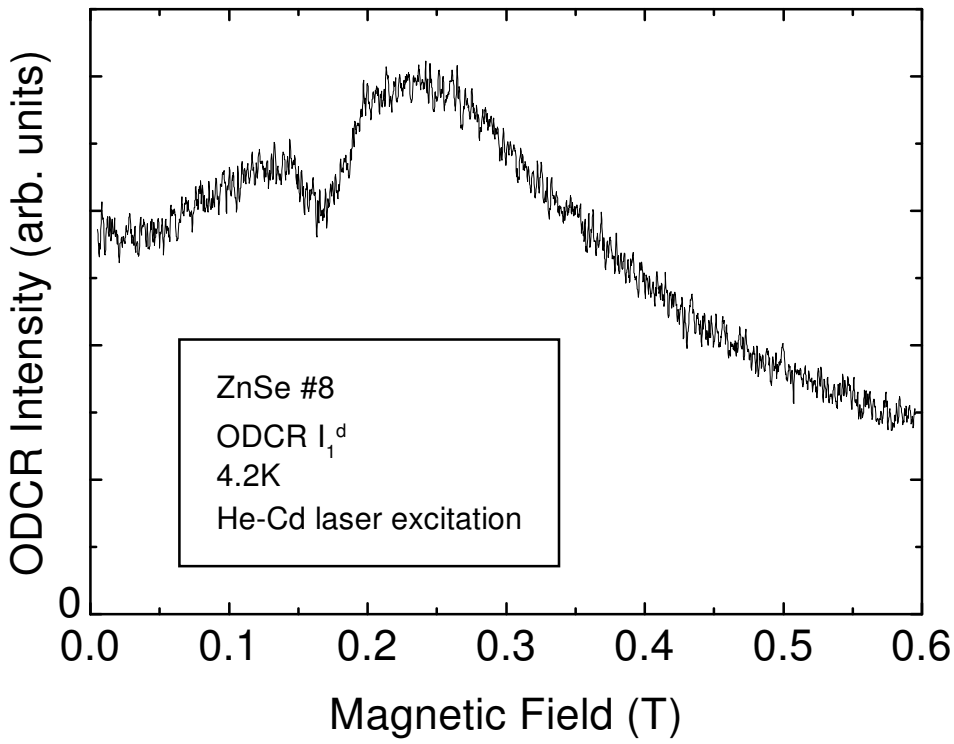

Figure 59: The ODCR spectrum for deep acceptor bound exciton I_1^d as a function of the magnetic field. The microwave power level is maximum. The line shape is different from that of the ODCR signal for free exciton.

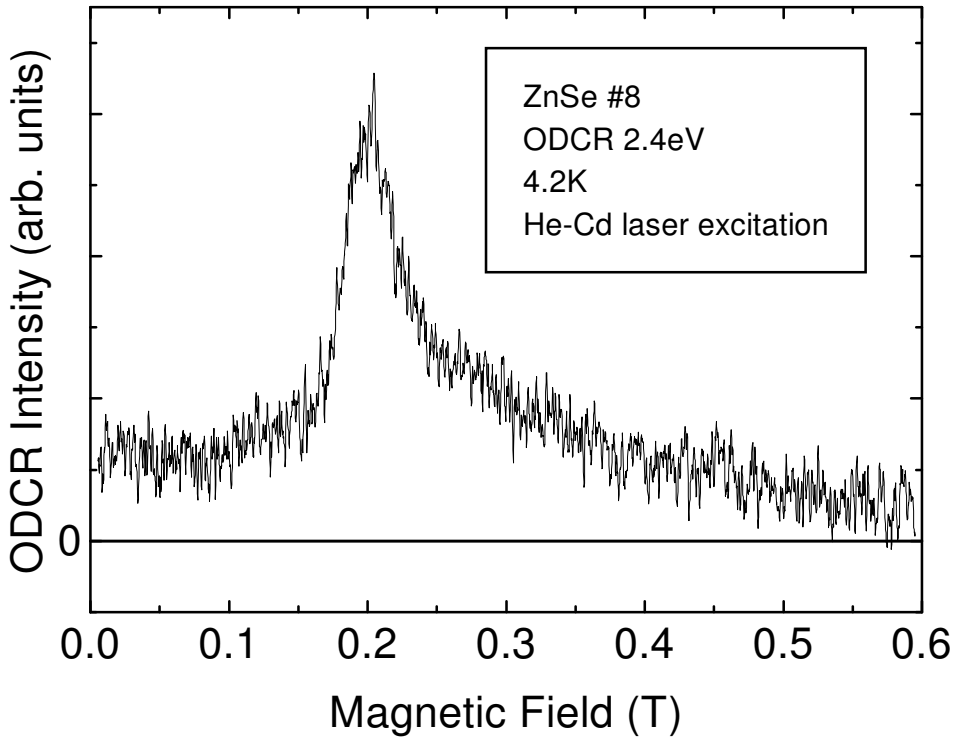

Figure 60: ODCR spectrum for the peak at 2.4eV. The signal is positive.

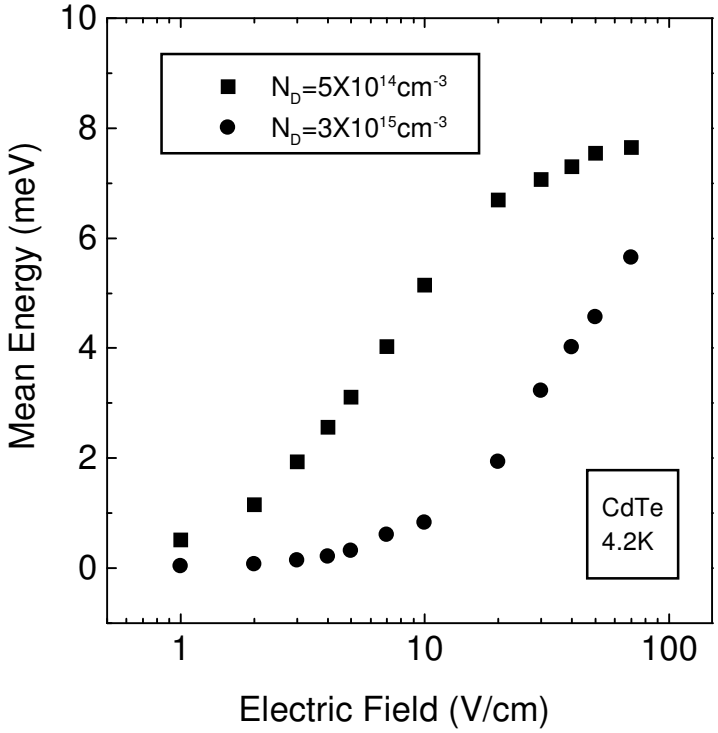

Figure 61: Mean energy of electrons plotted against the applied dc electric field.

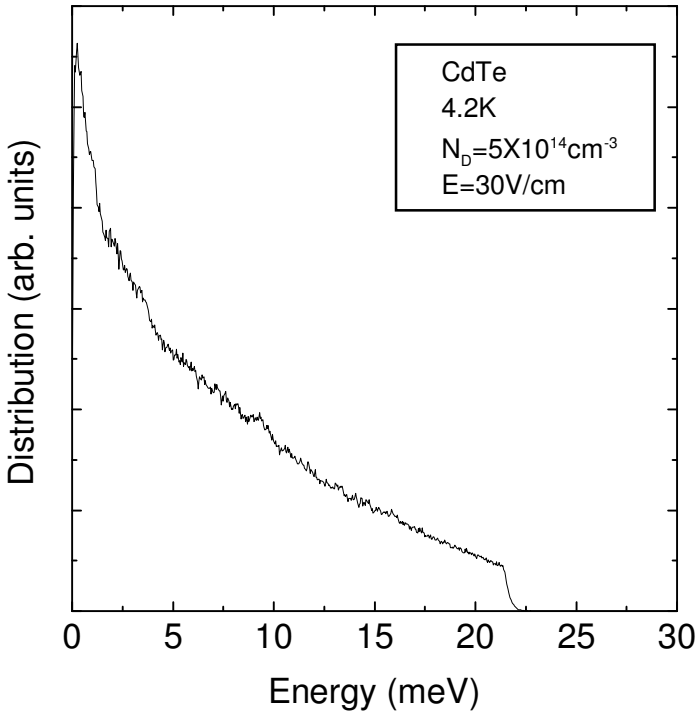

Figure 62: Distribution function of electrons at dc electric field of 30V/cm. One notes that there are some electrons that have kinetic energy above 13meV. The kink at 22meV corresponds to LO-phonon energy.

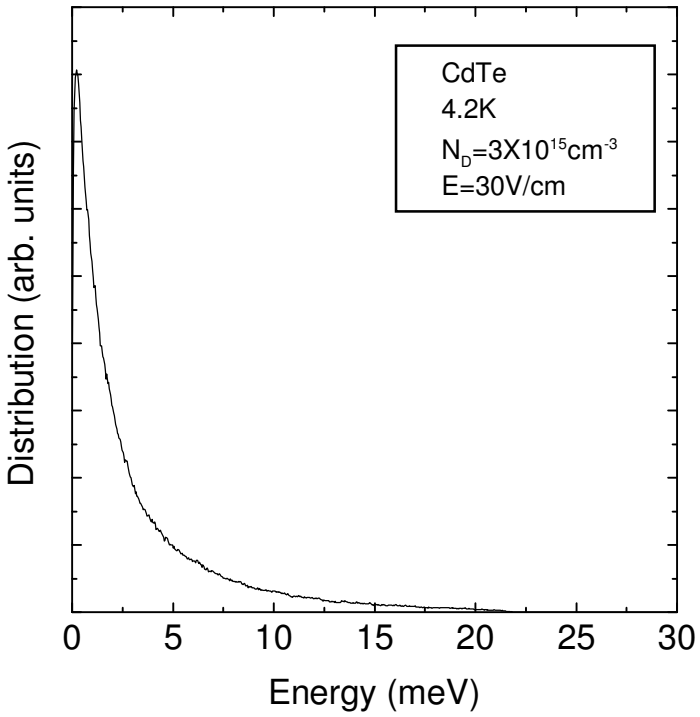

Figure 63: Distribution function of electrons at dc electric field of 30V/cm. There are few electrons that have kinetic energy above 13meV.

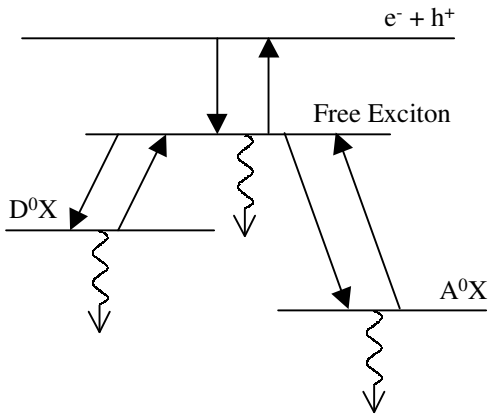

Figure 64: Energy diagram for free exciton, neutral donor bound exciton and neutral acceptor bound exciton.

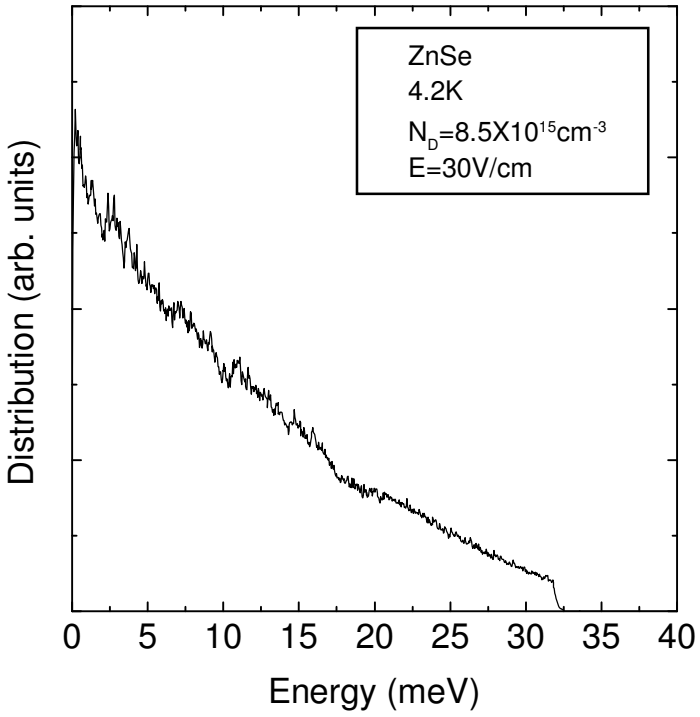

Figure 65: Distribution function of electrons at dc electric field of 30V/cm. There are a few electrons that have kinetic energy above 26meV. The kink at 32meV corresponds to LO-phonon energy.

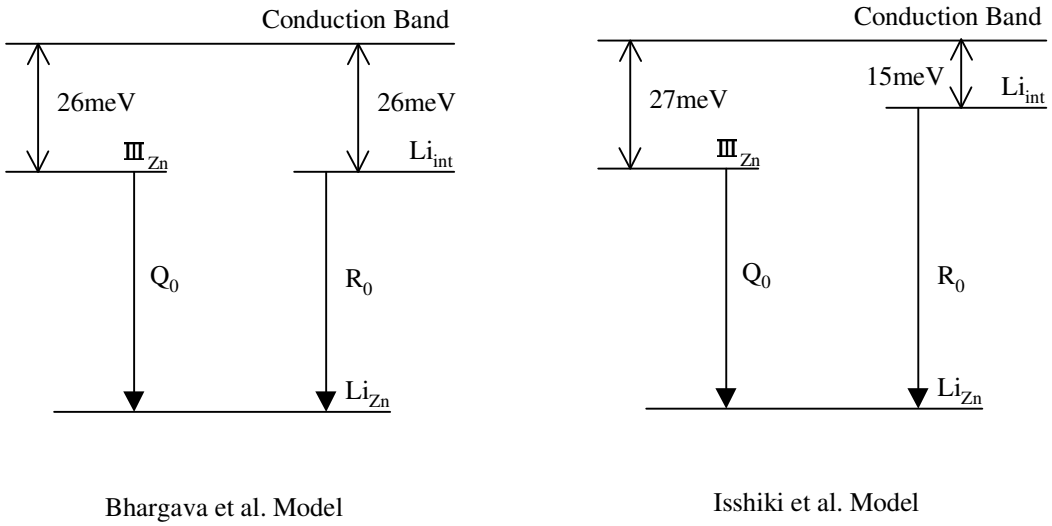

Figure 66: Energy diagram models proposed by Bhargava et al. and Isshiki at al.